Hadron-hadron scattering length from meson photoproduction

References

ωN **from** $\gamma p \rightarrow \omega p$

T. Ishikawa et al., PRC101, 052201 (R) (2020).

ηN **from** $\gamma d \rightarrow \eta pn$

S.X. Nakamura, H. Kamano, T. Ishikawa, PRC95, 042201 (R) (2017);
T. Ishikawa et al., Acta Phys. Polon. B51, 27 (2020).

ηN **from** $\gamma d \rightarrow \pi^0 \eta d$

T. Ishikawa et al., in preparation

nn **from** $\gamma^* d \rightarrow \pi^+ nn$

S.X. Nakamura, T. Ishikawa, T. Sato, arXiv: 2003.02497 (2020).

- Takatsugu Ishikawa (ishikawa@lns.tohoku.ac.jp)
- Research Center for Electron Photon Science (ELPH), Tohoku University, Japan

- Joint THEIA-STRONG2020 and JAEA/Mainz REIMEI Web-Seminar, Nov. 25, 2020

Contents

- **Introduction ~ low-energy scattering**
  - **internal structure**
  - **final-state interaction (FSI)**
  - **our activities**
    - **meson-nucleon scattering**
- **nn scattering length**
  - **charge symmetry breaking**
  - **photoproduction $\gamma d \to \pi^+ nn$**
  - **strategy to extract $\gamma d \to \pi^+ nn$**
    - **electroproduction**
    - **LT separation**

possible at the Mainz MAMI A1 facility

- **Summary**

Introduction

Scattering length

one of the fundamental parameters for describing hadron interactions

low-energy scattering is characterized with the *S*-wave phase shift $\delta(p)$

$$p\cot\delta(p) = -\frac{1}{a} + \frac{1}{2}rp^2 + O(p^4)$$

a **: scattering length** opposite sign is used for meson-nucleon scattering

r **: effective range**

negative (positive) a **provides attraction (repulsion)**

a **is positive if a bound state exists**

compositeness *X*:
overlap with the two-body scattering state

X* is directly given by the scattering length *a* and effective range *r

$$a = \frac{2X}{X+1}R, \quad r = \frac{X-1}{X}R, \quad R = \left(2\mu B\right)^{-1/2}$$

S. Weinberg, PR137, B672 (1965).

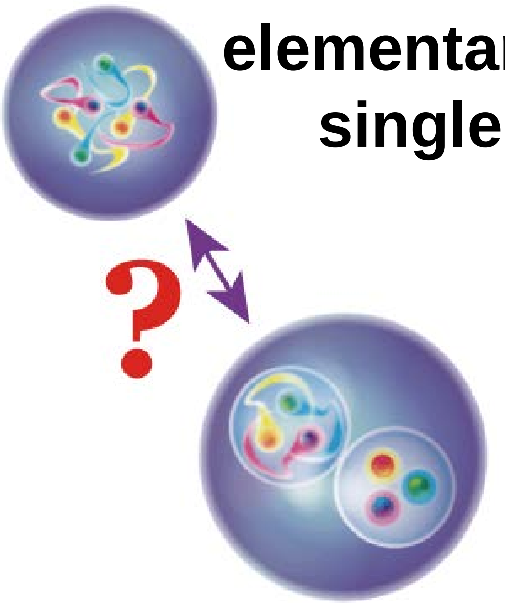

elementary:
single particle

composite:
molecule-like state

***X* can be also used for the near threshold resonances**

T. Hyodo, PRL111, 132002 (2013).

Final state interaction

- **the final-state interaction (FSI) is often utilized when a direct scattering experiment is difficult to be realized**

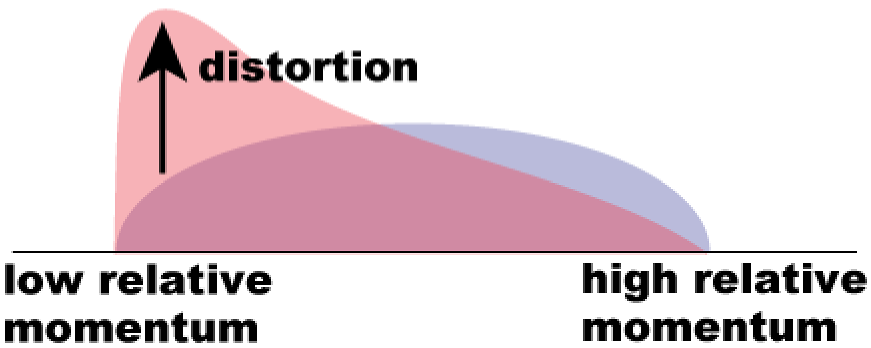

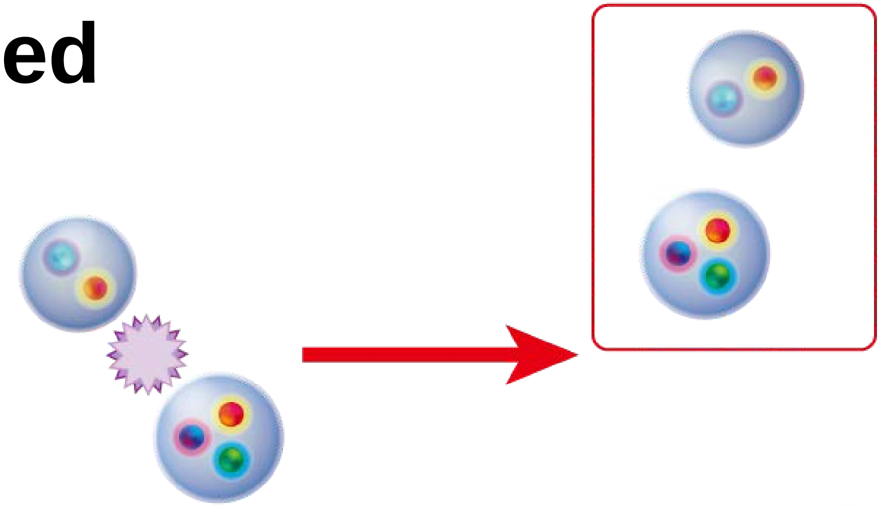

1) low relative momentum between the two hadrons of interest

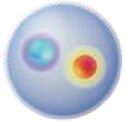

2) small or well-known FSI effects for the others
3) well-known production mechanism effects

Our activities

- ωN **scattering length from** $\gamma p \to \omega p$

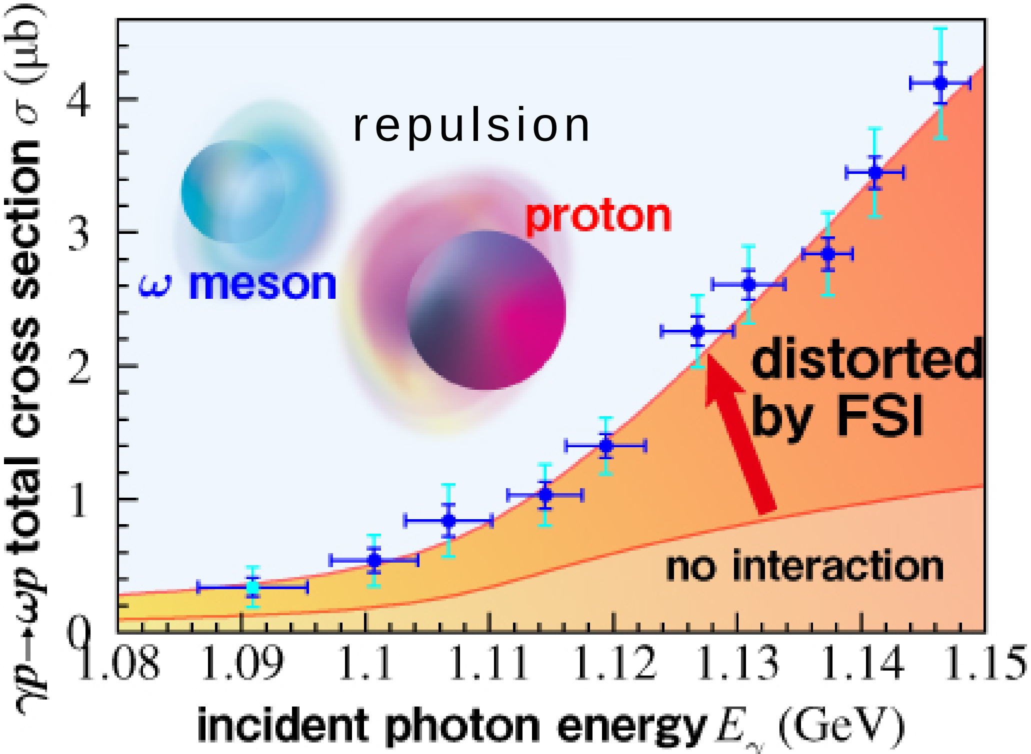

T. Ishikawa *et al.*, PRC101, 052201 (R) (2020).

complex ωN scattering parameters are determined for the first time

1) low relative momentum between ωN

2) no FSI effects for others (ωN alone in the final states)

3) insensitive production mechanism effects

Our activity ~ **ηN** (1)

$a_{\eta N}$ determination using $\gamma d \to \eta p n$ for understanding N(1535)S_{11}

the candidate for the chiral partner of the nucleon

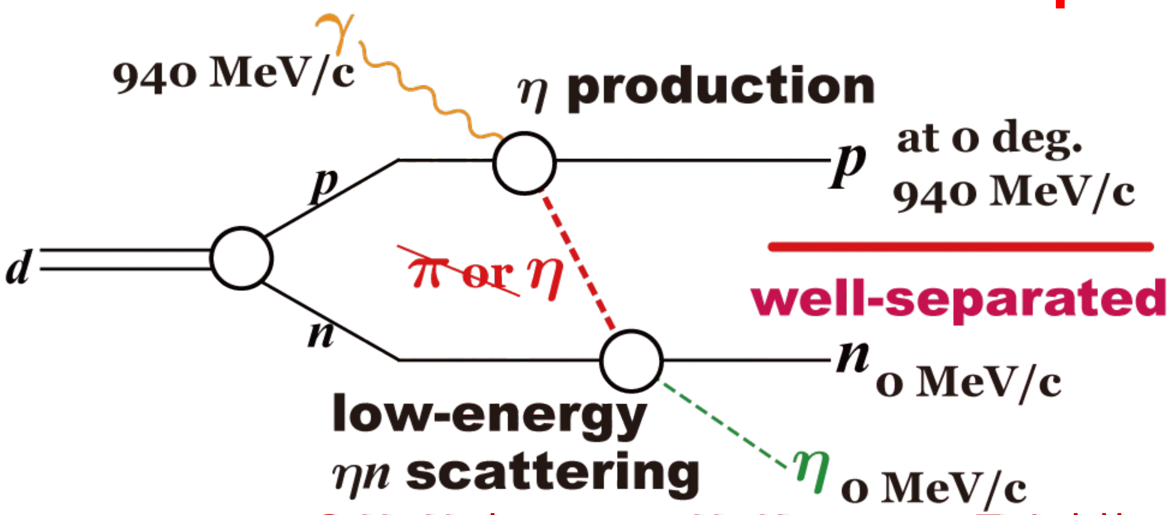

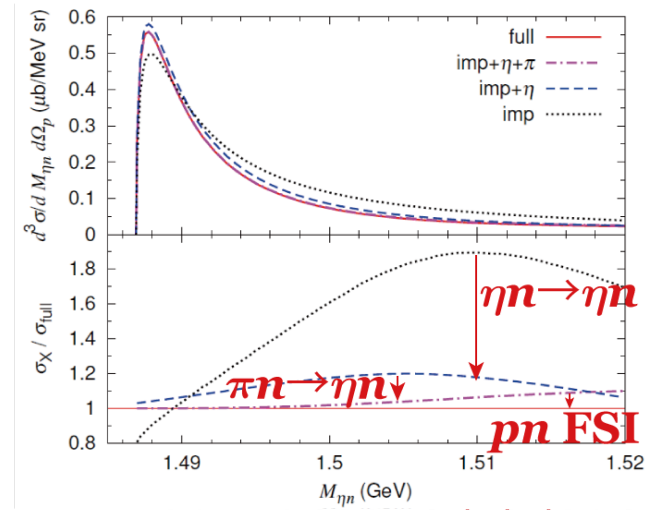

S.X. Nakamura, H. Kamano, T. Ishikawa, PRC95, 042201 (R) (2017).

1) low relative momentum between ηn
2) little FSI effects for others (pn & ηp)
3) little production mechanism uncertainties

the corresponding experiment is ongoing.

T. Ishikawa et al., Acta Phys. Polon. B51, 27 (2020).

Our activity ~ ηN (2)

$a_{\eta N}$ determination using $\gamma d \rightarrow \pi^0 \eta d$

calculation: M. Egorov, PRC101, 065205 (2020).

$$a_{\eta N} = 0.70 + i0.29 \text{ fm}$$

Migdal-Watson approximation gives

$$\mathrm{Re}\left[a_{\eta N}\right] = 0.72 \pm 0.05 \text{ fm}$$

$$\text{for } \mathrm{Im}\left[a_{\eta N}\right] = 0.2 \sim 0.4 \text{ fm}$$

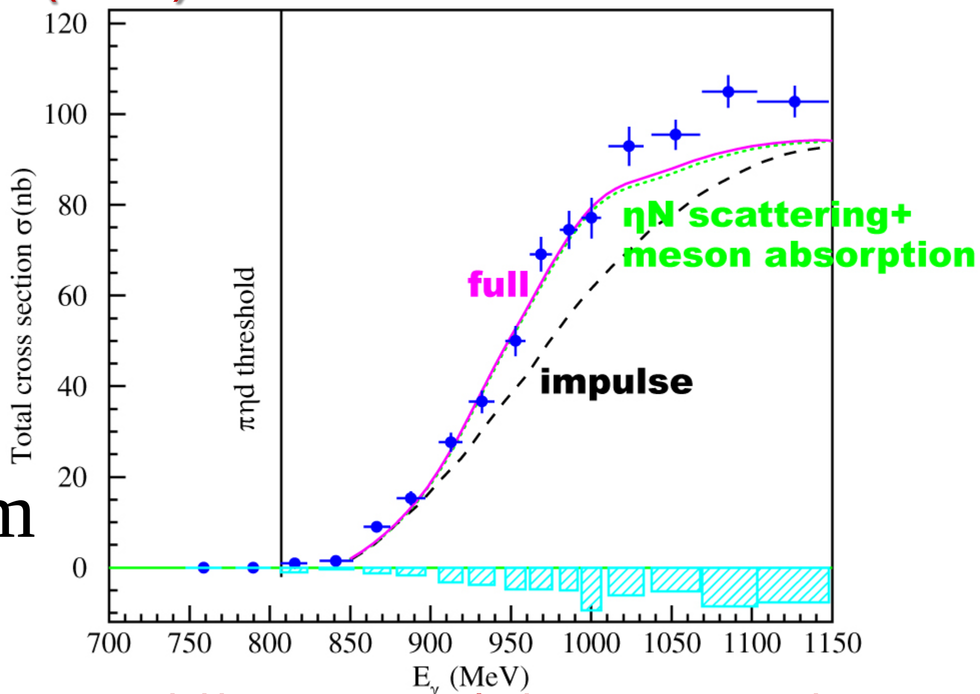

T. Ishikawa et al. in preparation

1) low relative momentum between ηN

2) little FSI effects for others (πN)

3) little production mechanism uncertainties [not clear]

absence of Δ-Kroll-Ruderman term and pion-pole term

nn scattering length

Charge Symmetry Breaking (CSB)

CS: invariance under interchange of *u* and *d* quarks

due to the difference of *u*-*d* masses and EM effects

***n*-*p* mass difference of 1.3 MeV**

charge dependence of nuclear force: a few percent

(ρ^0-ω mixing and *n*-*p* mass difference)

G.A. Miller and W.T.H. van Oers arXiv: nucl-th/9409013.

0.7-MeV difference in B between ^{3}H and ^{3}He

G.A. Miller and W.T.H. van Oers arXiv: nucl-th/9409013.

$A_n(\theta_n) \neq A_p(\theta_p)$ at $\theta_n = \theta_p$ for np scattering

R. Abegg et al., PRL56, 2571 (1986); PRD39, 2464 (1989).

$d\sigma/d\Omega_\pi(\theta) \neq d\sigma/d\Omega_\pi(\pi - \theta)$ for $np \to d\pi^0$

A.K. Opper et al., PRL91, 212302 (2003).

hypernuclear systems

0.3-MeV difference in E_x between $^4_\Lambda$H and $^4_\Lambda$He

T.O. Yamamoto et al., PRL115, 222501 (2015);

A. Esser et al., PRL114, 232501 (2015).

Charge symmetry breaking

low-energy *NN* scattering

characterized by the scattering length a and effective range r

$$p\cot\delta(p) = \boxed{-\frac{1}{a}} + \frac{1}{2} r p^2 + O(p^4)$$

the sign is different in meson-nucleon scattering

scattering parameters for the spin-singlet states

statistical uncertainty

$$a_{nn} = -18.9 \boxed{\pm 0.4 \text{ fm}}, \qquad r_{nn} = 2.75 \pm 0.11 \text{ fm} \quad \text{for } nn$$

$$a_{np} = -23.74 \pm 0.02 \text{ fm}, \quad r_{np} = 2.77 \pm 0.05 \text{ fm} \quad \text{for } np$$

$$a_{pp} = -17.3 \boxed{\pm 0.4 \text{ fm}}, \qquad r_{pp} = 2.85 \pm 0.04 \text{ fm} \quad \text{for } pp$$

systematic uncertainty of removing the EM effects

R. Machleidt and I. Slaus, JPG: NPP27, R69 (2001).

5.6-fm CIB: ***np*** and ***nn*** (***pp***)

1.6-fm CSB: ***nn*** and ***pp***

nn scattering length

a_{nn} determination: $-19 \sim -16$ fm

direct measurement W.I. Furman et al., JPG28, 2627 (2002); A.Yu. Muzichka et al., NPA789, 30 (2007).

nn **scattering: almost impossible**

indirect measurement

extraction from $nd \to nnp$ (Faddeev eq.)

$$a_{nn} = -16.1 \pm 0.4\ \text{fm}\ (E_n = 25.3\ \text{MeV},\ np\ \text{detected@Bonn})$$

V. Huhn et al., PRL85, 1190 (2000).

$$a_{nn} = -18.7 \pm 0.7\ \text{fm}\ (E_n = 13.0\ \text{MeV},\ nnp\ \text{detected@TUNL})$$

D.E. Gonzalez Trotter et al., PRC73, 034001 (2006).

$$a_{nn} = -16.5 \pm 0.9\ \text{fm}\ (E_n = 17.4\ \text{MeV},\ p\ \text{detected@Bonn})$$

W. Witsch et al., PRC74, 014001 (2006).

$\pi^- d \to nn\gamma$

C.R. Howell et al., PLB444, 252 (1998).

$$a_{nn} = -18.59 \pm 0.40\ \text{fm}\ (\text{stopped}\ \pi,\ n\gamma\ \text{detected@LAMPF})$$

the elementary (KR) amplitude is well determined for $\gamma p \to \pi^+ n$

FSI neutrons: ~2.4 MeV (efficiencies are measured for 5~13 MeV)

cross sections for $pp \to pp\gamma$ (analogous) is overestimated by 40% ?

E.S. Konobeevski et al., arXiv: 1703.00519 (2017). no KR in $pp \to pp\gamma$

New measurement of a_{nn}

a_{nn} determination using $\gamma d \to \pi^+ nn$

pointed out by Lensky et al. for the first time

based on chiral perturbation theory

too low E_γ (20 MeV above the threshold, $p_\pi <$ 80 MeV/c)

our consideration

experimental advantage

no need to detect neutrons

rather higher E_γ (200~300 MeV)

between the threshold (~150 MeV) and

Δ production (~340 MeV)

well-known π production amplitude

high nn FSI probability

weak πn FSI

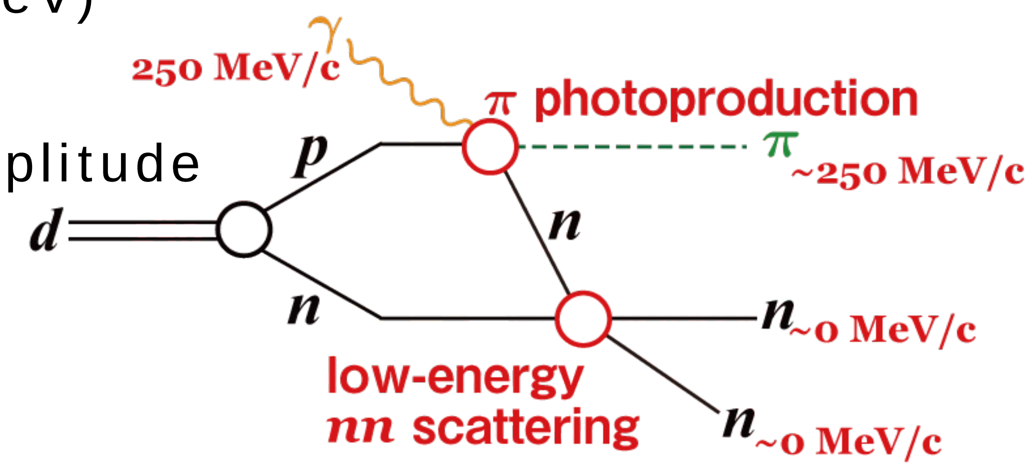

S.X. Nakamura, T. Ishikawa, T. Sato, arXiv: 2003.02497 (2020).

$$\gamma d \to \pi^+ nn$$

differential cross section

$$\frac{d^2\sigma(E_\gamma)}{d\Omega_{\vec{k}}\,dM_{nn}} = \boxed{\frac{1}{12}} \sum_{\lambda,s_d}\sum_{s_1,s_2} \frac{(2\pi)^4}{4E_\gamma}\frac{1}{2E_d(\vec{p}_d)}\int d\Omega_{\vec{p}_{nn}} \frac{p_{nn}k^2 m_n^2}{\left|kE - n\vec{q}\cdot\hat{k}\,E_\pi(\vec{k})\right|}\,|M(E)|^2$$

for $\gamma(\vec{q})+d(\vec{p}_d)\rightarrow\pi^+(\vec{k})+n_1(\vec{p}_1)+n_2(\vec{p}_2)$

$$M(E)=\sqrt{\frac{8E_\gamma E_d(\vec{p}_d)E_\pi(\vec{k})E_n(\vec{p}_1)E_n(\vec{p}_2)}{m_n^2}}$$

$$\times\left(t_{\mathrm{imp}}(E)+t_{NN}(E)+t_{\pi N}(E)+\{\text{exchange terms}\}\right)$$

initial spins γ, d
identity of n

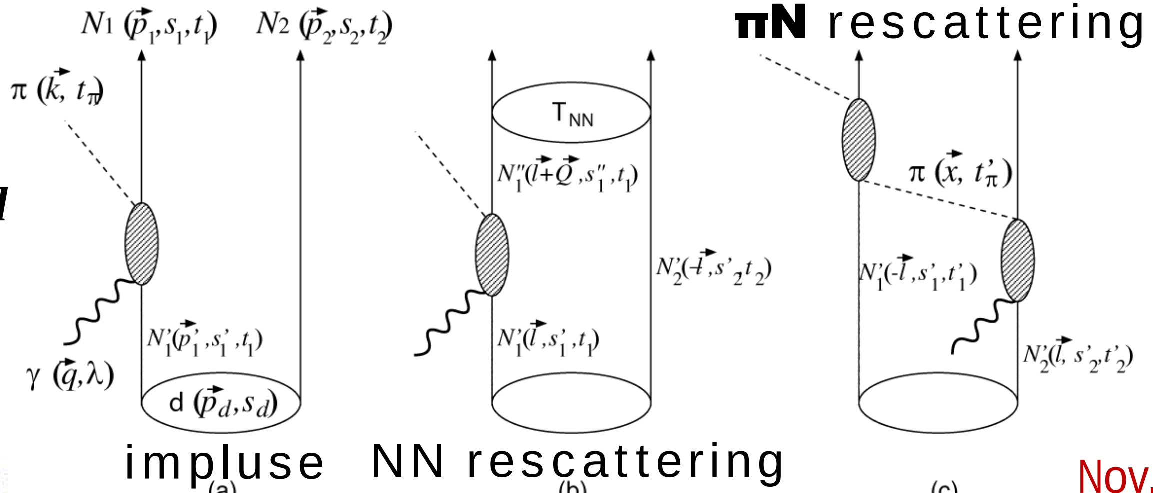

T. Ishikawa

Formalism

$\gamma N \to \pi N$ production amplitude

DCC, CM12

NN scattering amplitude

CD-Bonn, Reid93, Nijmegen I, Nijmegen II

πN scattering amplitude

DCC

meson-exchange current

considered

higher order effects

not considered

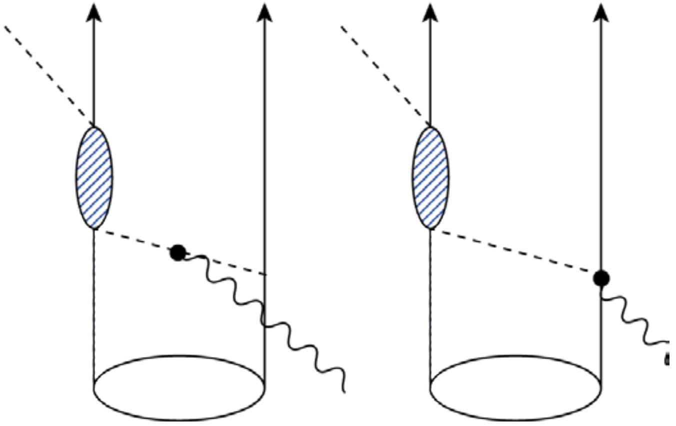

Formalism

$\gamma N \to \pi N$ production amplitude

DCC, CM12

elementary amplitudes: of primary importance

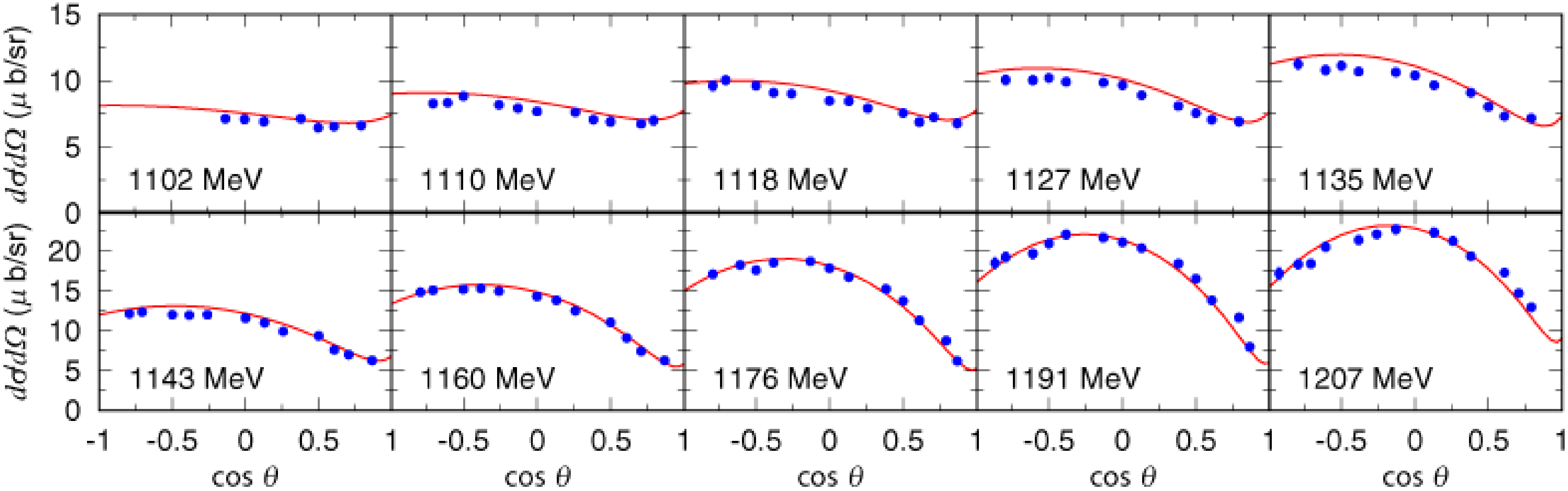

$$W = 1121 \text{ MeV for } E_\gamma = 200 \text{ MeV}$$

$$W = 1162 \text{ MeV for } E_\gamma = 250 \text{ MeV}$$

$$W = 1201 \text{ MeV for } E_\gamma = 300 \text{ MeV}$$

Results

$\gamma d \to \pi^+ nn$ cross sections at 250 MeV

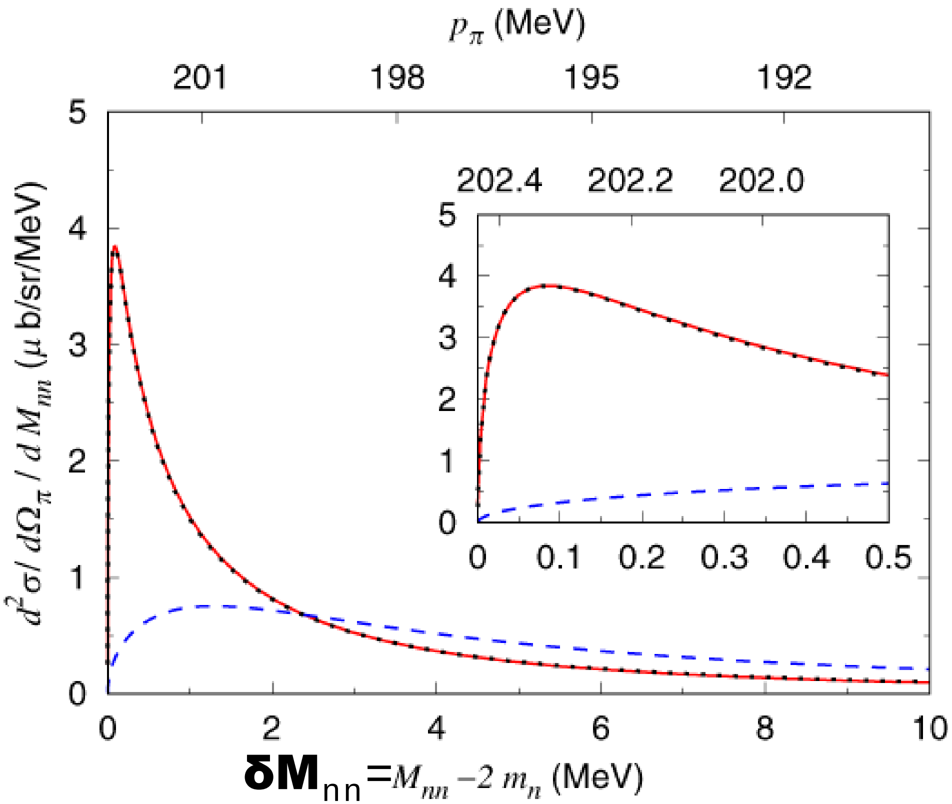

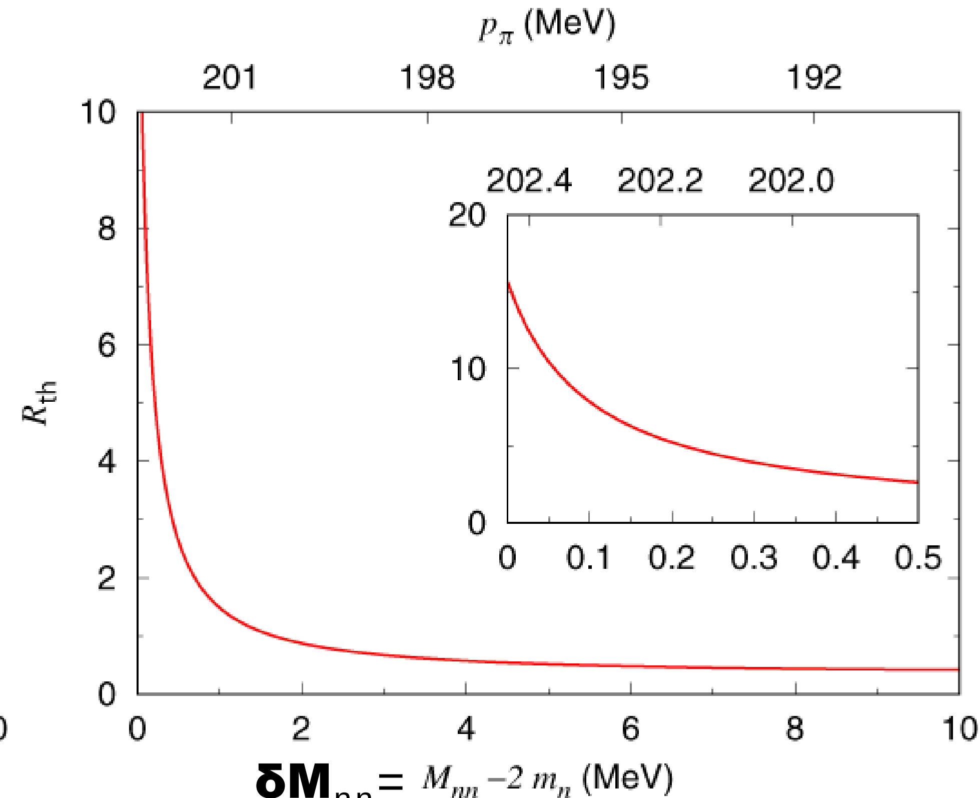

- - - - - **impulse**

· · · · · · · · · **impulse + NN rescattering**

——— **impulse + NN + πN rescattering**

$$E_\gamma = 250\text{MeV},\ \theta_\pi = 0^\circ$$

πN rescattering effect is very small, and hence higher order effects may be negligible

Results

$\gamma d \to \pi^+ nn$ cross sections at 250 MeV

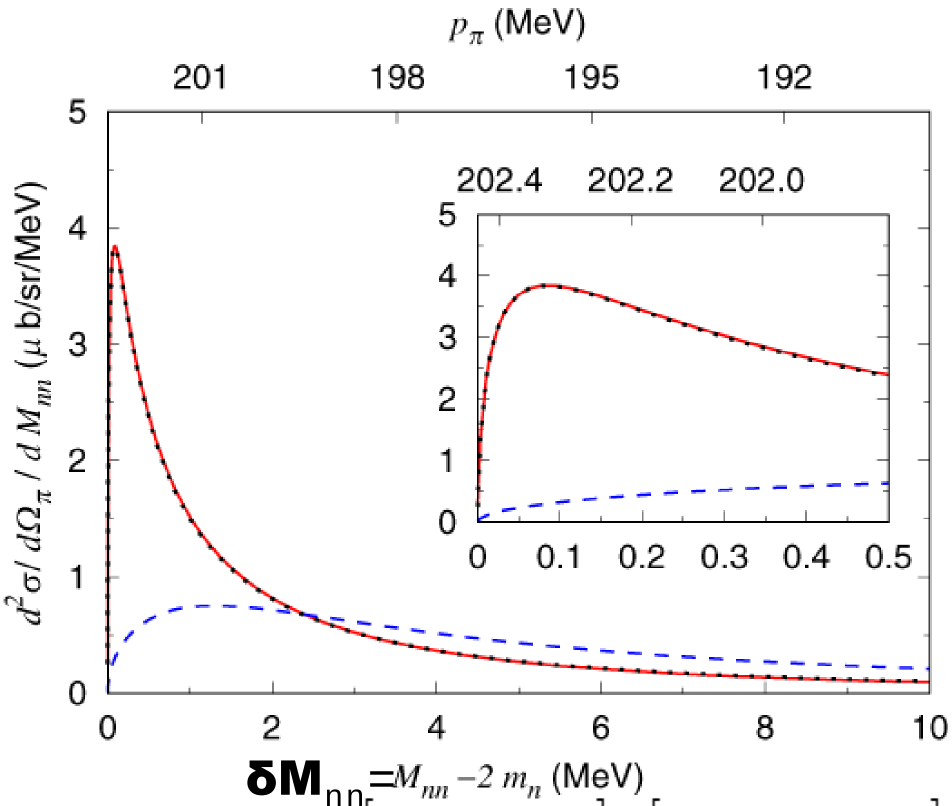

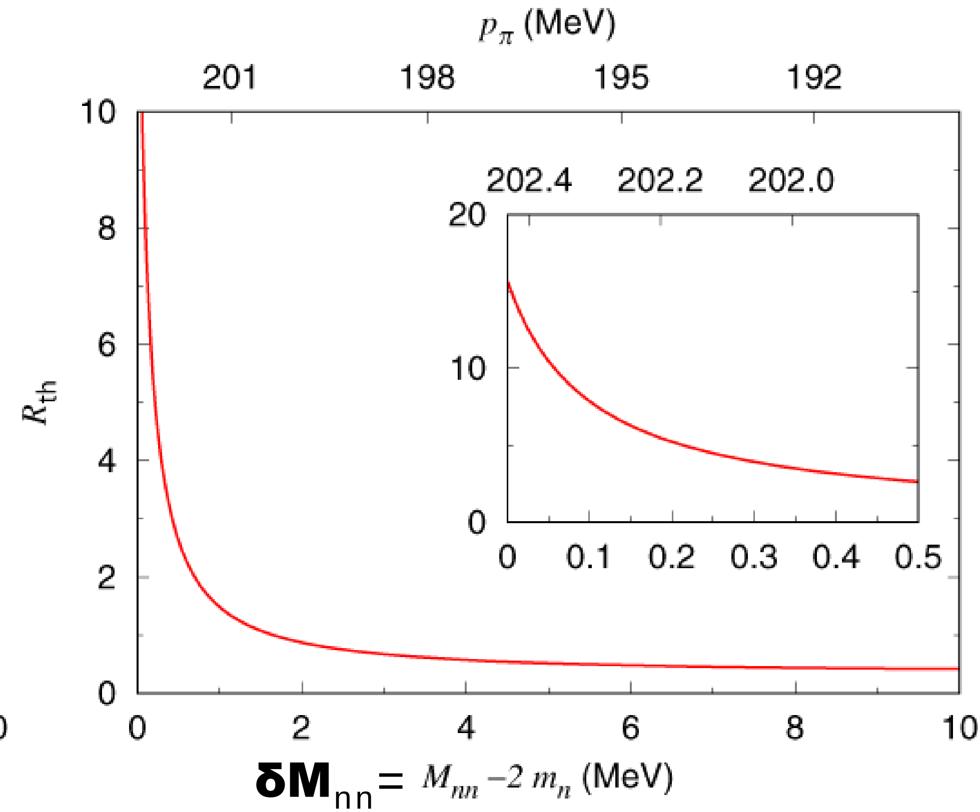

$$R_{\rm th} = \left[\frac{d^2\sigma(E_\gamma)}{d\Omega_{\vec{k}}dM_{nn}}\right] \Big/ \left[\frac{d^2\sigma_{\rm conv}(E_\gamma)}{d\Omega_{\vec{k}}dM_{nn}}\right]$$

nucleon momentum distribution inside the deuteron

$$\frac{d^2\sigma_{\rm conv}(E_\gamma)}{d\Omega_{\vec{k}}dM_{nn}} = \frac{d\sigma_{\gamma p\to\pi^+ n}(E_\gamma)}{d\Omega_{\vec{k}}} \int d^3 p_s \frac{m_n}{E_n(p_s)} |\Psi_d(p_s)|^2 \,\delta(M_{nn} - M_{nn}(\vec{p}_s, E_\gamma))$$

Results

$\gamma d \to \pi^+ nn$ cross sections at 250 MeV

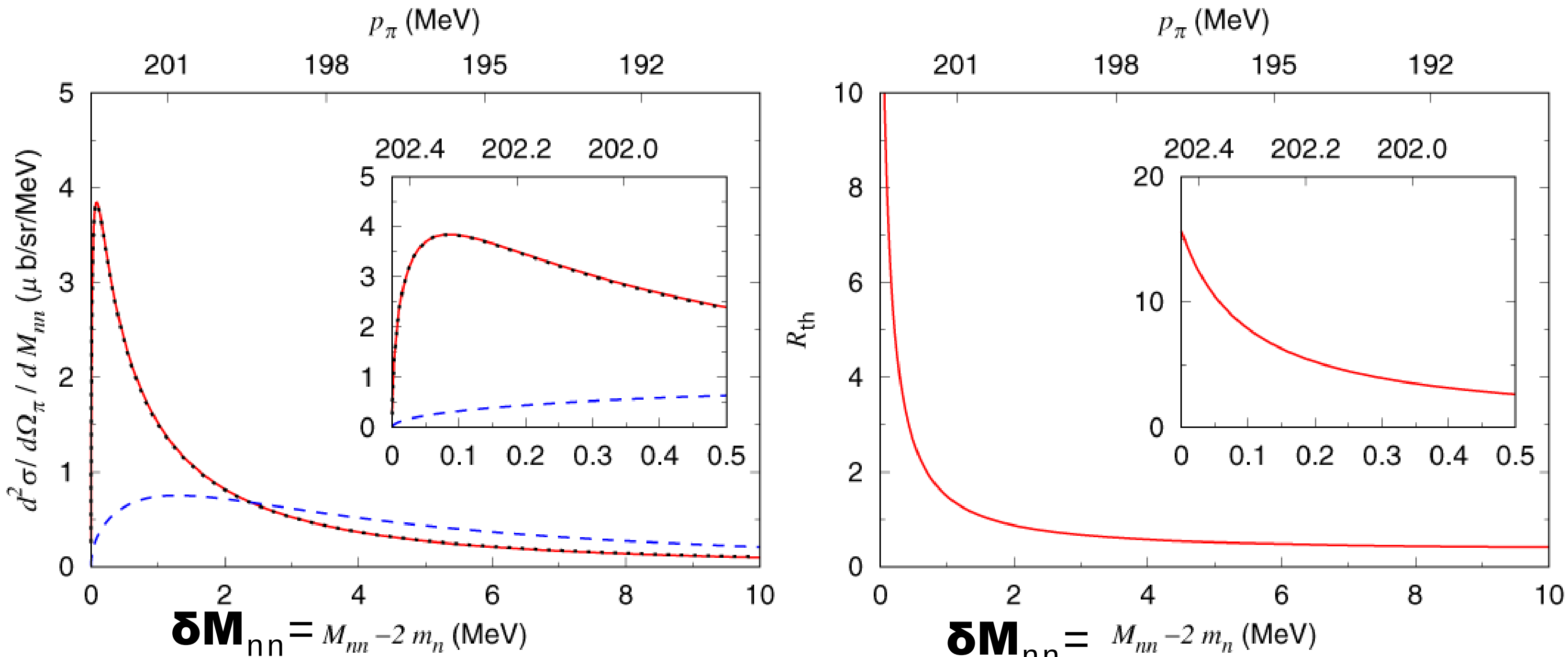

- - - - - - **impulse**

·········· **impulse + NN rescattering**

—— **impulse + NN + πN rescattering**

$$E_\gamma = 250\text{MeV}, \theta_\pi = 0^\circ$$

$\pi N \to \pi N$ rescattering effect is discernible at E_γ=300 MeV

$\gamma N \to \pi N$ production amplitude below the πN threshold contributes ~2% to the cross section at E_γ=200 MeV

the incident energy of 250 MeV (and θ_π=0°) is the best

a_{nn}, r_{nn} and $d^2\sigma / dM_{nn} / d\Omega_\pi$

$\gamma d \to \pi^+ nn$ cross sections for different a_{nn}

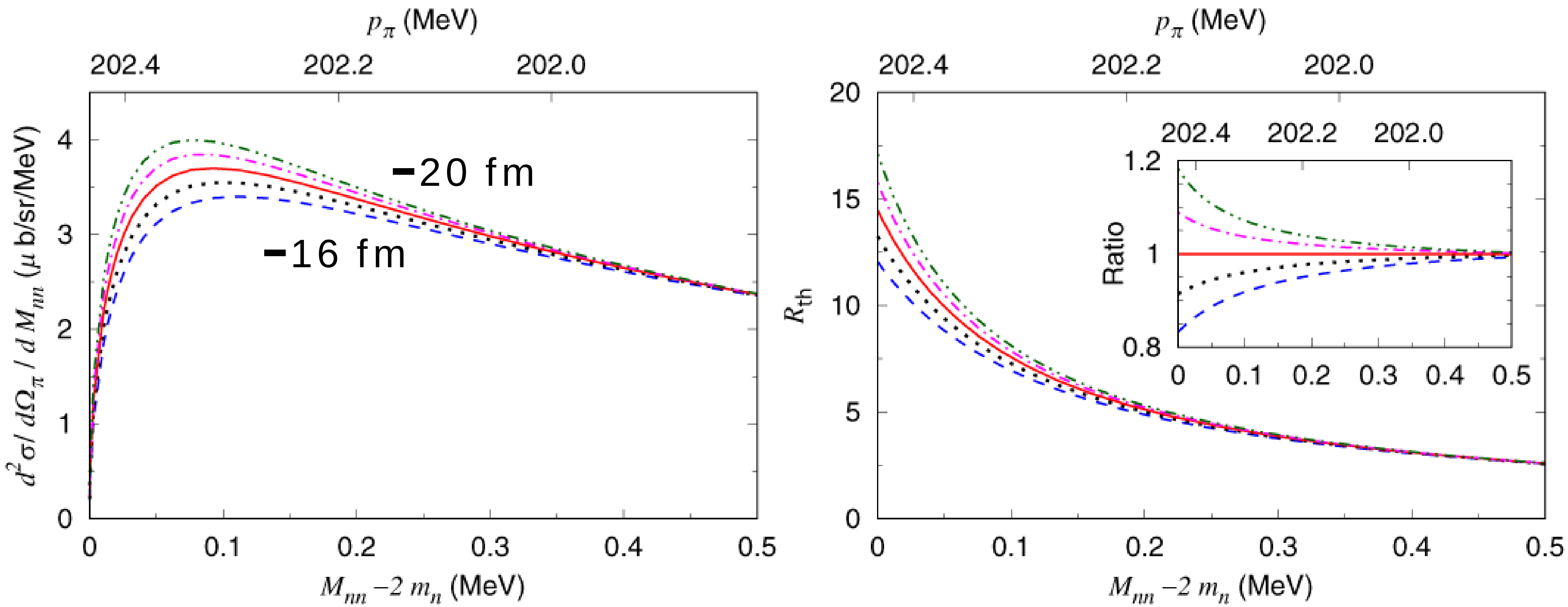

sensitive to $d^2\boldsymbol{\sigma}/dM_{nn}/\mathbf{d\Omega_\pi}$ **below** $\boldsymbol{\delta}\mathbf{M}_{nn}$=0.3 MeV

a_{nn}=−20 fm, −19 fm, −18 fm, −17 fm, −16 fm

r_{nn}=2.75 fm

$\gamma d \rightarrow \pi^+ nn$ cross sections for different r_{nn}

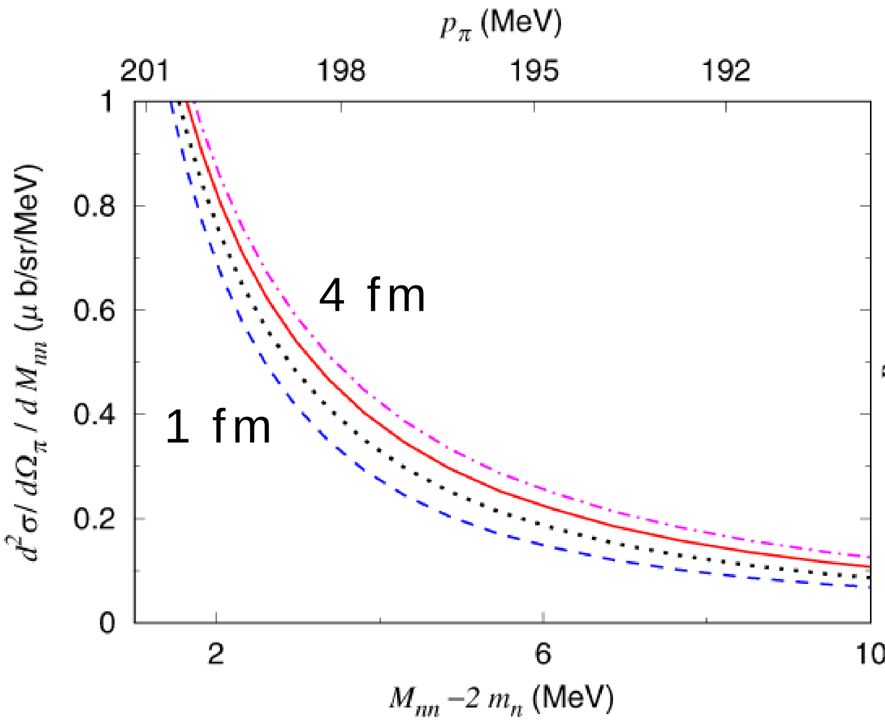

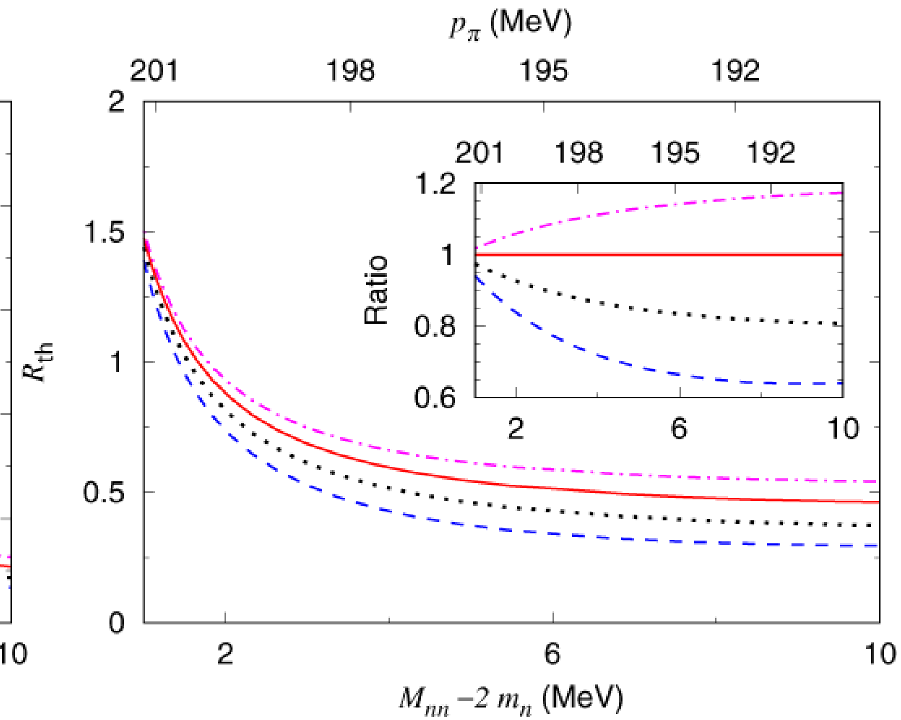

sensitive to $d^2\sigma/dM_{nn}/d\Omega_\pi$ from δM_{nn}=2 to 10 MeV

a_{nn}=−18.9 fm

r_{nn}=1 fm, 2 fm, 3 fm, 4 fm

a_{nn}, r_{nn} and $d^2\sigma / dM_{nn} / d\Omega_\pi$

R_{th} with 2% error, resolved into ΔM_{nn}=0.04 MeV can determine a_{nn} and r_{nn} with the uncertainties σ_a and σ_r of ±0.21 fm and ±0.06 fm, respectively

σ_a=0.13~0.27 fm, σ_r=0.23~0.06 fm for ΔM_{nn}=0.01~0.08 MeV

σ_a and σ_r are independent of a_{nn} and r_{nn}, respectively

σ_a gradually increases with increase of a_{nn}

σ_r rapidly increases with increase of r_{nn}

theoretical uncertainty does not affect σ_a so much

Strategy to extract

$$\gamma d \to \pi^+ nn$$

Electroproduction

Requirements

1. **High momentum resolution for the incident photon & emitted positive pion:**
   ~0.1 MeV/c (5×10^{-4}) or better
2. **Precision for the cross section:**
   ~2% or higher

difficult to achieve such a high resolution at the real photon facilities in the world

electroproduction is considered instead at the Mainz MAMI A1 facility

Electroproduction

Mainz MAMI A1 facility

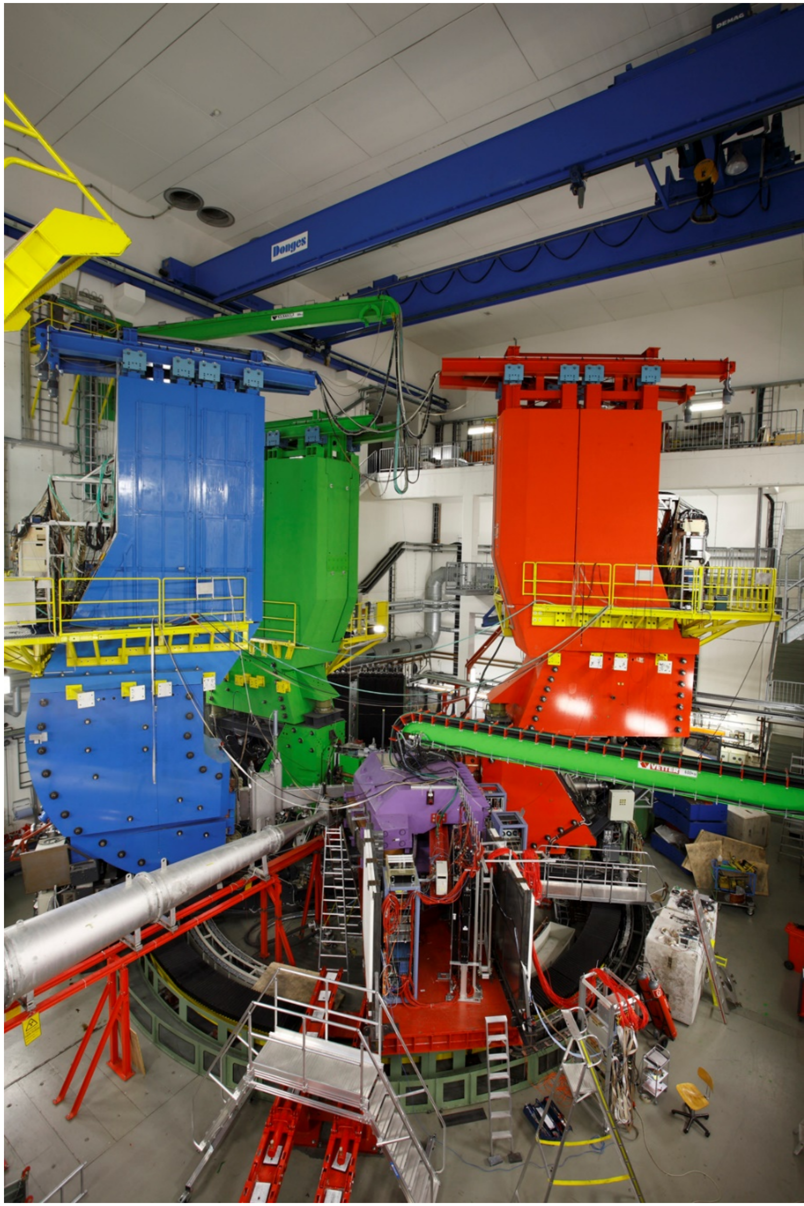

momentum resolution
electron beam: ~10^{-6}
spectrometer: ~10^{-4}

high statistics enables us to use a convolution technique even if such a high resolution is not achieved

Electron scattering

triple-differential cross section for $(e,e'\pi)$

$$\frac{d^3\sigma^{ed}}{dE_{e'}\,d\Omega_{e'}\,d\Omega_\pi}=\Gamma_\gamma\left\{\frac{d\sigma_{\mathrm{T}}^{\gamma d}}{d\Omega_\pi}+\epsilon_{\mathrm{L}}\frac{d\sigma_{\mathrm{L}}^{\gamma d}}{d\Omega_\pi}+\sqrt{2\epsilon_{\mathrm{L}}\left(1+\epsilon_{\mathrm{T}}\right)}\frac{d\sigma_{\mathrm{LT}}^{\gamma d}}{d\Omega_\pi}\cos\phi_\pi+\epsilon_{\mathrm{T}}\frac{d\sigma_{\mathrm{TT}}^{\gamma d}}{d\Omega_\pi}\cos 2\phi_\pi\right\}$$

for a unpolarized electron beam

$$\epsilon_{\mathrm{T}}=\left(1+\frac{2\left|\vec{q}\right|^2}{Q^2}\tan^2\frac{\theta_{e'}}{2}\right)^{-1}\quad\text{and}\quad\epsilon_{\mathrm{L}}=\frac{Q^2}{\omega^2}\epsilon_{\mathrm{T}}$$

$\epsilon_{\mathrm{T}}=\epsilon$

$$\Gamma_\gamma=\frac{\alpha}{2\pi^2 Q^2}\frac{E_\gamma}{1-\epsilon_{\mathrm{T}}}\frac{E_{e'}}{E_e}\quad\text{and}\quad E_\gamma=\omega-\frac{Q^2}{2m_d}$$

to give the same W

triple-differential cross section for $(e,e'\pi)$

$$\frac{d^3\sigma^{ed}}{dE_{e'}\,d\Omega_{e'}\,d\Omega_\pi}=\Gamma_\gamma\left\{\frac{d\sigma_{\mathrm{T}}^{\gamma d}}{d\Omega_\pi}+\epsilon_{\mathrm{L}}\frac{d\sigma_{\mathrm{L}}^{\gamma d}}{d\Omega_\pi}+\sqrt{2\epsilon_{\mathrm{L}}\left(1+\epsilon_{\mathrm{T}}\right)}\frac{d\sigma_{\mathrm{LT}}^{\gamma d}}{d\Omega_\pi}\cos\phi_\pi+\epsilon_{\mathrm{T}}\frac{d\sigma_{\mathrm{TT}}^{\gamma d}}{d\Omega_\pi}\cos 2\phi_\pi\right\}$$

$$\frac{d\sigma_{\mathrm{LT}}^{\gamma d}}{d\Omega_\pi}\propto\sin\theta_\pi \quad \text{and} \quad \frac{d\sigma_{\mathrm{TT}}^{\gamma d}}{d\Omega_\pi}\propto\sin^2\theta_\pi$$

$$\frac{d^3\sigma^{ed}}{dE_{e'}\,d\Omega_{e'}\,d\Omega_\pi}=\Gamma_\gamma\left\{\frac{d\sigma_{\mathrm{T}}^{\gamma d}}{d\Omega_\pi}+\epsilon_{\mathrm{L}}\frac{d\sigma_{\mathrm{L}}^{\gamma d}}{d\Omega_\pi}\right\}\quad\text{for }\theta_\pi=0^\circ$$

π^+ should be detected in the same direction as the virtual photon

$\cancel{\epsilon_{\mathrm{L}}\frac{d\sigma_{\mathrm{L}}^{\gamma d}}{d\Omega_\pi}\ll\frac{d\sigma_{\mathrm{T}}^{\gamma d}}{d\Omega_\pi}}$ for available placements of spectrometers

T. Ishikawa

Three spectrometers

Spektrometer		A	B	C
Magnetkonfiguration		QSDD	D	QSDD
Maximale Magnetfeldstärke	[T]	1.51	1.50	1.40
Maximaler Impuls	[MeV/c]	735	870	551
Länge der Zentralbahn	[m]	10.75	12.03	8.53
Streuwinkelbereich				
- minimaler Winkel		18°	7°	18°
- maximaler Winkel		160°	62.4°	160°
Impulsakzeptanz	[%]	20	15	25
Raumwinkelakzeptanz	[msr]	28	5.6	28
Winkelakzeptanzen				
- dispersive Ebene	[mrad]	±70	±70	±70
- nichtdispersive Ebene	[mrad]	±100	±20	±100
- Raumwinkel	[msr]	28	5.6	28
Langes-Target-Akzeptanz	[mm]	50	50	50
Impulsauflösungsvermögen		10^{-4}	10^{-4}	10^{-4}
Winkelauflösung am Target	[mrad]	≤ 3	≤ 3	≤ 3
Ortsauflösung am Target	[mm]	$3-5$	1	$3-5$

I. Ewald, Phd thesis, Mainz Univ. (2000).

Electron scattering

e' and π^+ detected with SpekA and SpekB, respectively

incident electron

scattered electron

electron energy

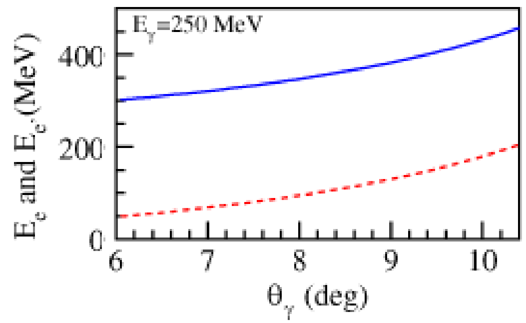

scattering angle of the electron

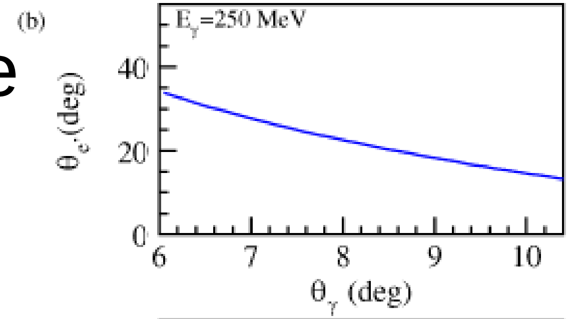

longitudinal polarization

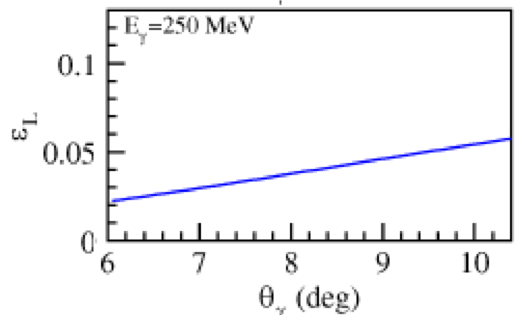

as a function of emission angle of the virtual photon

$$Q^2 = 0.0050\ \mathrm{GeV}^2/c^2$$

difference of $d\sigma_{\mathrm{T}}/d\Omega_\pi$ is $\sim 1\%$ between $Q^2 = 0$, and $0.0050\ \mathrm{GeV}^2/c^2$

LT separation

taking advantage of the linear ϵ_{L} dependence

$$\frac{d^3\sigma^{ed}}{dE_{e'}\,d\Omega_{e'}\,d\Omega_{\pi}} = \Gamma_{\gamma}\left\{\frac{d\sigma_{\mathrm{T}}^{\gamma d}}{d\Omega_{\pi}} + \epsilon_{\mathrm{L}}\frac{d\sigma_{\mathrm{L}}^{\gamma d}}{d\Omega_{\pi}}\right\} \quad \text{for } \theta_{\pi} = 0^{\circ}$$

$\dfrac{d\sigma_{\mathrm{T}}^{\gamma d}}{d\Omega_{\pi}}$ can be obtained from several $\dfrac{d^3\sigma^{ed}}{dE_{e'}\,d\Omega_{e'}\,d\Omega_{\pi}}$s

for different ϵ_{L} and same Q^2

like Rosenbluth separation

E_e (GeV)	$E_{e'}$ (GeV)	$\theta_{e'}$	k_{γ} (GeV)	ω (GeV)	Q^2 (GeV$^2/c^2$)	Γ_{γ} (10^{-3})	ε_{T}	ε_{L}	θ_{γ} (deg)
0.3020	0.0493	33.8	0.2500	0.2527	0.0050	0.0042	0.2836	0.0224	6.0
0.3220	0.0693	27.4	0.2500	0.2527	0.0050	0.0064	0.3795	0.0299	7.0
0.3487	0.0960	22.3	0.2500	0.2527	0.0050	0.0098	0.4832	0.0381	8.0
0.3847	0.1320	18.1	0.2500	0.2527	0.0050	0.0154	0.5899	0.0465	9.0
0.4350	0.1823	14.4	0.2500	0.2527	0.0050	0.0251	0.6937	0.0547	10.0

SpekB covers 2.3°

SpekA covers 11.5°

LT separation

E_e (GeV)	$E_{e'}$ (GeV)	$\theta_{e'}$	k_γ (GeV)	ω (GeV)	Q^2 (GeV$^2/c^2$)	Γ_γ (10^{-3})	ε_T	ε_L	θ_γ (deg)
0.3020	0.0493	33.8	0.2500	0.2527	0.0050	0.0042	0.2836	0.0224	6.0
0.3220	0.0693	27.4	0.2500	0.2527	0.0050	0.0064	0.3795	0.0299	7.0
0.3487	0.0960	22.3	0.2500	0.2527	0.0050	0.0098	0.4832	0.0381	8.0
0.3847	0.1320	18.1	0.2500	0.2527	0.0050	0.0154	0.5899	0.0465	9.0
0.4350	0.1823	14.4	0.2500	0.2527	0.0050	0.0251	0.6937	0.0547	10.0

A candidate for spectrometer setting

- Electron beam: 385 MeV/c
- SpekA: 18°, 132 MeV/c
- SpekB: 9°, 185 MeV/c

Possible background contributions

- Møller scattering
  - out of range
- Coulomb scattering of post-bremsstrahlung electrons
  - out of range
- π^+, e^- accidental coincidence for $\gamma d \to \pi^+ nn$

LT separation

kinematic coverage for

e⁻ beam: 385 MeV/c, SpekA: 18º, 132 MeV/c, SpekB: 9º, 185 MeV/c

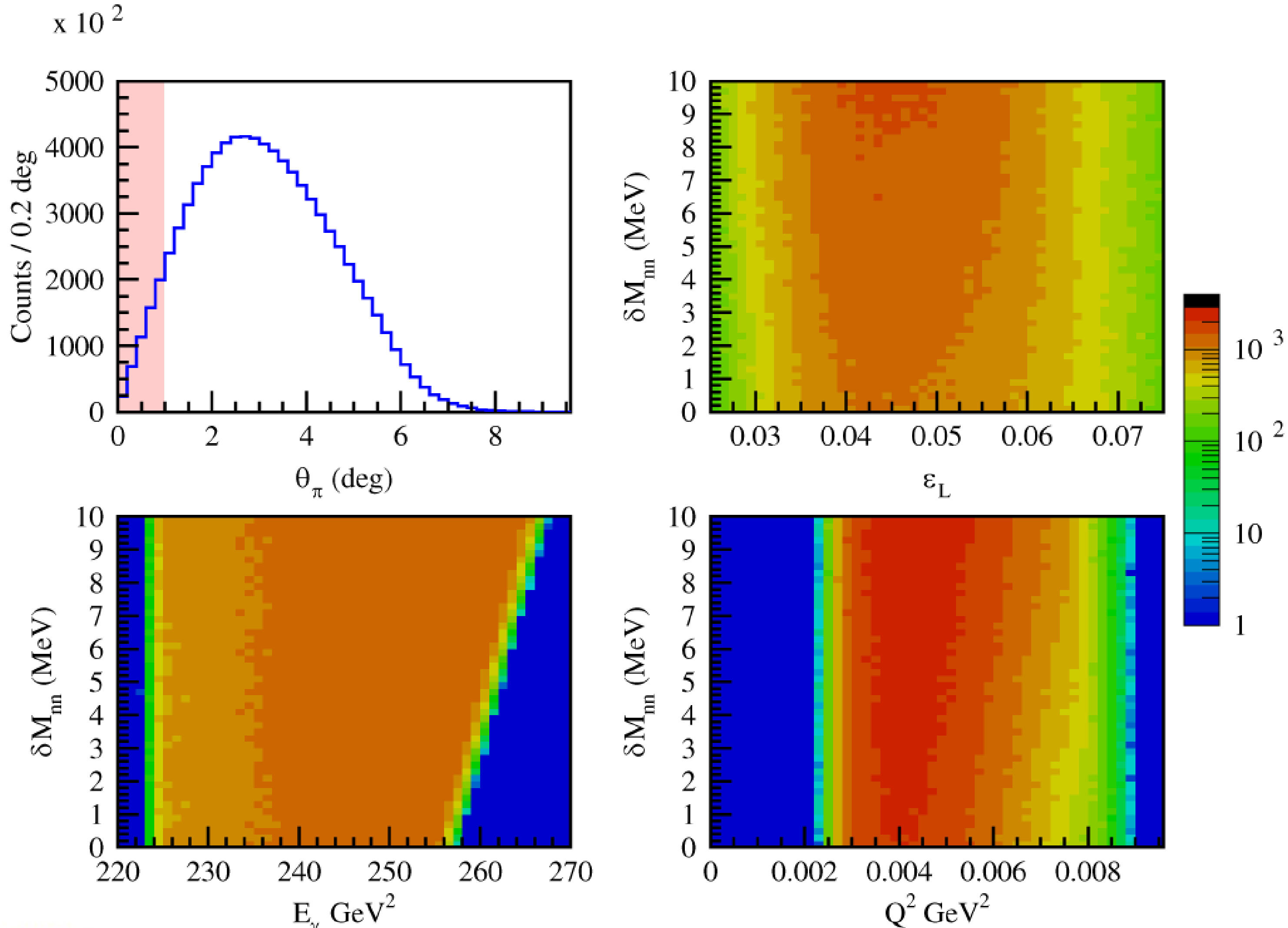

LT separation

E_γ dependence: linear

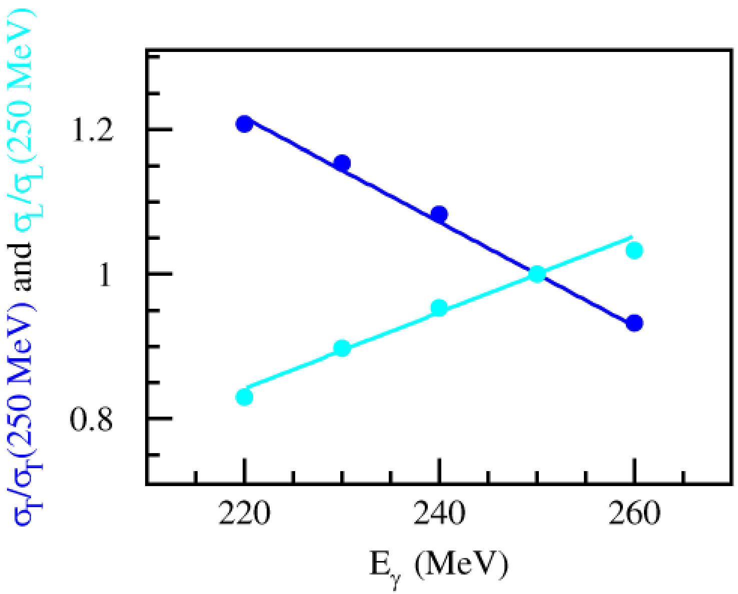

$$\sigma(E_\gamma)\,/\,\sigma(250\ \mathrm{MeV}) = 1 + \alpha E_\gamma$$

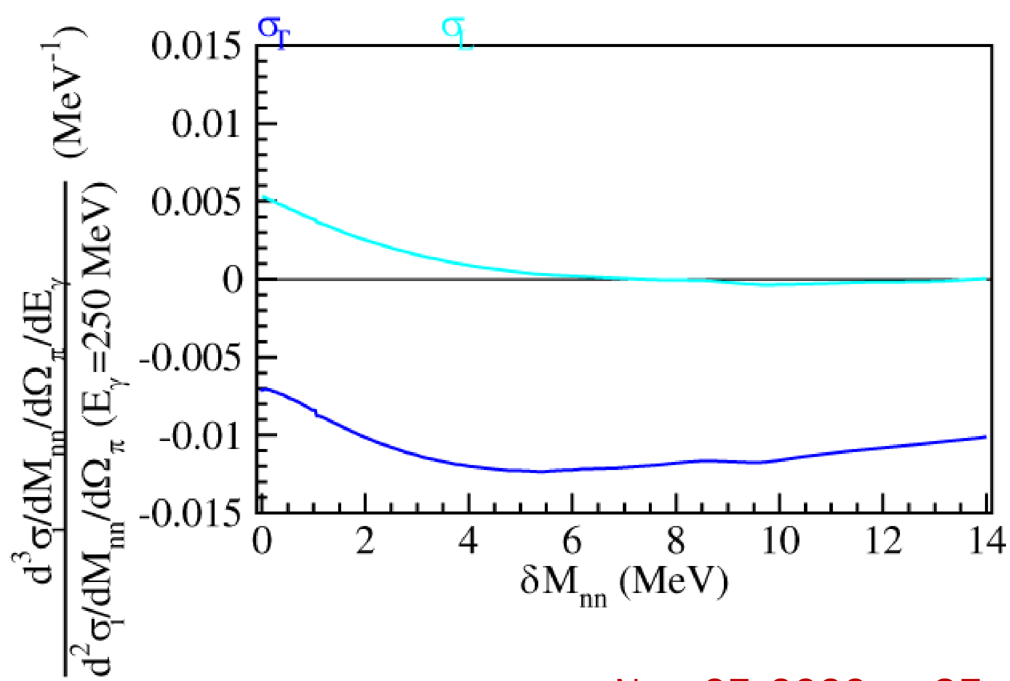

Q^2 dependence: linear

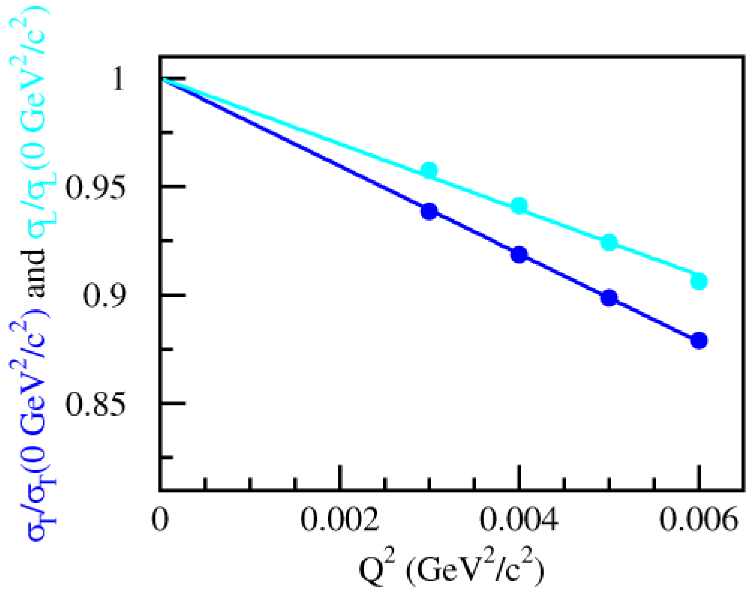

$$\sigma(Q^2)/\sigma(0\ \mathrm{GeV}/c\wedge 2) = 1 + \alpha Q^2$$

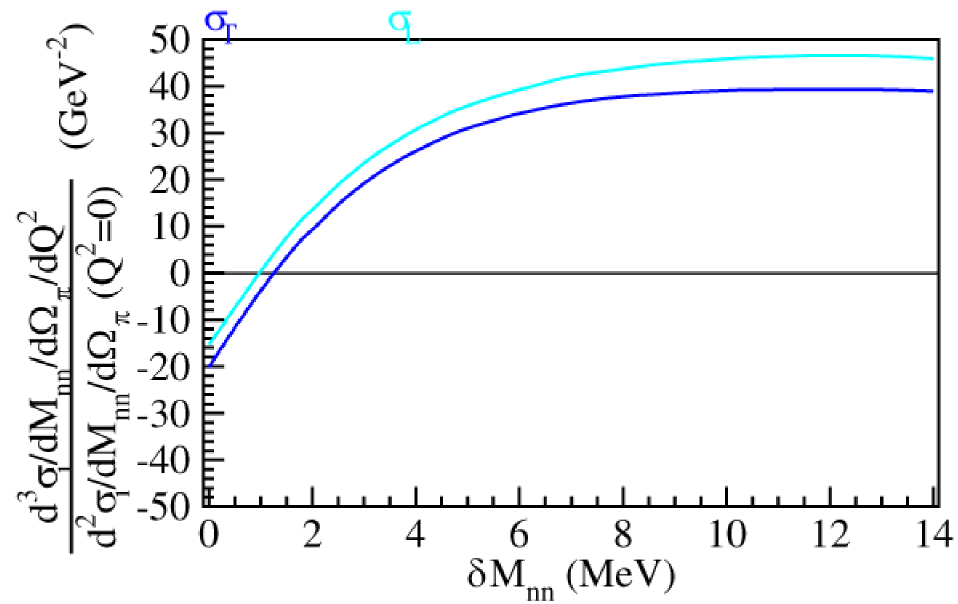

LT separation

θ_π dependence:

quadratic in T and L **(almost linear for θ_π** <0.5°)

linear in LT and TT

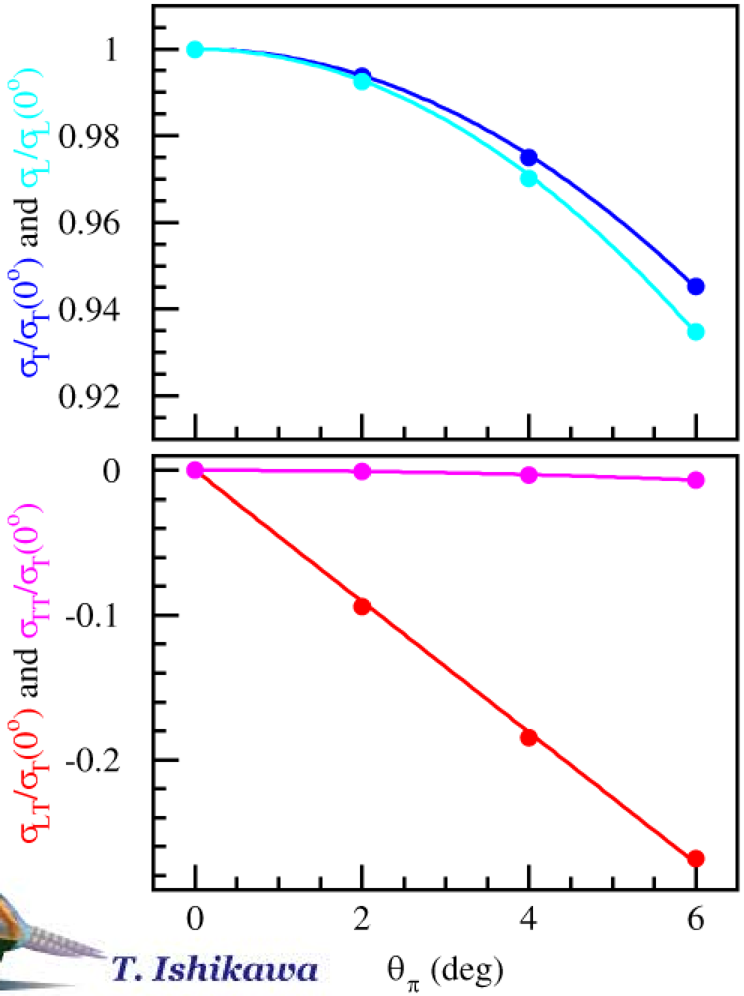

$$\sigma(\theta_\pi)/\sigma(0^\circ) = 1 + \alpha\theta_\pi^{\,2}/2 \text{ for T, and L}$$

$$\sigma(\theta_\pi)/\sigma_T(0^\circ) = \alpha\theta_\pi \text{ for LT, and TT}$$

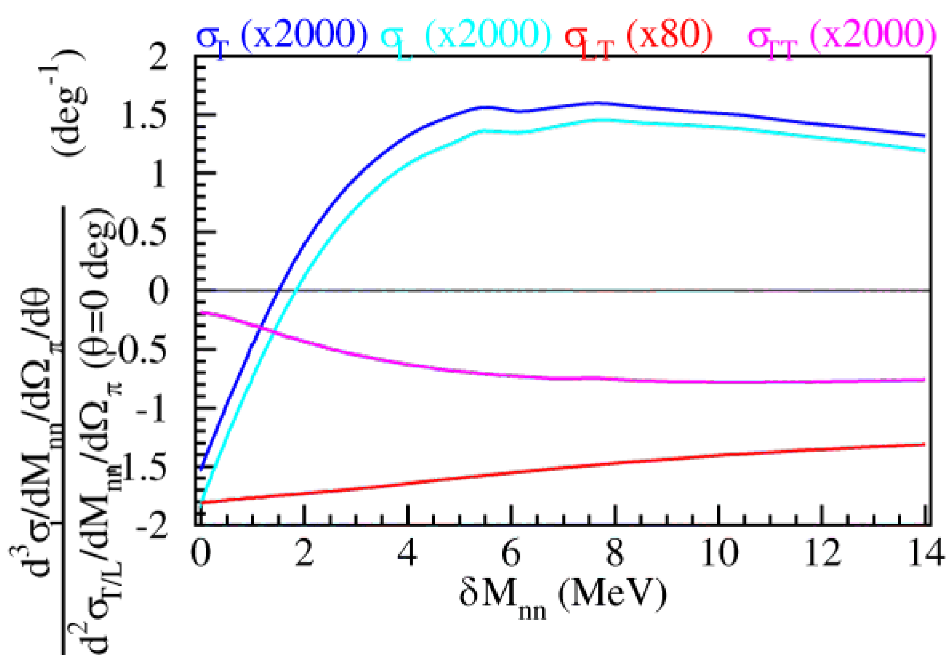

LT separation

a wide kinematic coverage enables us to get the data at E_γ=250 MeV, Q^2=0 GeV^2/c^2, θ_π=0^o

the following conditions

- ~ **μ**b/sr/MeV at δM_{nn}=2 MeV
- $\sigma_L \sim 4\sigma_T$ and ε_L:0.03~0.07 requires x10 to get the limit at 0
- 0.04 MeV δM_{nn} bin
- 2.0 deg = 1.2 msr **tolerance for π^+**
- 50 mm thick liquid D_2 = 2.6 b^{-1}
- 40 **μA** for a beam current
- Γ_γ~15 x 10^{-6} MeV^{-1}sr^{-1} x 28 msr **for γ^*** flux

shows a 20-day measurement to achieve 2% precision at δM_{nn}=2 MeV giving δa_{nn}=0.2 fm (5-day: δa_{nn}=0.4 fm)

Summary

Summary

Meson photoproduction

hadron-hadron scattering parameters can be determined using FSI
it is useful when a direct scattering experiment is difficult to be realized

Our activities

ωN **from** $\gamma p \rightarrow \omega p$

T. Ishikawa et al., PRC101, 052201 (R) (2020).

ηN **from** $\gamma d \rightarrow \eta pn$

S.X. Nakamura, H. Kamano, T. Ishikawa, PRC95, 042201 (R) (2017);
T. Ishikawa et al., Acta Phys. Polon. B51, 27 (2020).

ηN **from** $\gamma d \rightarrow \pi^0 \eta d$

T. Ishikawa et al., in preparation

nn **from** $\gamma^* d \rightarrow \pi^+ nn$

S.X. Nakamura, T. Ishikawa, T. Sato, arXiv: 2003.02497 (2020).

Summary ~ nn

photoproduction

possibility of extracting a_{nn} and r_{nn} is discussed

$\gamma d \to \pi^+ nn$ at $\theta_\pi = 0^\circ$ and E_γ=250 MeV is suitable

$R_{\rm th}$, $d^2\sigma/dM_{nn}/d\Omega_\pi$ normalized by $\gamma p \to \pi^+ n$ cross sections and the deuteron wave function, with 2% error, resolved into ΔM_{nn}=0.04 MeV can determine a_{nn} and r_{nn} with the uncertainties of ±0.21 fm and ±0.06 fm, respectively

electroproduction

Such high M_{nn} resolution can be achieved with an electron scattering experiment at Mainz A1 facility

$d(e,e'\pi^+)$ cross sections at different ϵ_L values but the same $Q^2 \simeq 0$ gives $d^2\sigma_T/dM_{nn}/d\Omega_\pi$ s corresponding to the photoproduction cross sections

S.X. Nakamura, T. Ishikawa, T. Sato, **arXiv:2003.02497**

Backup Slides~nn

$\gamma d \to \pi^+ nn$ cross sections at 200 MeV

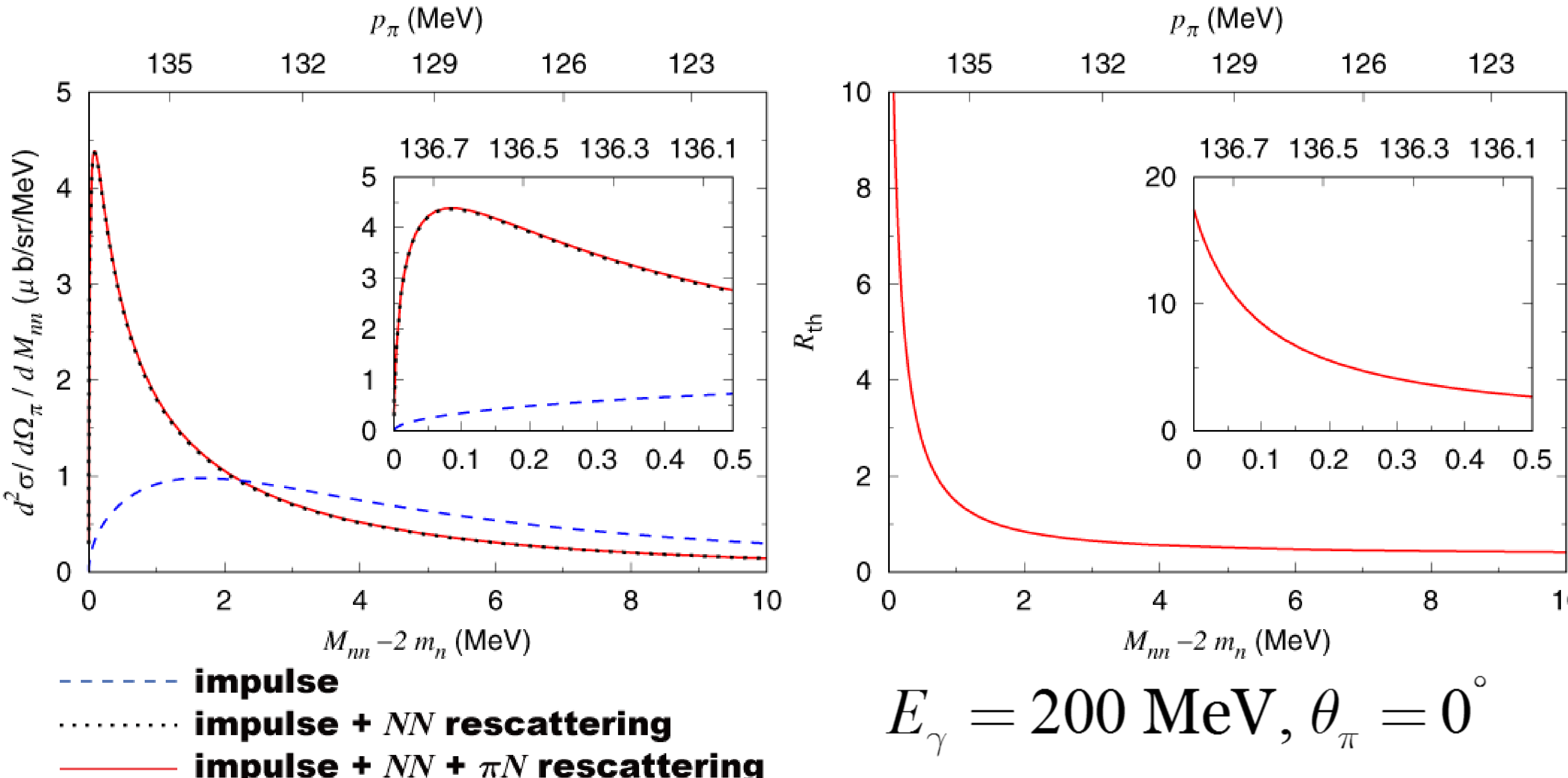

$$E_\gamma = 200 \text{ MeV}, \theta_\pi = 0^\circ$$

$\gamma N \to \pi N$ production amplitude below the πN threshold contributes ~2% to the cross section

negligibly small for $E_\gamma \geqq$ **250 MeV**

Results

$\gamma d \to \pi^+ nn$ cross sections at 300 MeV

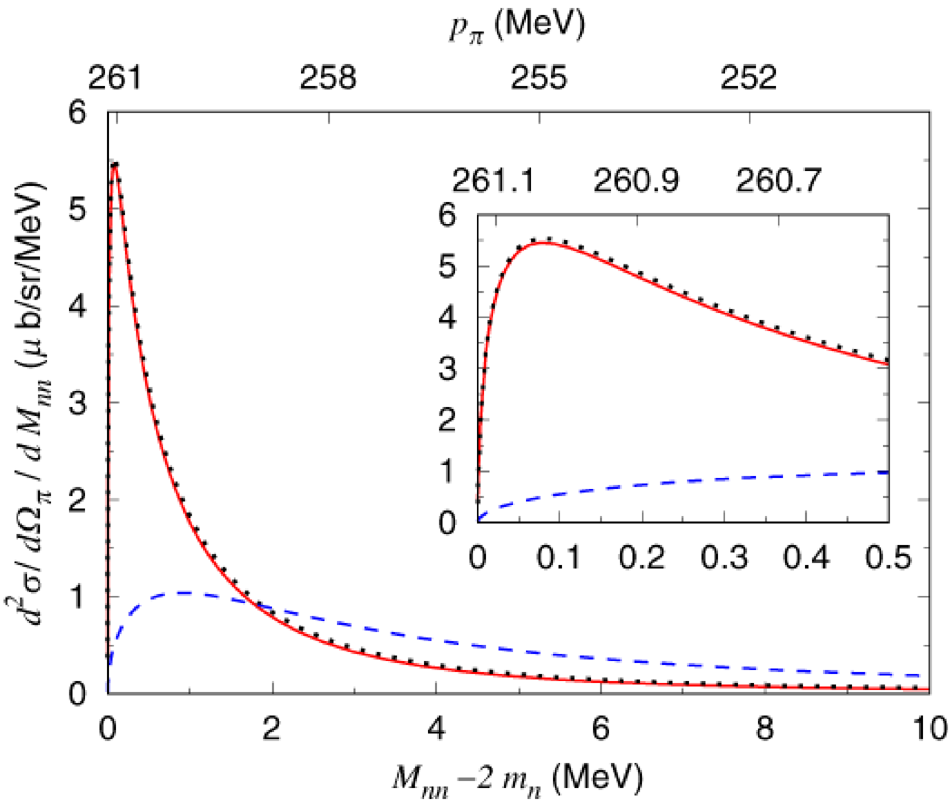

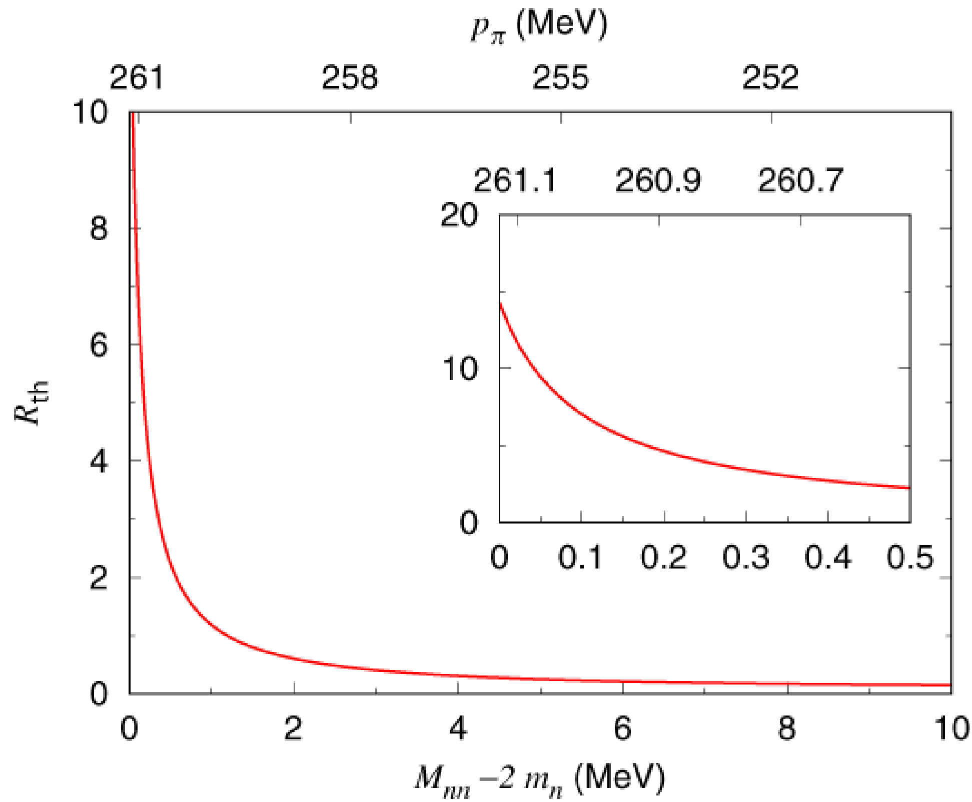

impulse
impulse + NN rescattering
impulse + NN + πN rescattering

$$E_\gamma = 300\ \mathrm{MeV},\ \theta_\pi = 0^\circ$$

$\pi N \to \pi N$ rescattering effects: discernible at this energy

the incident energy of 250 MeV is the best

Results

$\gamma d \to \pi^+ nn$ cross sections for different pion-emission angles

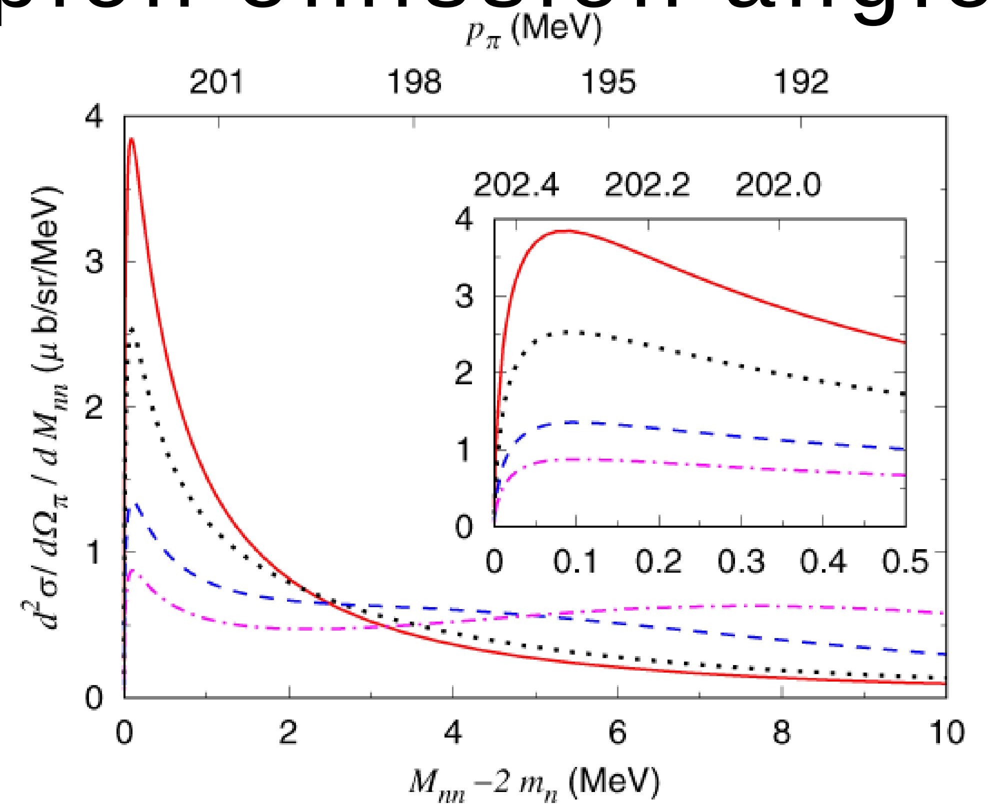

small M_{nn} region, the most sensitive to the nn scattering length, the cross section is significantly larger for smaller emission angle

the pion emission angle of 0 deg is the best

250 MeV & 0 deg is the optimal setting

Theoretical uncertainties

different *NN* potentials

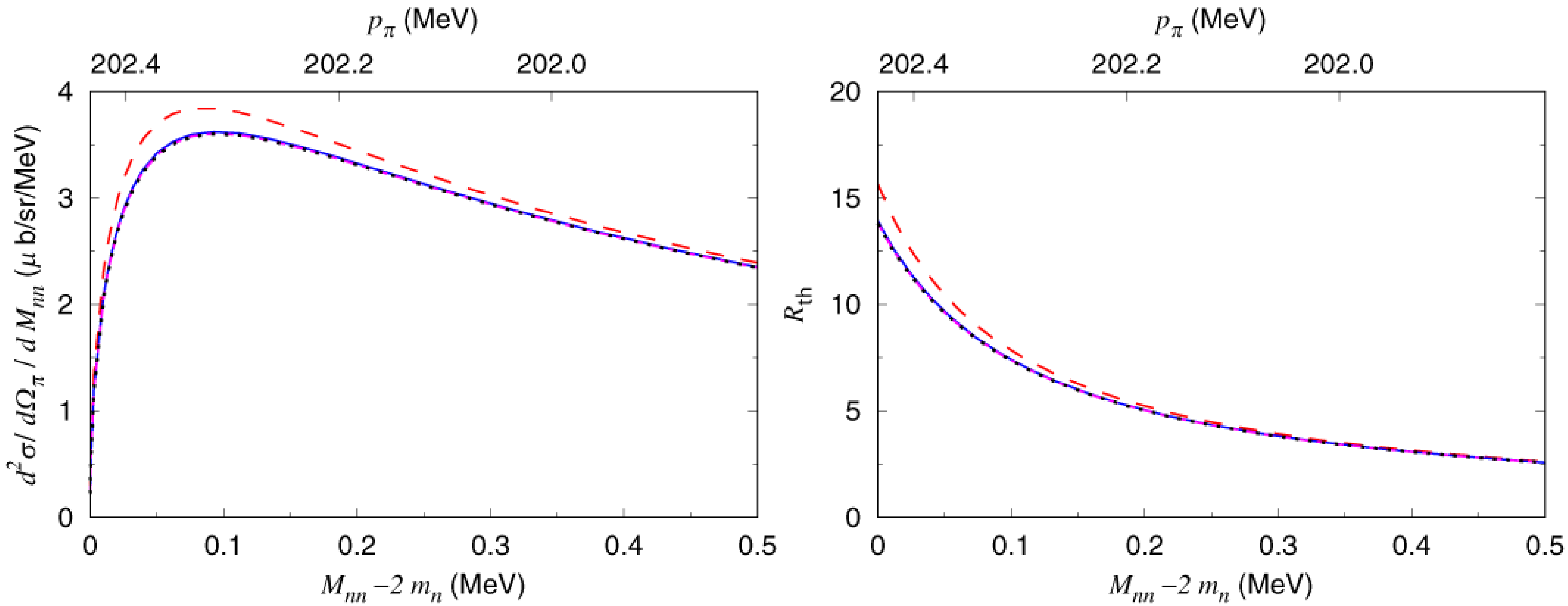

CD-Bonn $a_{nn} = -18.9\ \mathrm{fm}$

Reid93
Nijmegen I
Nijmegen II

$\left.\right\}\ a_{nn} = -17.3\ \mathrm{fm}$

different off-shell behaviors

not negligible for $\pi^- d \to nn\gamma$ analysis

Theoretical uncertainties

different *NN* potentials

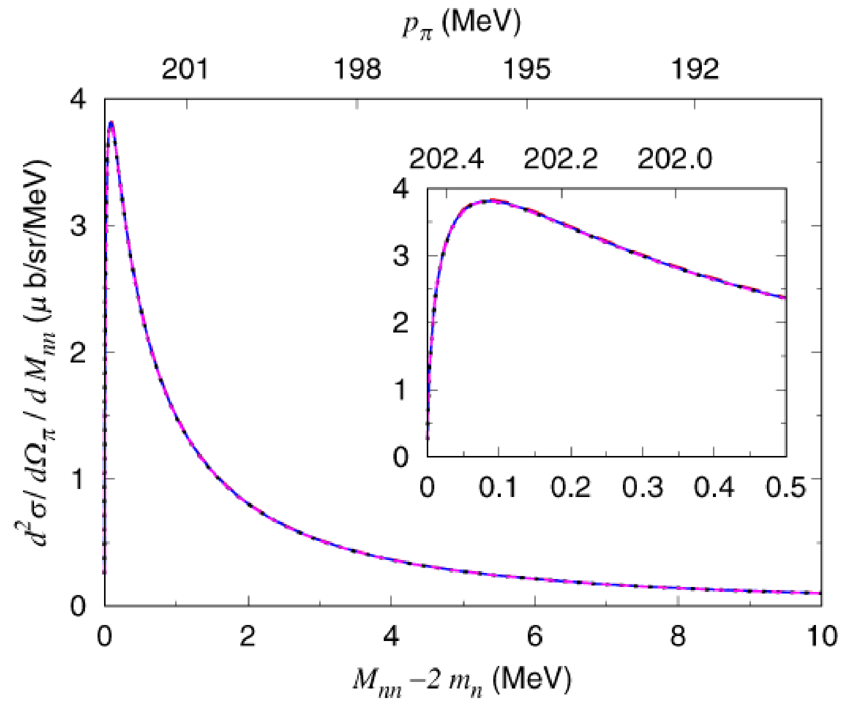

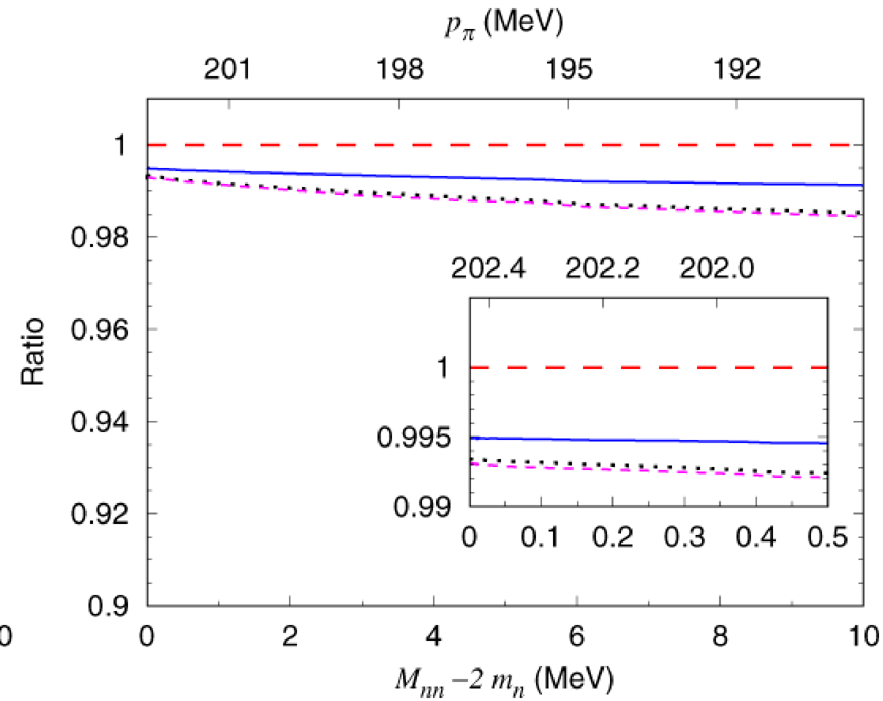

CD-Bonn $a_{nn} = -18.9$ fm

Reid93
Nijmegen I
Nijmegen II
$\Big\}$ $a_{nn} = -17.3$ fm

$$t_{NN}(M_{N_1N_2}) \Rightarrow t^{\mathrm{ERE}}_{NN,NN}(M_{N_1N_2}) \times \left[\frac{t_{NN}(M_{N_1N_2})}{t^{\text{on-shell}}_{NN,NN}(M_{N_1N_2})} \right]$$

Theoretical uncertainties

different $\gamma p \to \pi^+ n$ amplitudes

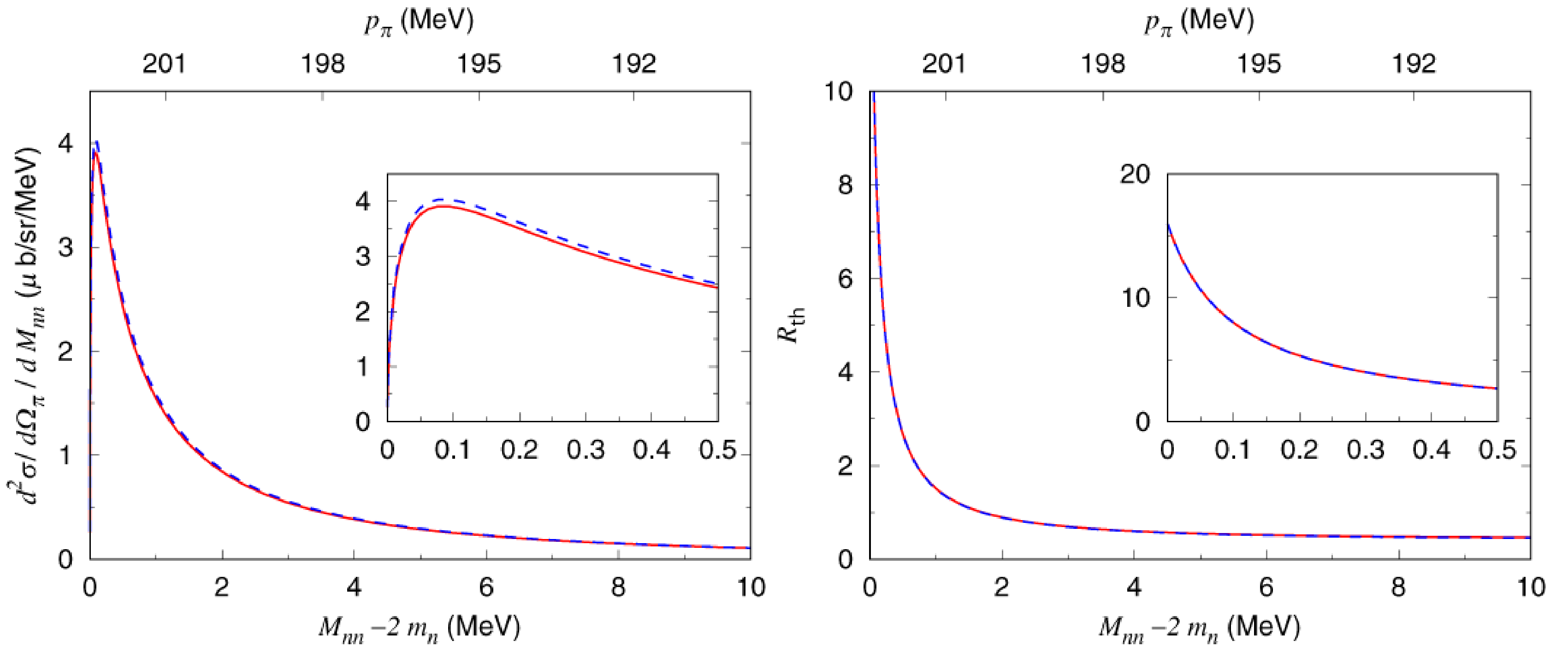

DCC and Chew-Mandelstam (CM12) parametrization
(on-shell amplitude is used for the off-shell one here)
uncertainty from different on-shell $\gamma p \to \pi^+ n$ amplitude can be removed by using R_{th}

Theoretical uncertainties

off-shell effects from $\gamma p \to \pi^+ n$

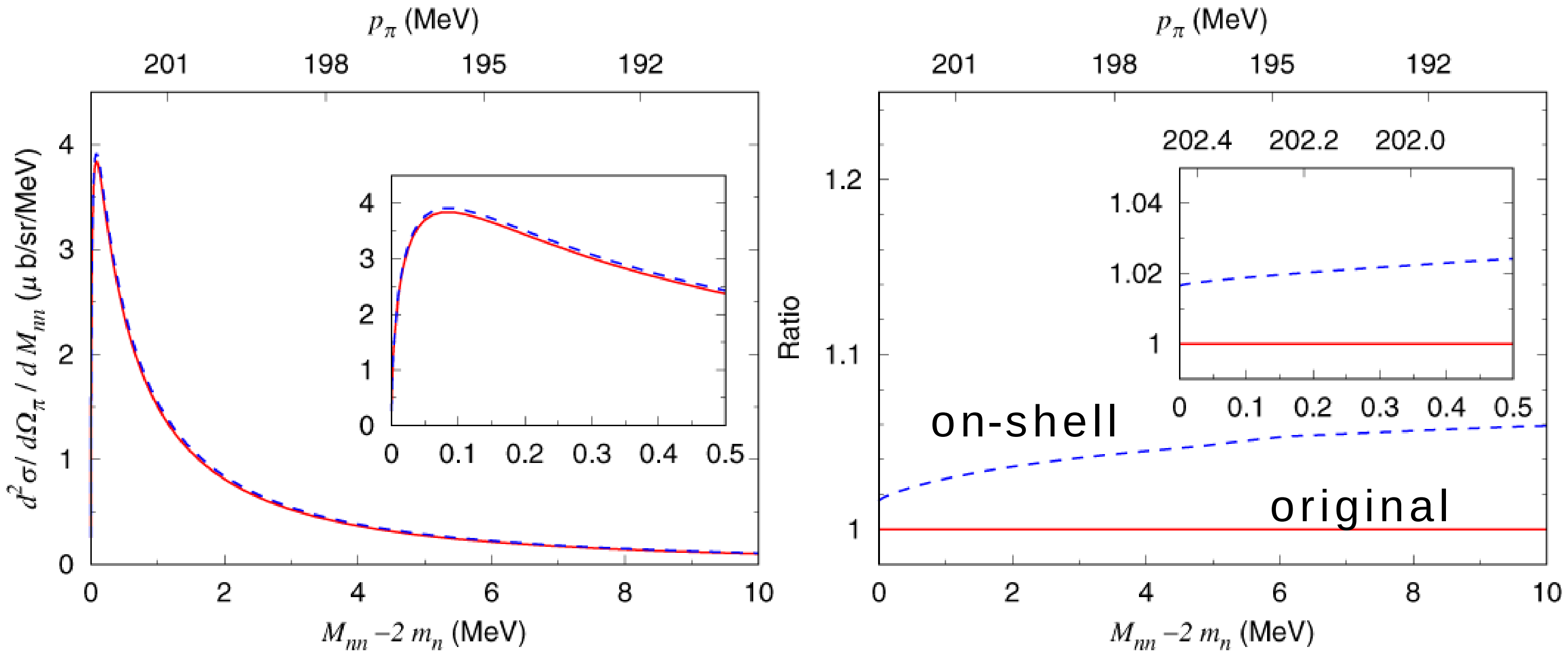

off-shell $\gamma p \to \pi^+ n$ amplitude is replaced by on-shell one

meson exchange current

higher order effects

relative deviation: $0.002(M_{nn} - 2m_n)/\mathrm{MeV}$

Monte Carlo simulation for estimating a_{nn} and r_{nn} uncertainties

quadratic sum of theoretical uncertainties

1) $\mathring{R}_{\rm exp}(\mathring{a}_{nn}, \mathring{r}_{nn}; M_{nn}) \equiv R_{\rm th}(\mathring{a}_{nn}, \mathring{r}_{nn}; M_{nn}) + g\boxed{\Delta R_{\rm th}^{\rm all}(M_{nn})}$

g: random number according to the $N(0,1)$

2) $\mathring{R}_{\rm exp}(\mathring{a}_{nn}, \mathring{r}_{nn}; i)$ for i-th M_{nn} bin

average of $\mathring{R}_{\rm exp}(\mathring{a}_{nn}, \mathring{r}_{nn}; M_{nn})$ over the bin width

3) $R_{\rm exp}(i)$ is generated from $\mathring{R}_{\rm exp}(\mathring{a}_{nn}, \mathring{r}_{nn}; i)$ with a statistical fluctuation corresponding to the given precision

4) a_{nn} and r_{nn} are simultaneously searched for so that $R_{\rm exp}(a_{nn}, r_{nn}; M_{nn})$ reproduces $R_{\rm exp}(i)$

the obtained $a_{nn}(r_{nn})$ distribution provides the $a_{nn}(r_{nn})$ uncertainty

obtained a_{nn} and r_{nn} distribution

centroid: δ_a and δ_r

width: σ_a and σ_r

with theoretical uncertainty

a_{nn} -r_{nn} fit in [0.0,6.0) MeV

a_{nn} fit in [0.0,0.5) MeV / r_{nn} fit in [1.0,6.0) MeV

without theoretical uncertainty

a_{nn} -r_{nn} fit in [0.0,6.0) MeV

a_{nn} fit in [0.0,0.5) MeV / r_{nn} fit in [1.0,6.0) MeV

ΔM_{nn}=0.04 MeV

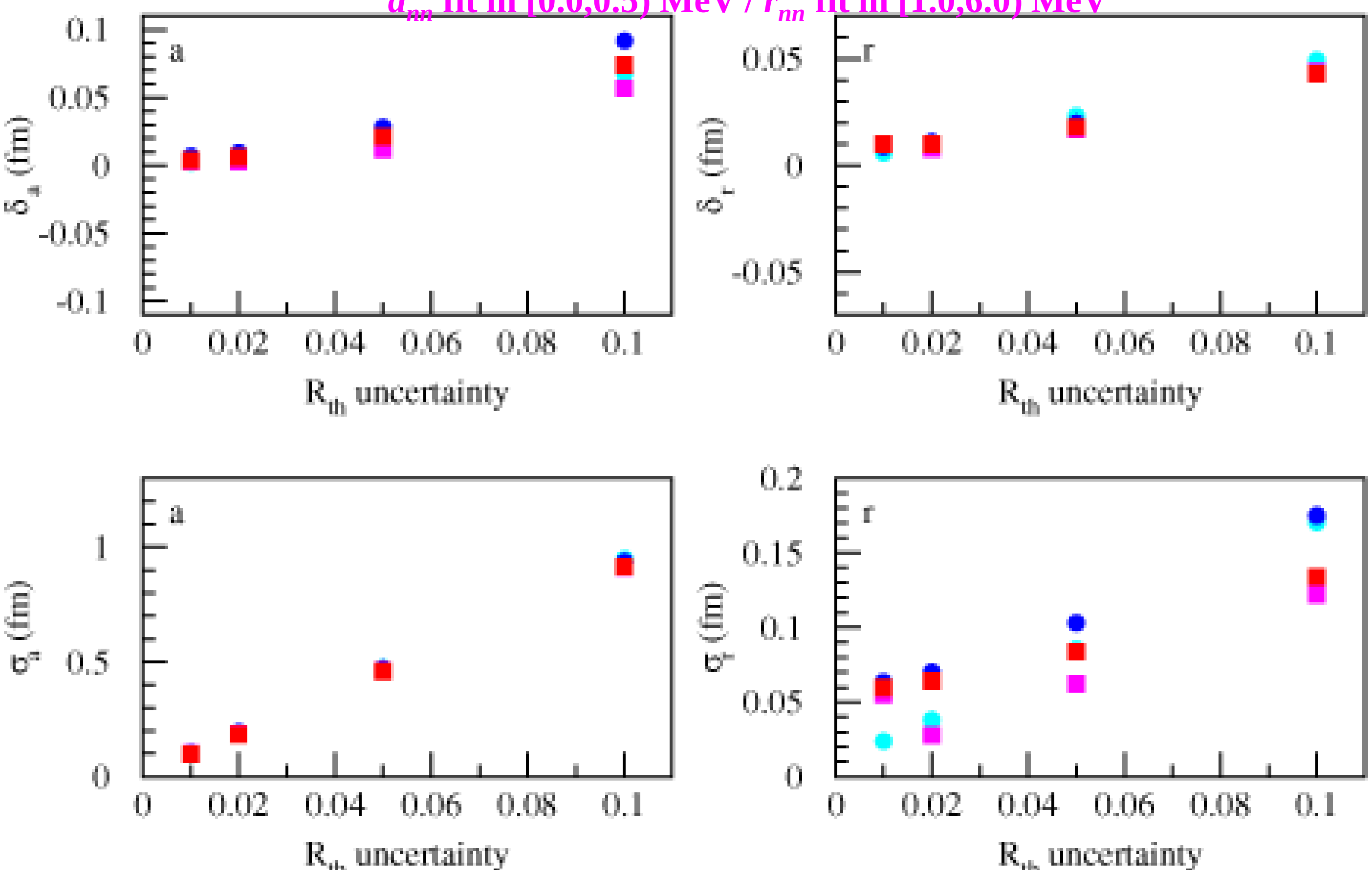

controllable

obtained a_{nn} and r_{nn} distribution

centroid: δ_a and δ_r

width: σ_a and σ_r

with theoretical uncertainty

a_{nn} -r_{nn} fit in [0.0,6.0) MeV

a_{nn} fit in [0.0,0.5) MeV / r_{nn} fit in [1.0,6.0) MeV

without theoretical uncertainty

a_{nn} -r_{nn} fit in [0.0,6.0) MeV

a_{nn} fit in [0.0,0.5) MeV / r_{nn} fit in [1.0,6.0) MeV

$\sigma(R_{th})/R_{th}=0.02$

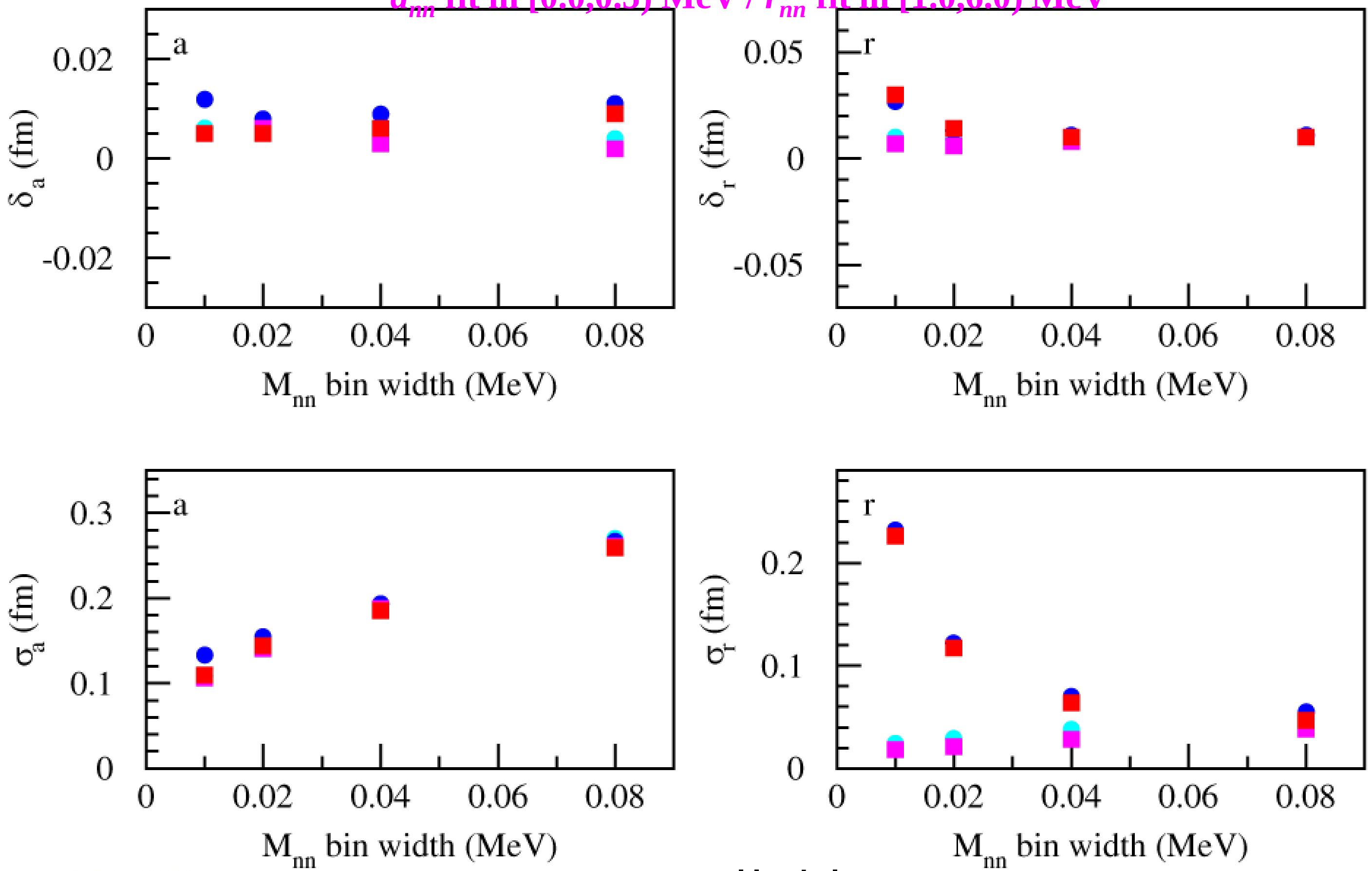

controllable

obtained a_{nn} and r_{nn} distribution

centroid: δ_a and δ_r

width: σ_a and σ_r

with theoretical uncertainty

a_{nn} -r_{nn} fit in [0.0,6.0) MeV

a_{nn} fit in [0.0,0.5) MeV / r_{nn} fit in [1.0,6.0) MeV

without theoretical uncertainty

a_{nn} -r_{nn} fit in [0.0,6.0) MeV

a_{nn} fit in [0.0,0.5) MeV / r_{nn} fit in [1.0,6.0) MeV

ΔM_{nn}=0.04 MeV, $\sigma(R_{\mathrm{th}})/R_{\mathrm{th}}$=0.02

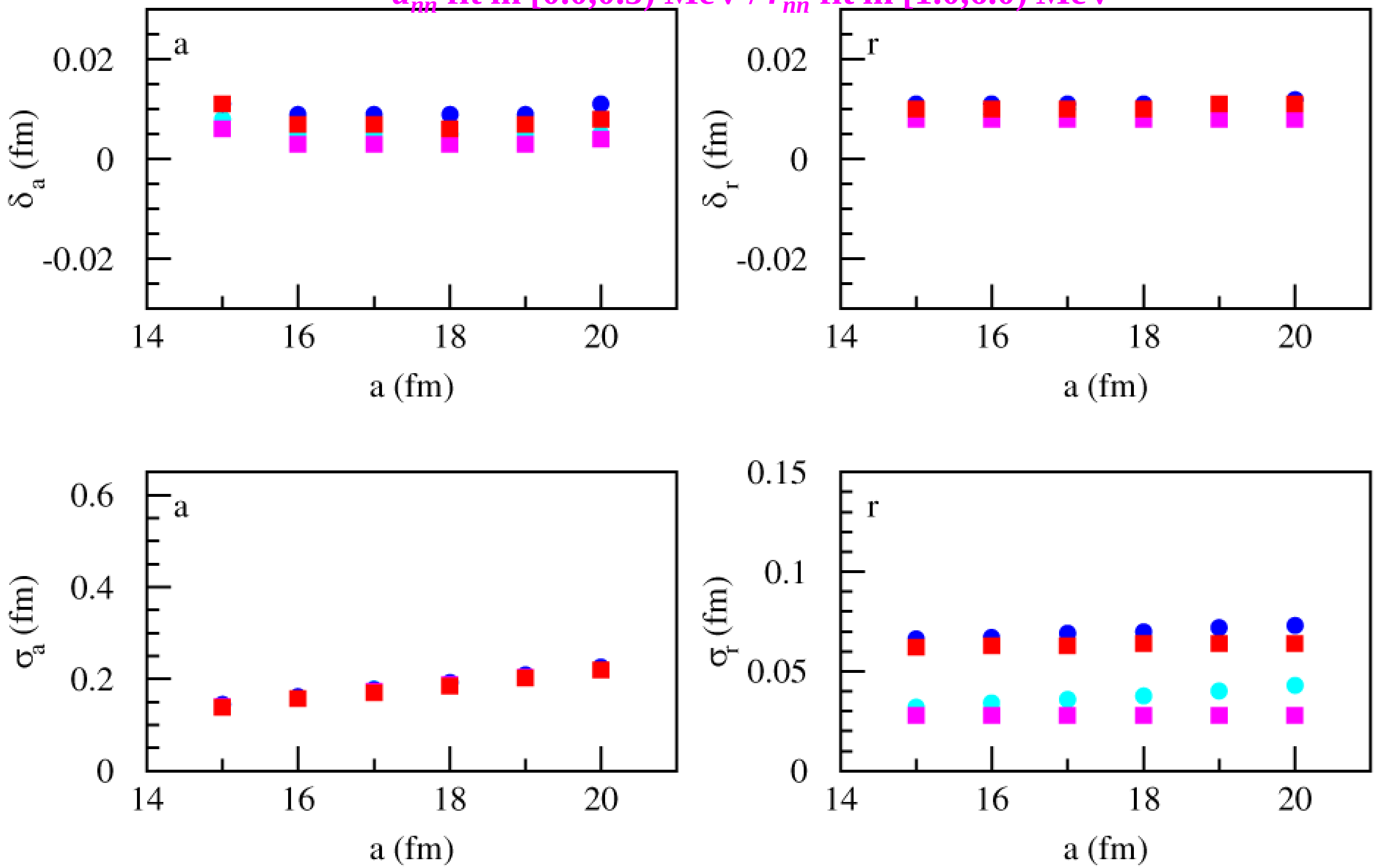

uncontrollable

obtained a_{nn} and r_{nn} distribution

centroid: δ_a and δ_r

width: σ_a and σ_r

with theoretical uncertainty

a_{nn} -r_{nn} fit in [0.0,6.0) MeV

a_{nn} fit in [0.0,0.5) MeV / r_{nn} fit in [1.0,6.0) MeV

without theoretical uncertainty

a_{nn} -r_{nn} fit in [0.0,6.0) MeV

a_{nn} fit in [0.0,0.5) MeV / r_{nn} fit in [1.0,6.0) MeV

ΔM_{nn}=0.04 MeV, $\sigma(R_{th})/R_{th}$=0.02

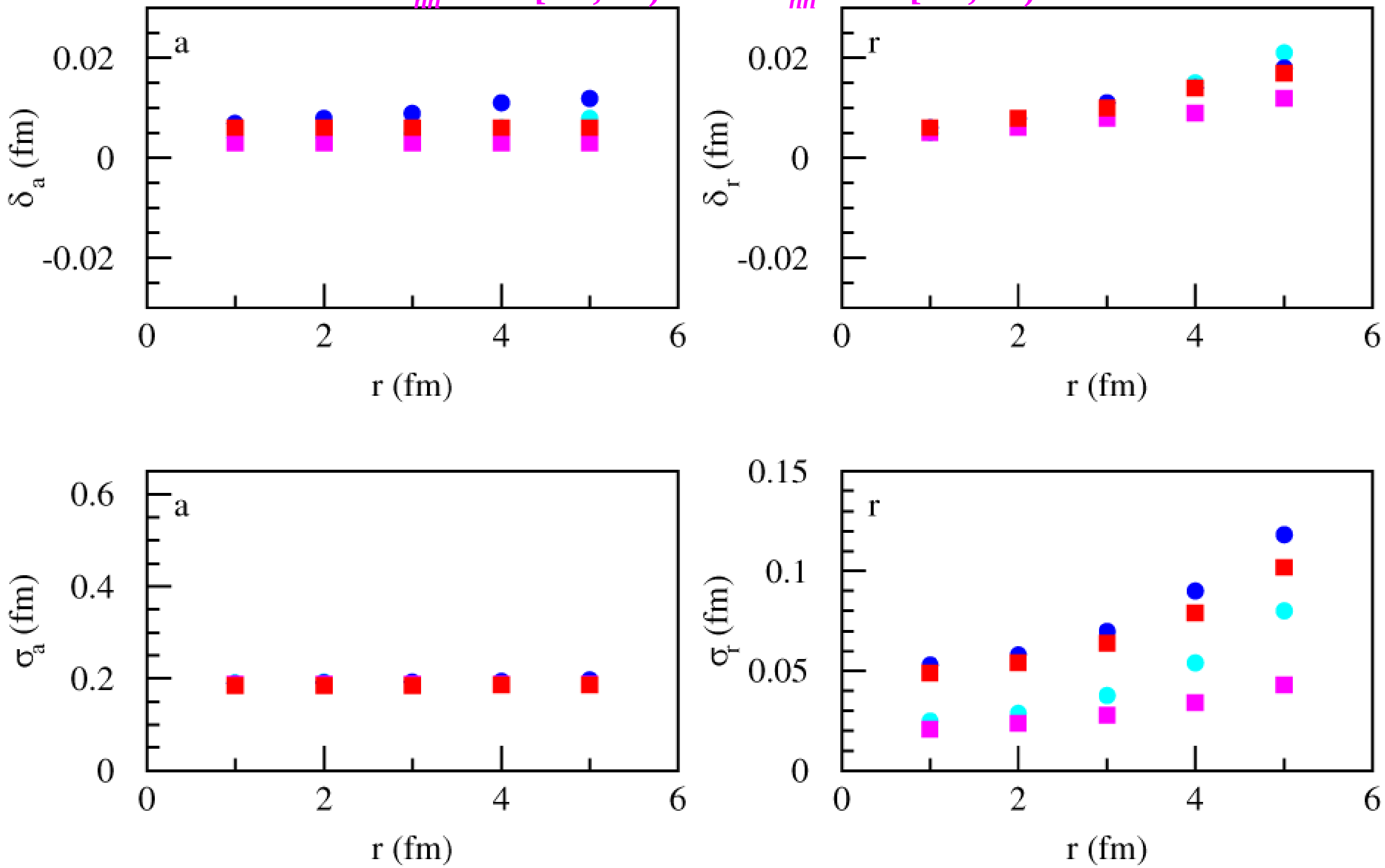

uncontrollable

Theoretical uncertainties

all the uncertainties

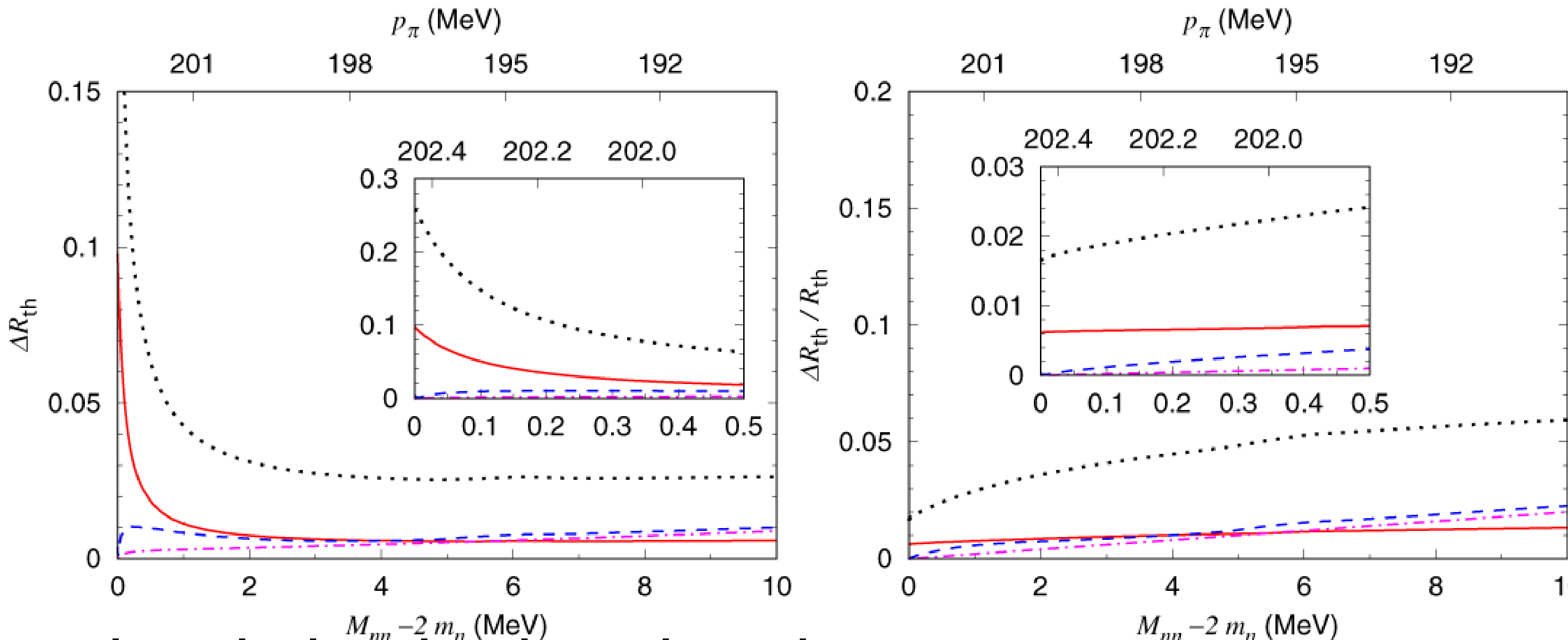

standard deviation is given as an error curve from each source

- different NN potentials
- off-shell effects
- different on-shell amplitudes
- meson exchange current

a_{nn}, r_{nn} and $d^2\sigma / dM_{nn} / d\Omega_\pi$

$\gamma d \to \pi^+ nn$ cross sections for different r_{nn}

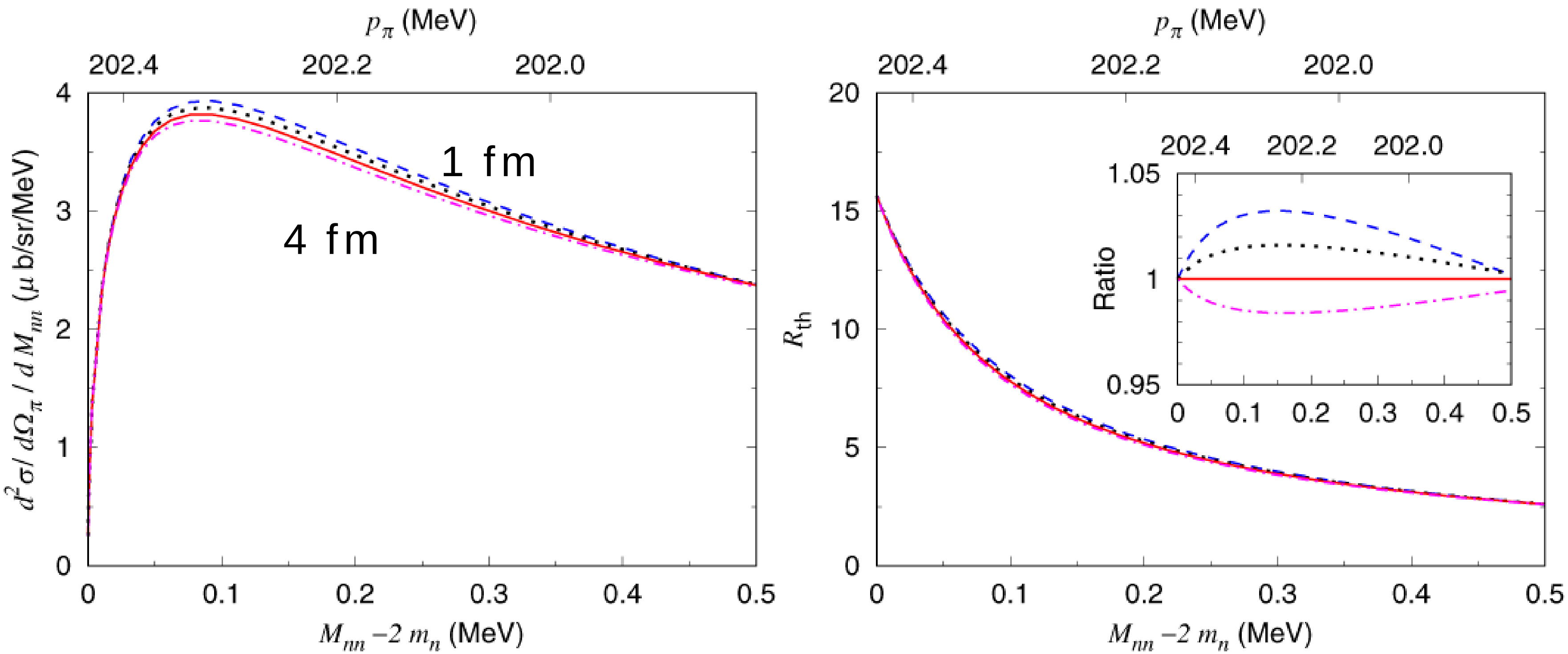

less sensitive to $d^2\sigma/dM_{nn}/d\Omega_\pi$ **below** δM_{nn}=0.3 MeV

a_{nn}=−18.9 fm

r_{nn}=1 fm, 2 fm, 3 fm, 4 fm

Backup slides ~ ωN

ω meson

ω meson plays an important role in describing
short-range repulsive central force, and
strong spin-orbit (LS) force
of the NN interaction:

$$V_\omega \simeq \frac{g_\omega^2}{q^2 + m_\omega^2}\left[1 - 3\frac{\vec{L}\cdot\vec{S}}{2M^2}\right]$$

one of the best established hadrons

nevertheless, scattering between the ω meson and nucleon is not well-known

ωN scattering length

Only one experiment deduce the ωN scattering length assuming the vector dominance model:

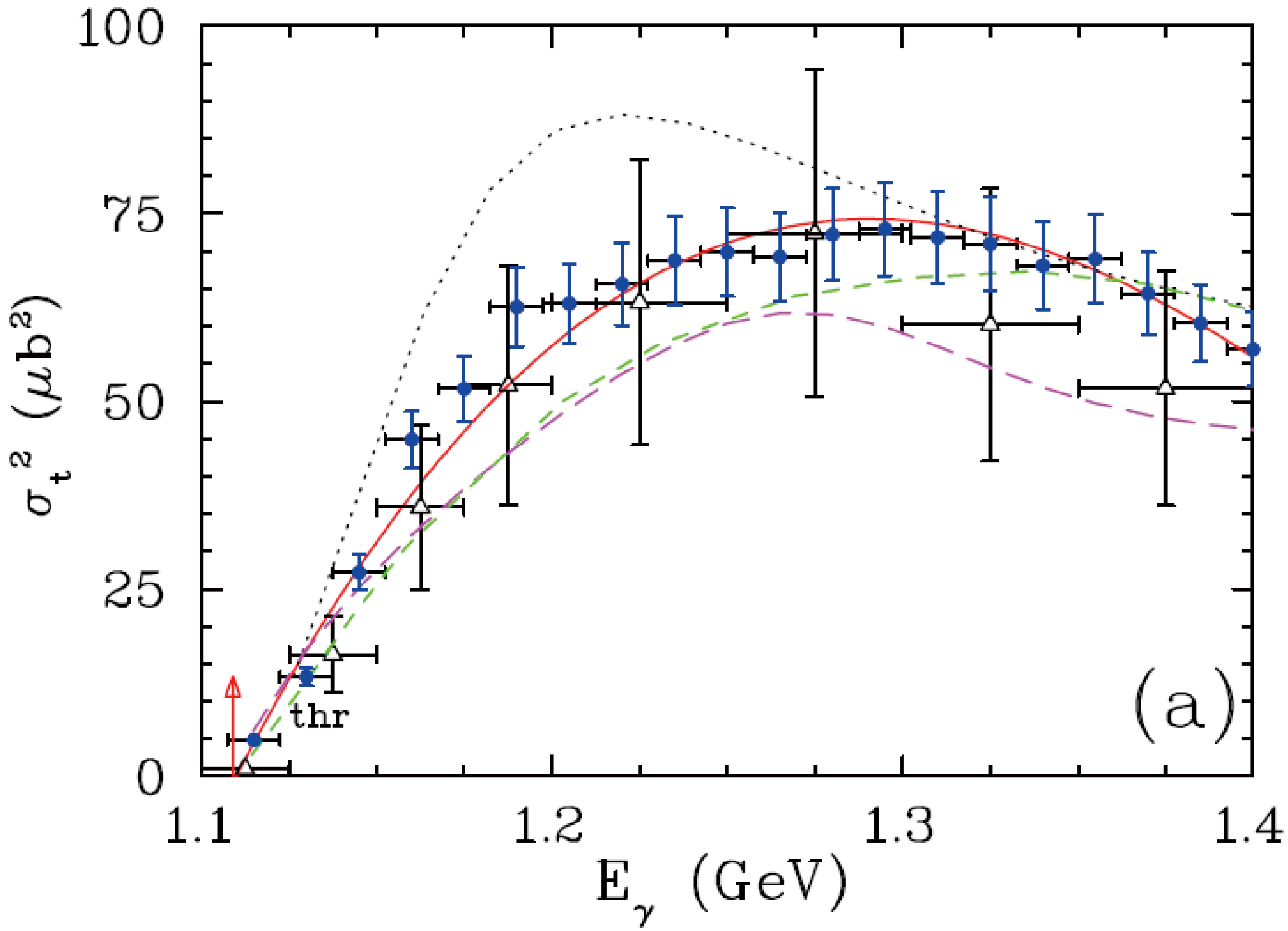

$\gamma p \rightarrow \omega p$ I.I. Strakovsky et al. PRC91, 045207 (2015).

ωN scattering length

Only one experiment deduce the ωN scattering length assuming the vector dominance model:

$$\sigma = \frac{q}{k}\frac{4\alpha\pi^2}{\gamma^2}\left|a_{\omega p}\right|^2 \qquad \left|a_{\omega p}\right| = 0.82 \pm 0.03 \text{ fm}$$

I.I. Strakovsky et al. PRC91, 045207 (2015).

$k:$ incident γ momentum in the CM frame

$q:$ ω momentum in the CM frame

$\alpha:$ fine structure constant

$\gamma = 8.53 \pm 0.14:$ $\gamma\omega$ coupling constant

Only the absolute value is provided, the finite ω width in the final state is not taken into account

ωN scattering length

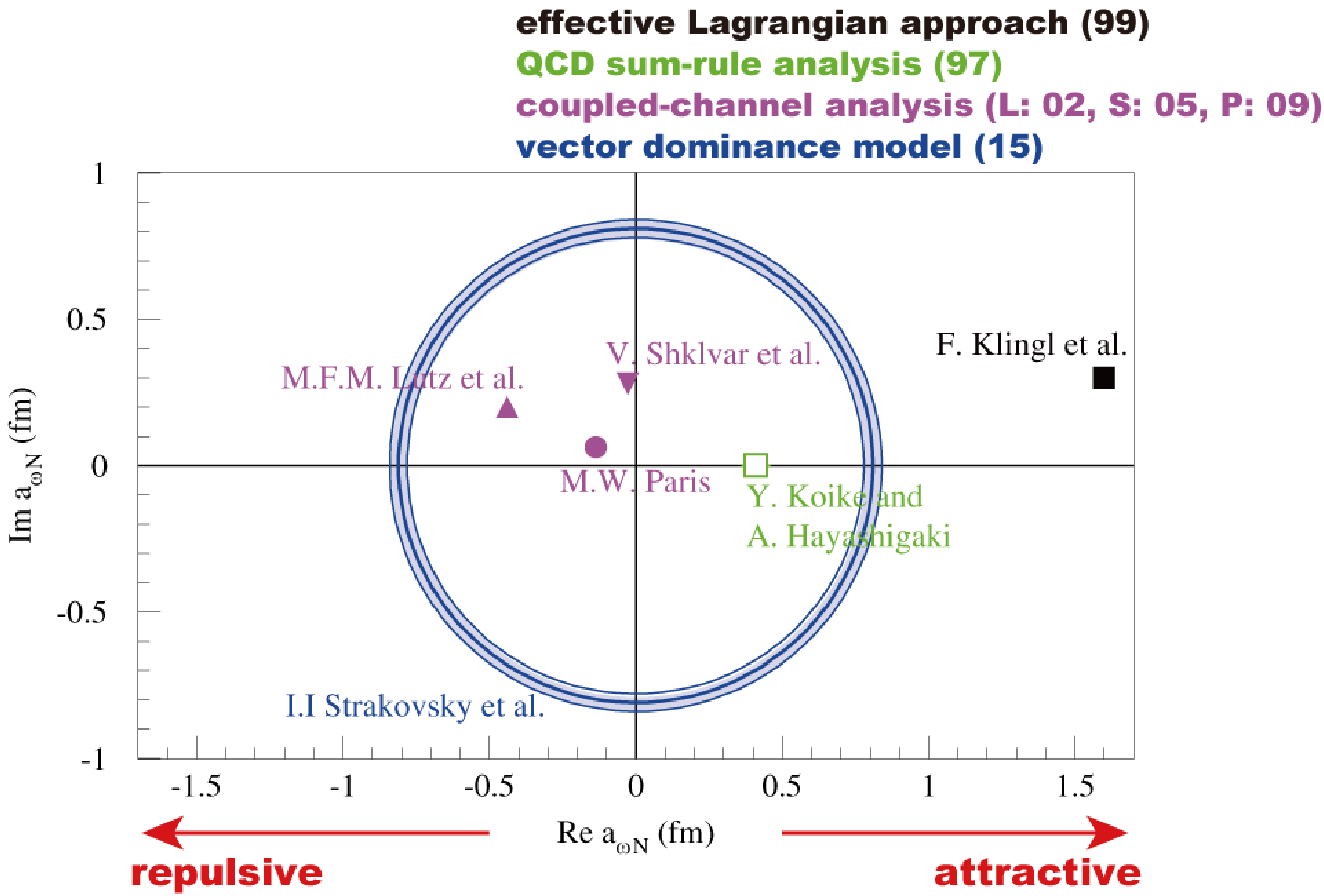

ωA potential

The imaginary part is deduced from the transparency reatio $\gamma A \to \omega X$:

$$T_A = \frac{\sigma_A}{A\sigma_N}$$

V. Metag et al., Prog. Part. Nucl. Phys. 97, 199 (2017).

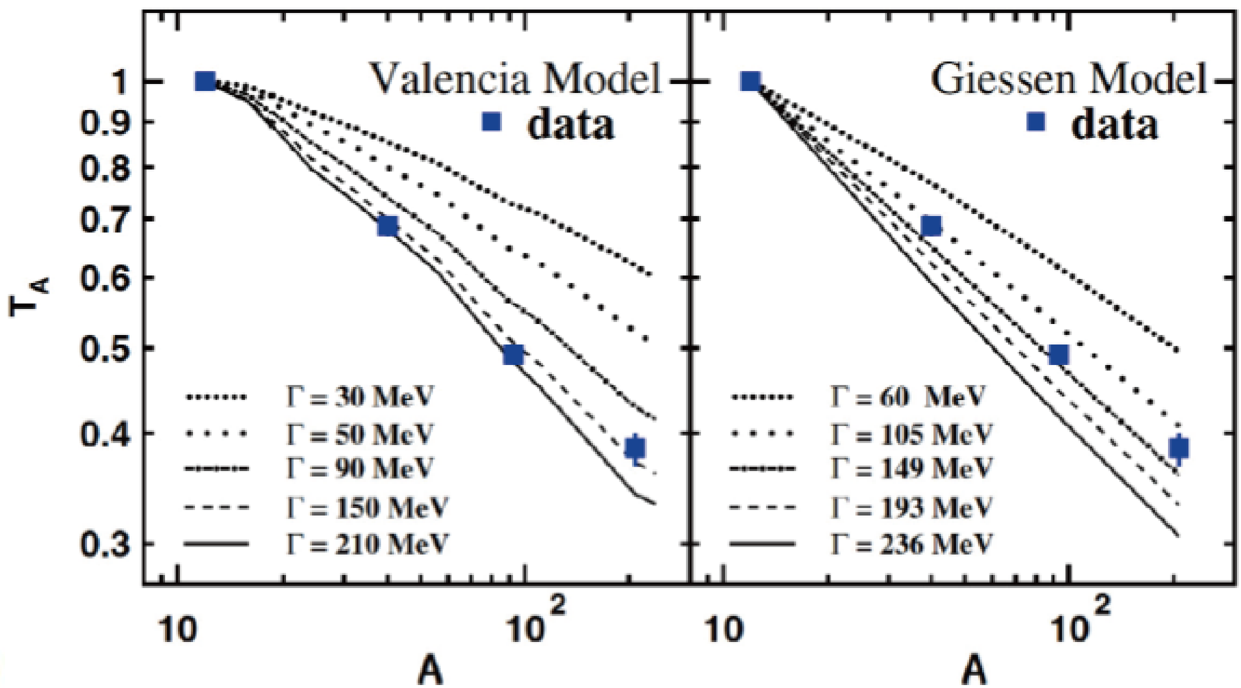

M. Kotulla et al., PRL100, 192302 (2008); ibid 114, 199903 (2015).

Scattering parameters

determine

the low-energy *S*-wave scattering parameters

from

the shape of the excitation function of the total cross section for $\gamma p \rightarrow \omega p$ near the threshold

through

the final-state interaction (ωp rescattering)

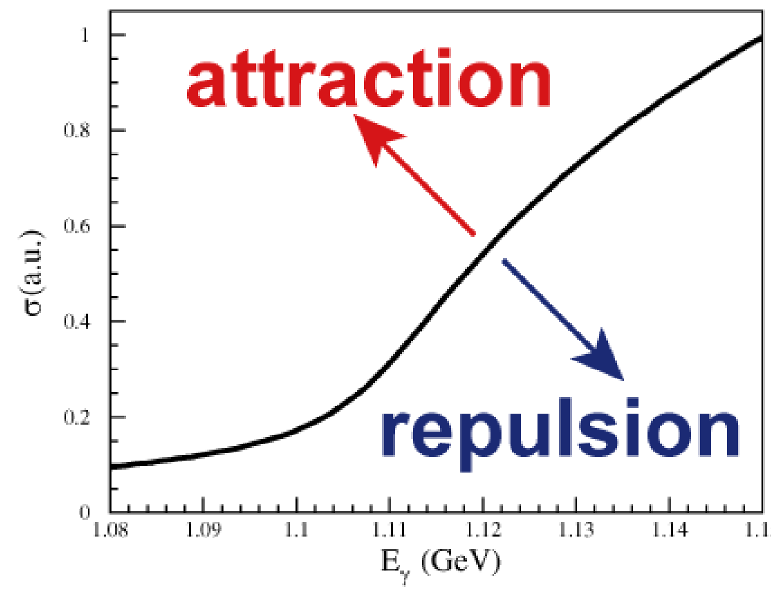

excitation function for $\gamma p \rightarrow \omega p$

without FSI

ω width is taken into account

ωN scattering length

Only one experiment deduce the ωN scattering length assuming the vector dominance model:

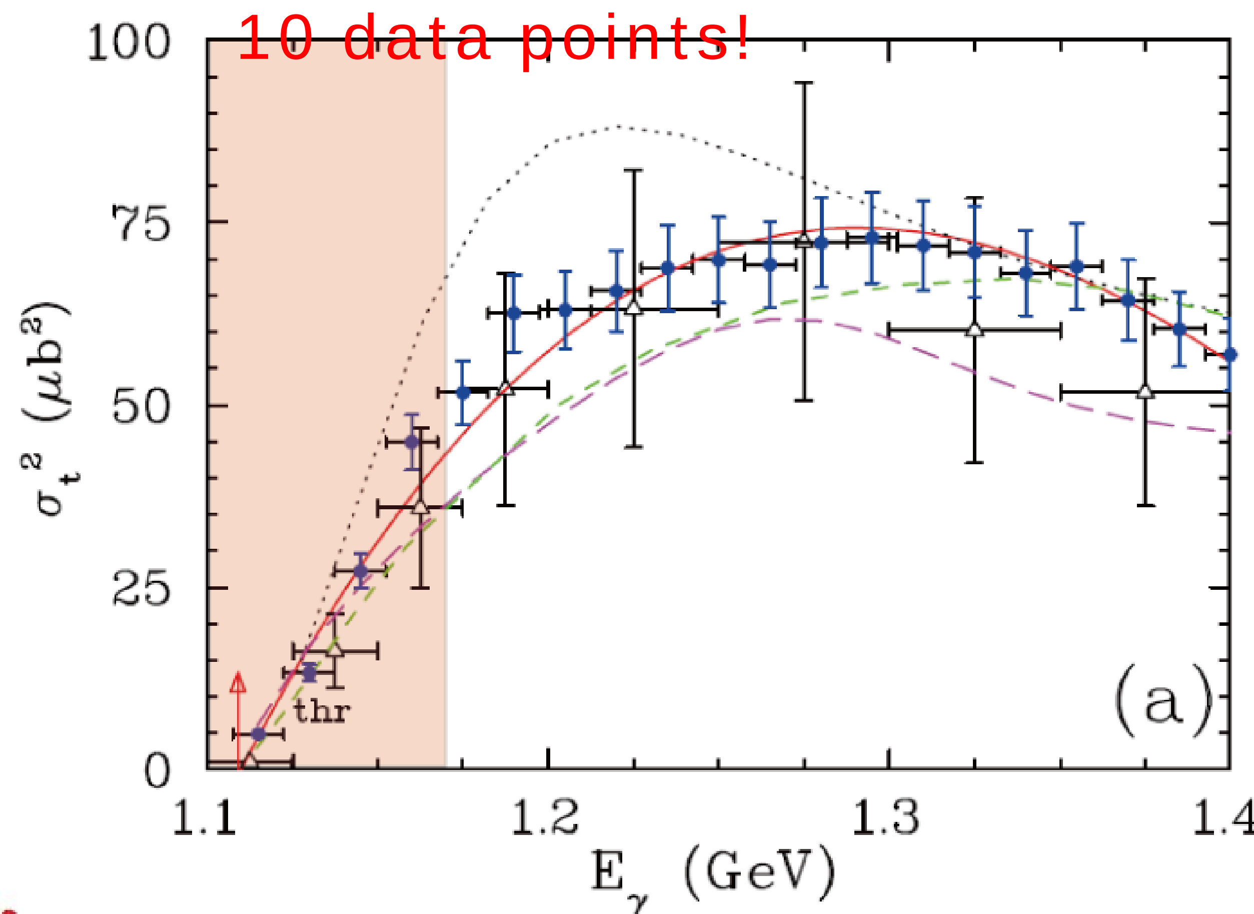

$\gamma p \rightarrow \omega p$

I.I. Strakovsky *et al.*, PRC91, 045207 (2015).

Selection ~ $\gamma p \to \omega p \to \pi^0 \gamma p$

1. 3 neutral particles and 1 charged particle
2. neutral pion: $\gamma\gamma$ decay, $M_{\gamma\gamma}$: 50~220 MeV
3. additional photon: > 200 MeV
4. time difference is less than $3\sigma_t$
   between every 2 neutral clusters out of 3
4. p is detected with SPIDER
   (response of SCISSORS III is not required)
   time delay is larger than 0 ns wrt average $\gamma\gamma\gamma$ time
5. sideband background subtraction
   to remove accidental coincidence
   between STB-Tagger II and FOREST

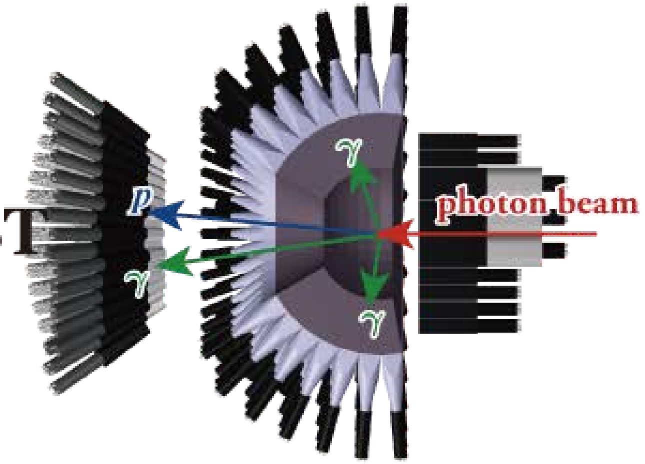

Selection ~ $\gamma p \to \omega p \to \pi^0 \gamma p$

1. 3 neutral particles and 1 charged particle
2. neutral pion: $\gamma\gamma$ decay, $M_{\gamma\gamma}$: 50~220 MeV
3. additional photon: > 200 MeV
4. time differe
   between eve
4. p is detecte
   (response o
   time delay i
5. sideband ba
   to remove a
   between ST

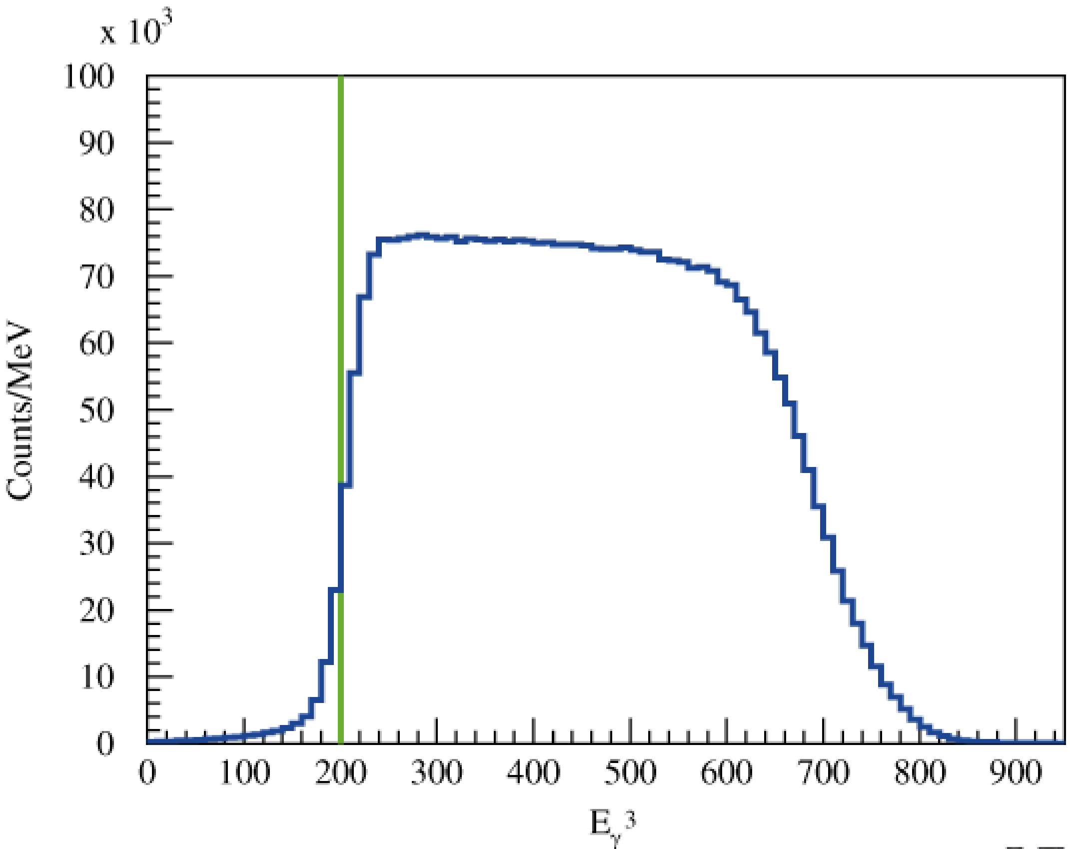

γ time

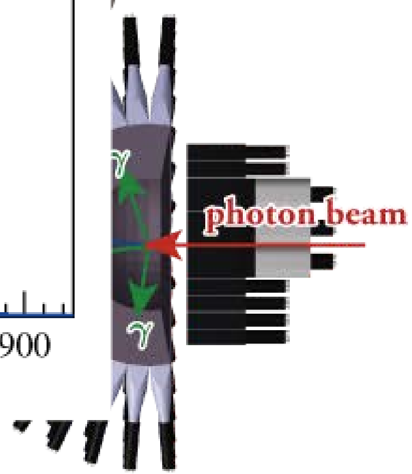

Further event selection:

- **a kinematic fit with 5 constraints is applied**
  - **energy and momentum conservation (4)**
  - **$\gamma\gamma$ invariant mass is m_{π^0} (1)**
  - **χ^2 probability is higher than 0.1**

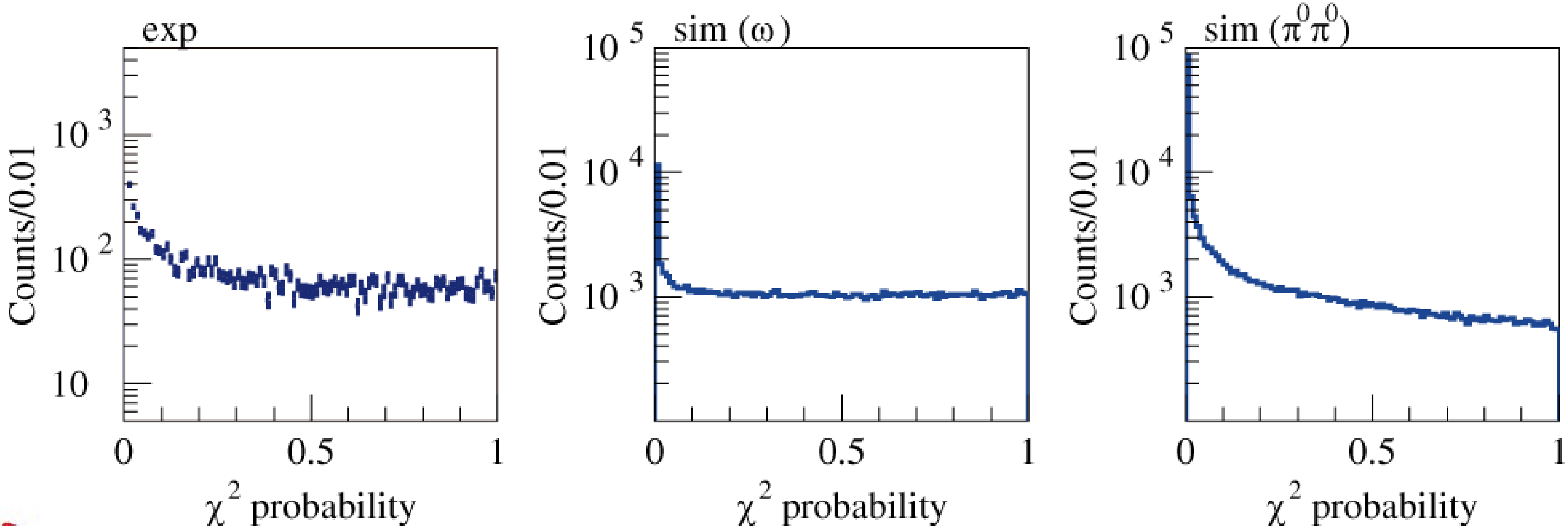

$\pi^0\gamma$ invariant mass

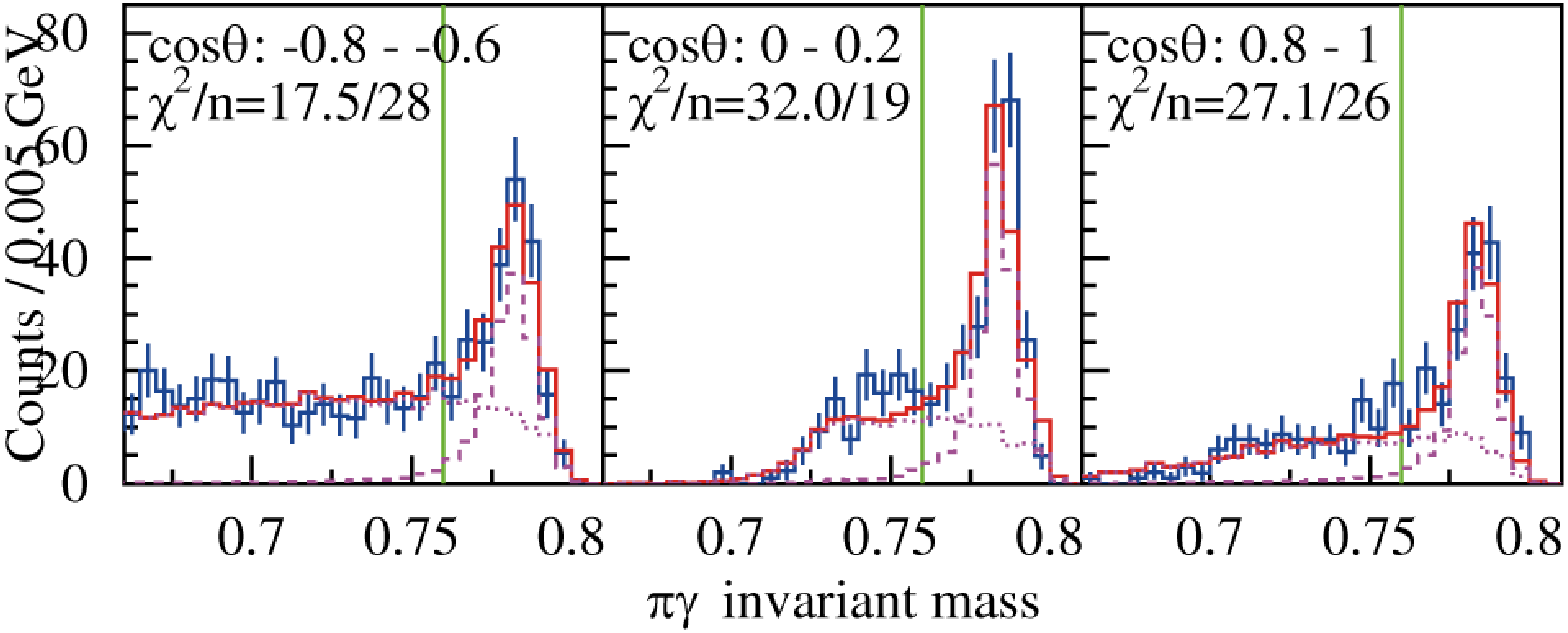

mass distributions are well-reproduced by a sum of

- **ω production**
- **$\pi^0\pi^0$ production (1γ missing)**

$d\sigma/d\Omega$ as a function of $\cos\theta$

$$\frac{d\sigma}{d\Omega}(\cos\theta) = \frac{d\sigma}{2\pi d\cos\theta}(\cos\theta) = \frac{N_\omega(\cos\theta)}{2\pi\Delta\cos\theta N_\gamma N_T \eta_{\mathrm{acc}}(\cos\theta)\mathrm{BR}(\omega\to\pi^0\gamma)\mathrm{BR}(\pi^0\to\gamma\gamma)}$$

acceptance

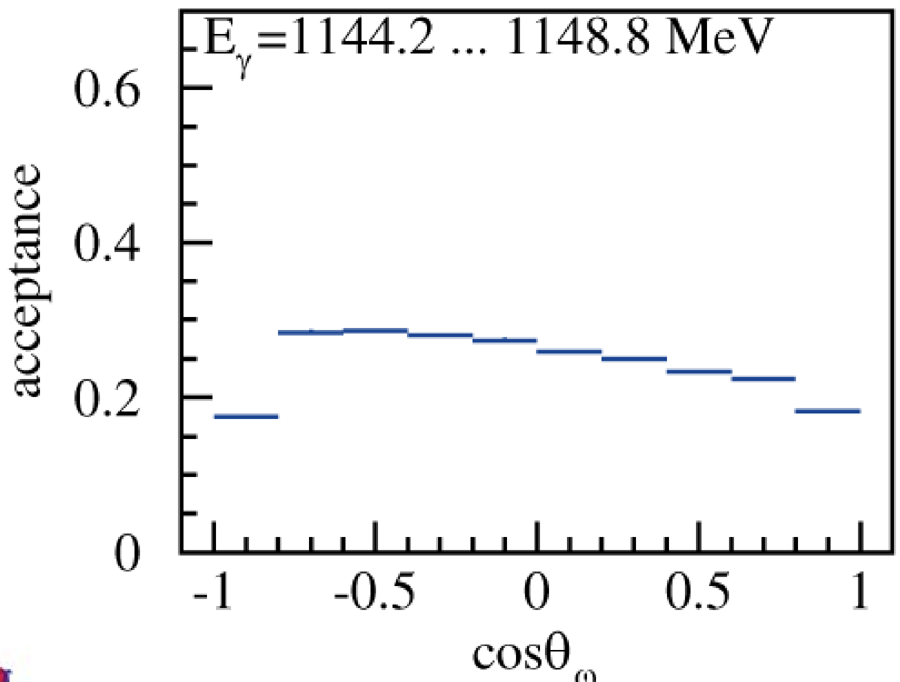

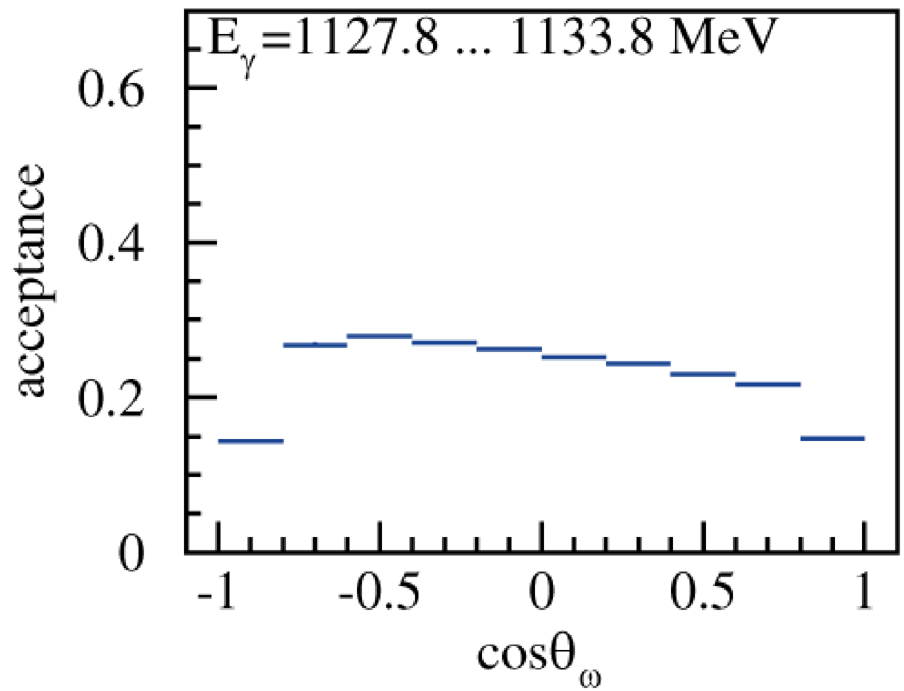

Differential cross sections

$d\sigma/d\Omega$ as a function of $\cos\theta$

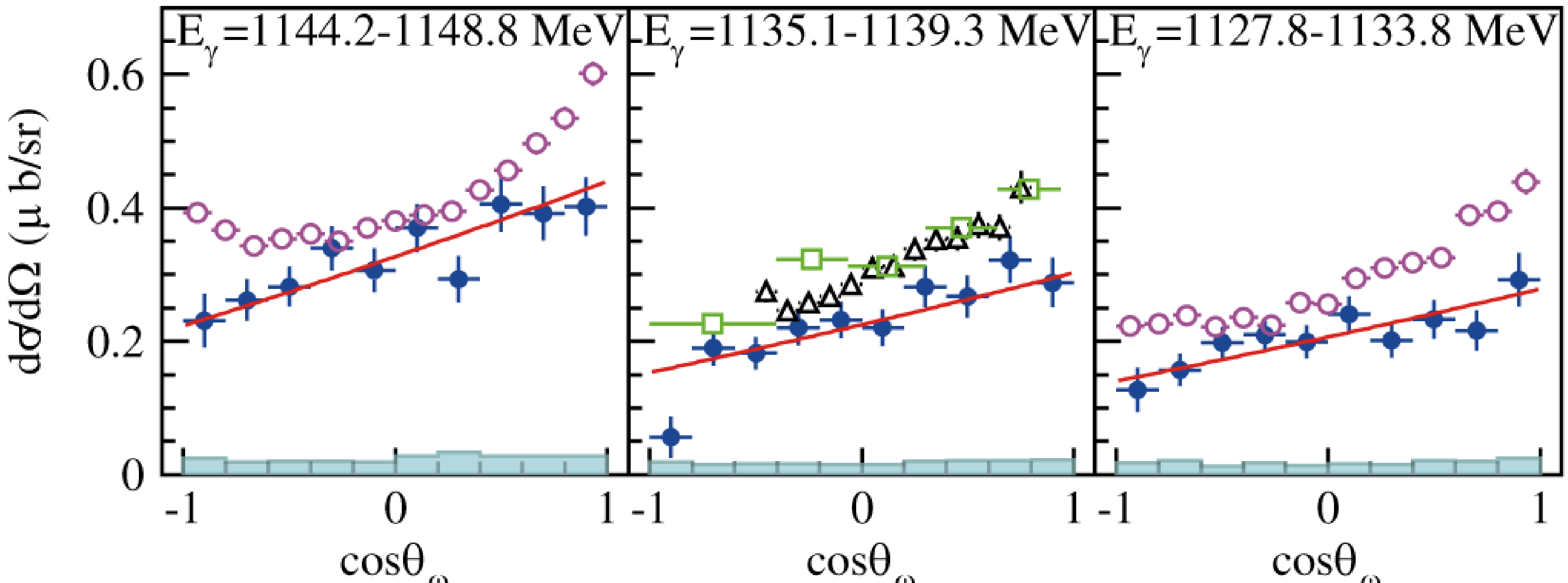

Mainz (15 MeV) JLAB (18 MeV) SAPHIR (25 MeV)

almost isotropically generated in CM

different tagging energies by a few MeV

relative difference

Systematic uncertainties

1) angular distribution in CM
   [decay angular distribution is flat]
2) $\pi\pi$ background level
3) kinematic fit
4) lower limit of $\pi\gamma$ invariant mass
5) target position
6) energy loss of the emitted proton

7) number of target protons
8) number of incident photons
   including DAQ efficiency

Total cross section

integrating $d\sigma/d\Omega$

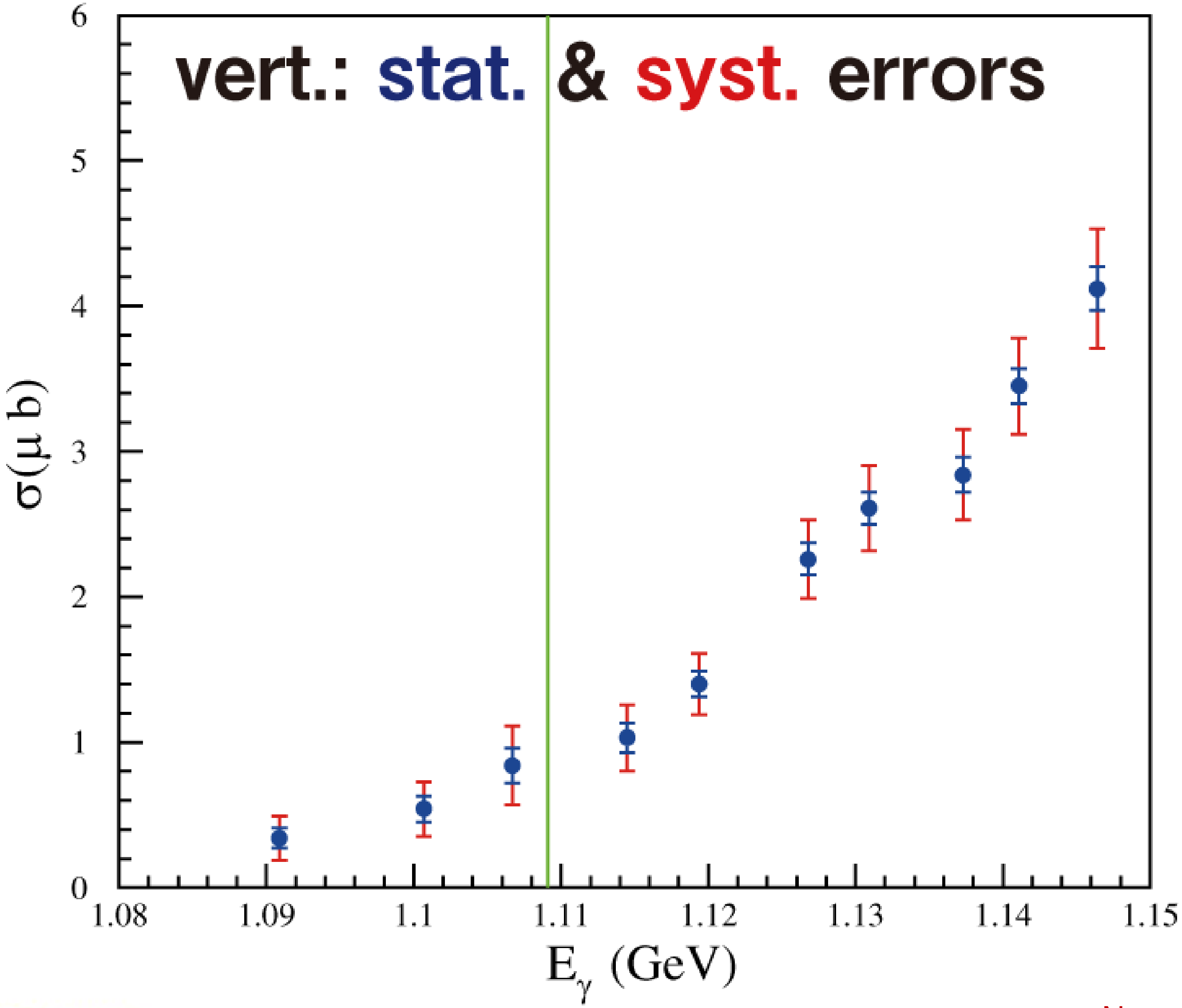

Excitation function & $a_{\omega N}$

a model with ωp final-state interaction (FSI) based on Lippmann-Schwinger equation

$$T_{\gamma p \to \omega p} = \left(1 + T_{\omega p \to \omega p} G_{\omega p}\right) V_{\gamma p \to \omega p}$$

final-state interaction (ωp scattering)

ωp propagator

ω production

$V_{\gamma p \to \omega p}$ is assumed to be constant

on-shell approximation

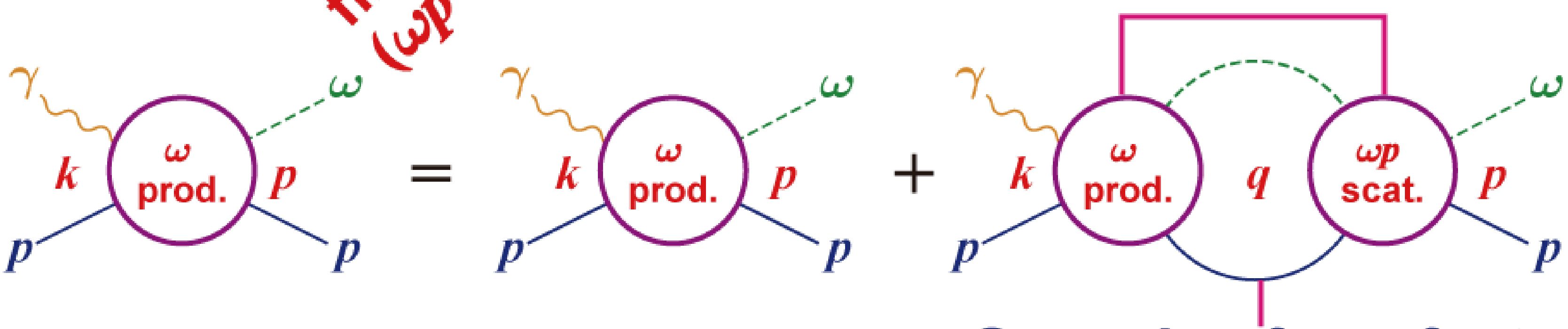

Gaussian form factor

Excitation function & $a_{\omega N}$

systematic uncertainty is estimated from that of the mean incident energy (±3%)

Parameters	Re $a_{\omega p}$ (fm)	Im $a_{\omega p}$ (fm)	Re $r_{\omega p}$ (fm)	Im $r_{\omega p}$ (fm)
$\Lambda = 0.8$ GeV/c	$-0.97^{+0.16+0.03}_{-0.16-0.00}$	$+0.07^{+0.15+0.17}_{-0.14-0.09}$	$+2.78^{+0.67+0.11}_{-0.54-0.12}$	$-0.01^{+0.46+0.06}_{-0.50-0.00}$
$\Lambda = 0.6$ GeV/c	$-1.11^{+0.14+0.03}_{-0.16-0.04}$	$+0.12^{+0.17+0.12}_{-0.17-0.11}$	$+2.78^{+0.81+0.04}_{-0.57-0.16}$	$+0.00^{+0.44+0.11}_{-0.54-0.10}$
$\Lambda = 1.0$ GeV/c	$-0.89^{+0.16+0.01}_{-0.18-0.00}$	$+0.04^{+0.14+0.13}_{-0.12-0.04}$	$+2.78^{+0.62+0.23}_{-0.51-0.09}$	$+0.01^{+0.47+0.11}_{-0.50-0.05}$
P-wave contribution	$-0.96^{+0.16+0.04}_{-0.16-0.01}$	$+0.10^{+0.14+0.14}_{-0.14-0.09}$	$+2.85^{+0.77+0.15}_{-0.53-0.15}$	0.00
Single N^* contribution	$-0.87^{+0.15+0.04}_{-0.22-0.02}$	$+0.22^{+0.14+0.11}_{-0.12-0.11}$	$+2.69^{+0.62+0.06}_{-0.55-0.12}$	$-0.04^{+0.48+0.04}_{-0.69-0.14}$

the parameters do not change among the realistic Λ cut-off values

Im[$r_{\omega N}$] is consistent with 0

P-wave contribution is small

the parameters do not change with an extreme energy-dep of V (single N* resonance near the threshold, M=1.7 GeV, Γ=0.2 GeV)

T. Ishikawa

Summary of $a_{\omega N}$

effective Lagrangian approach (99)
QCD sum-rule analysis (97)
coupled-channel analysis (L: 02, S: 05, P: 09)
vector dominance model (15)

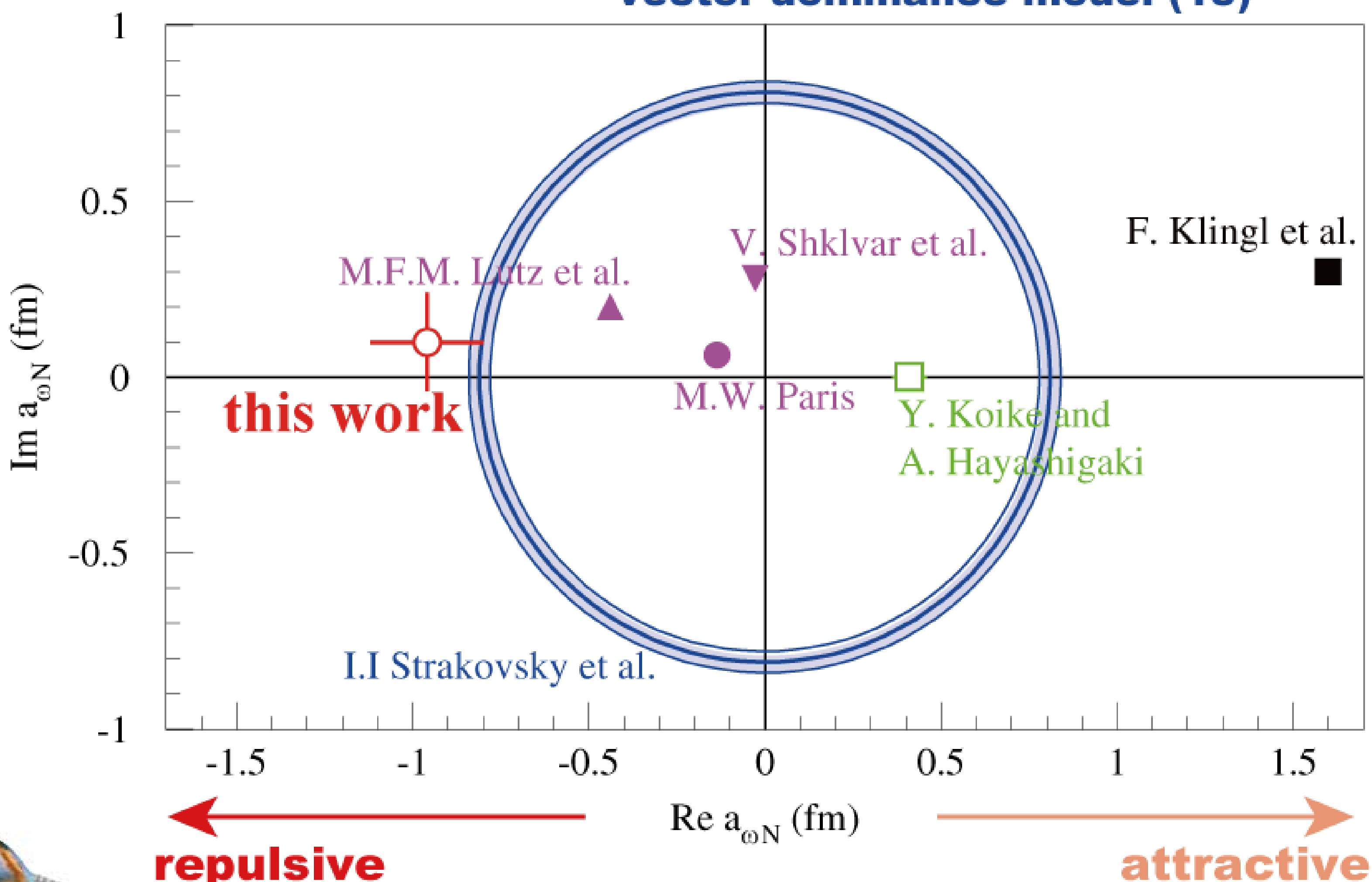

ωN interaction

seems inconsistent between attractive results

1. ωA potential from excitation function for ω photoproduction from nuclei
2. mass decrease by $9.2\% \pm 0.2\%$ from line-shape analysi in dilepton spectroscopy

possible reasons:

spin-dependent terms?

in-medium mass modification can be disguished from the basic interaction?

Backup slides ~ **ηN** (1)

N(1535) with J^{π}=1/2$^-$

chiral partner of the nucleon N(940) ?

N(940) and N(1535) degenerate at high density and/or high temperature

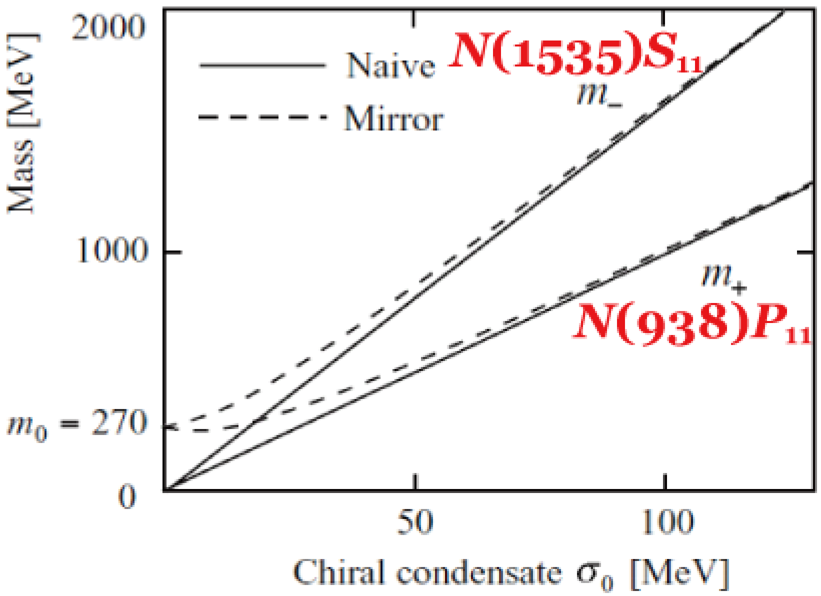

C. DeTar and T. Kunihiro, PRD 39, 2805 (1989);
T. Hatsuda and M. Prakash, PLB 224, 11 (1989);
D. Jido, M. Oka, and A. Hosaka, PTP106, 873 (2001).

strongly couples to the eta meson (η) and nucleon (N)

$N(1535)S_{11}$

N(1535) with J^{π}=1/2^{-}

chiral partner of the nucleon N(940) ?
N(940) and N(1535) degenerate at high density and/or high temperature

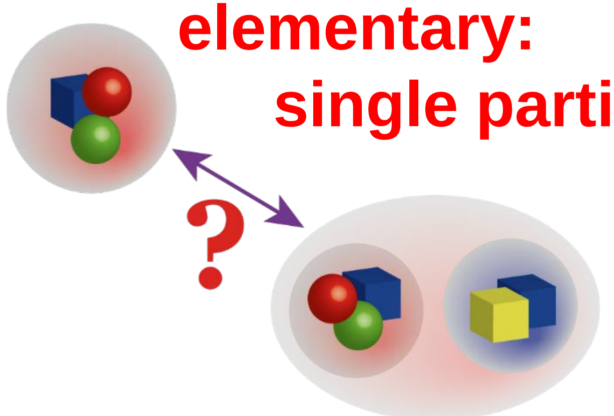

elementary: single particle

composite: molecule-like state

strongly couples to the eta meson (η) and nucleon (N)

$$X_{\eta N} = 0.04 + i0.37$$

T. Sekihara *et al.*, PRC 93, 035204 (2016).

ηN scattering length

eta-nucleon scattering
Im: ~ 0.25 fm
Re: scattered

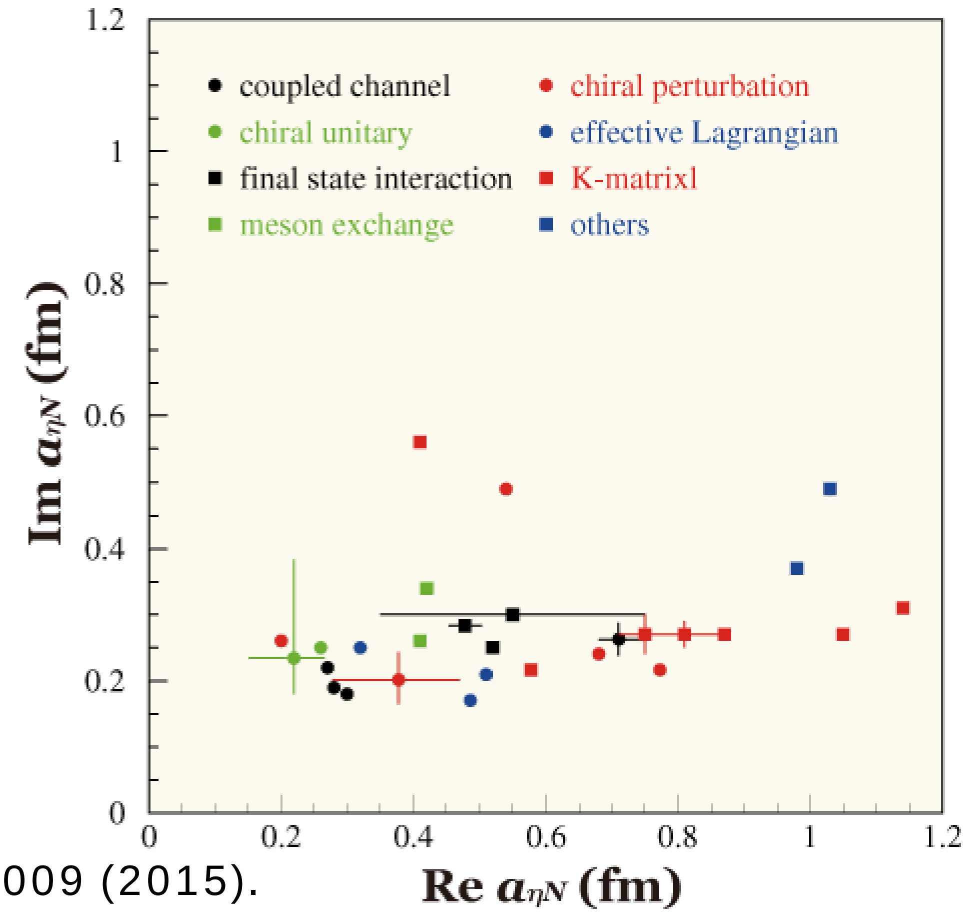

combined analysis of cross sections for

$$\pi N \to \pi N, \pi N \to \eta N,$$
$$\gamma N \to \pi N, \gamma N \to \eta N$$

Q. Haider and L.C. Liu,
J. Mod. Phys. E 24, 1530009 (2015).

proposed kinematics for $a_{\eta N}$ determination using $\gamma d \to \eta p n$

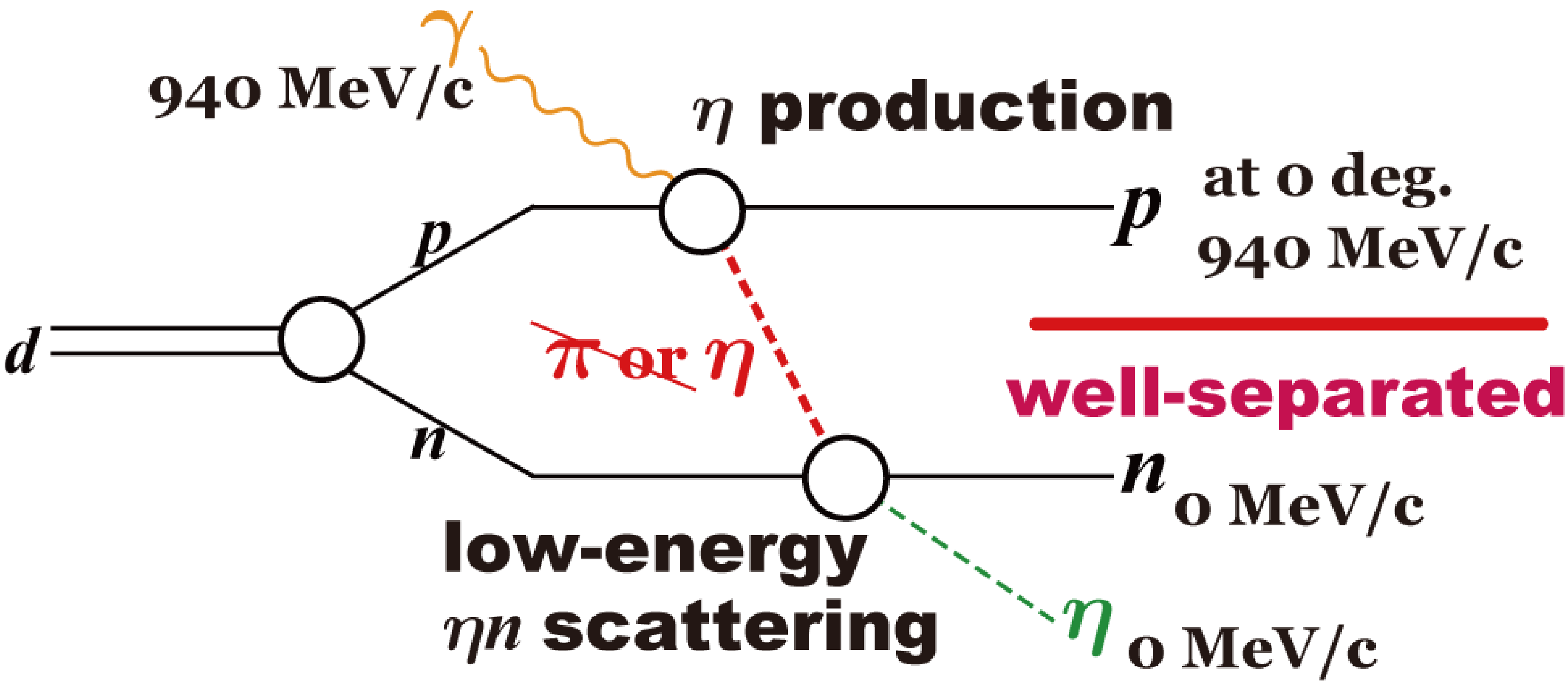

ηN scattering length

differential cross section for for $\gamma d \to \eta p n$ as a function of ηn invariant mass

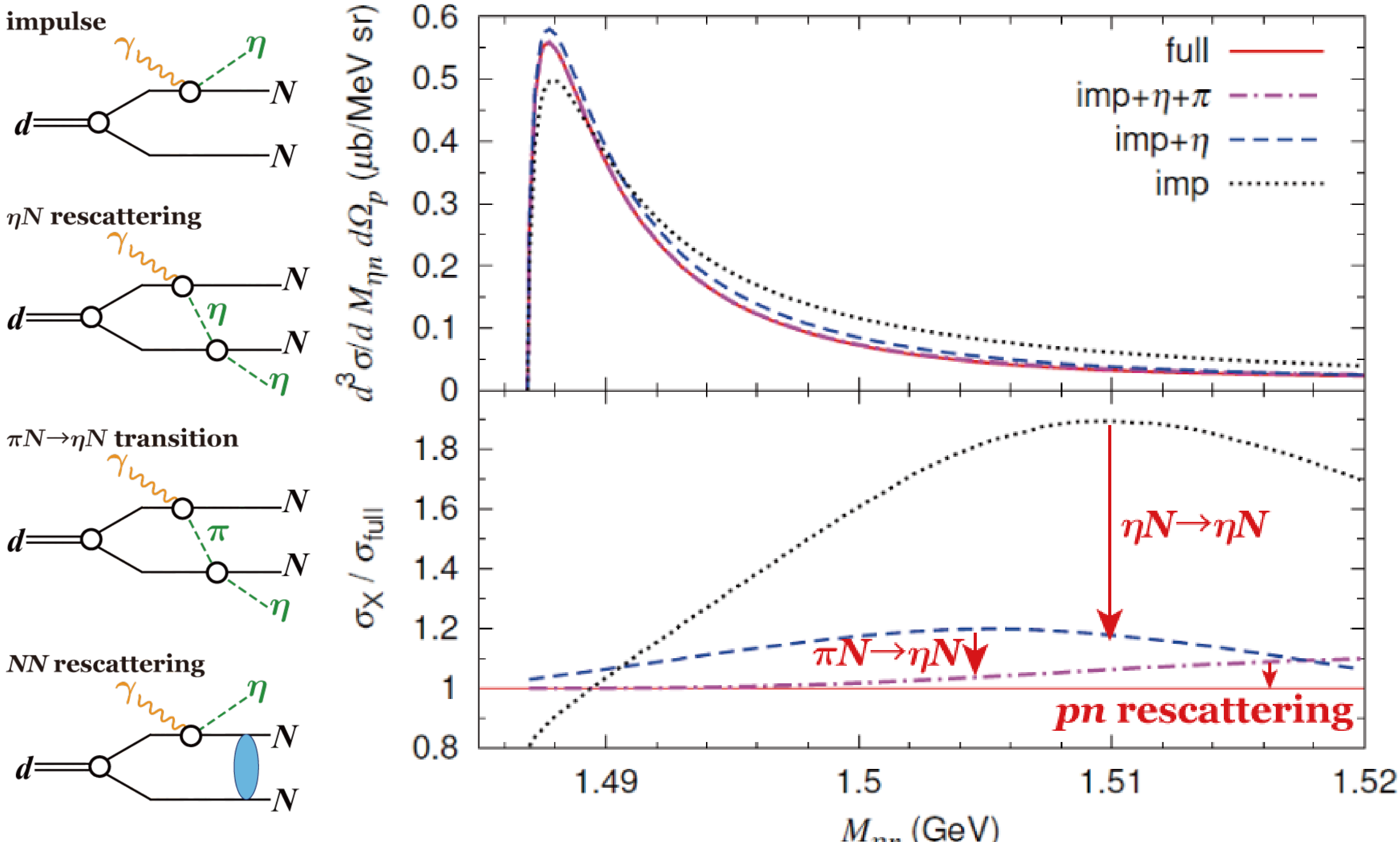

S.X. Nakamura, H. Kamano, T. Ishikawa, Phys. Rev. C 96, 042201 (R) (2017).

1) energy-tagged photon beam
2) eta-meson identification (EM calorimeter)
3) forward proton detection (spectrometer)

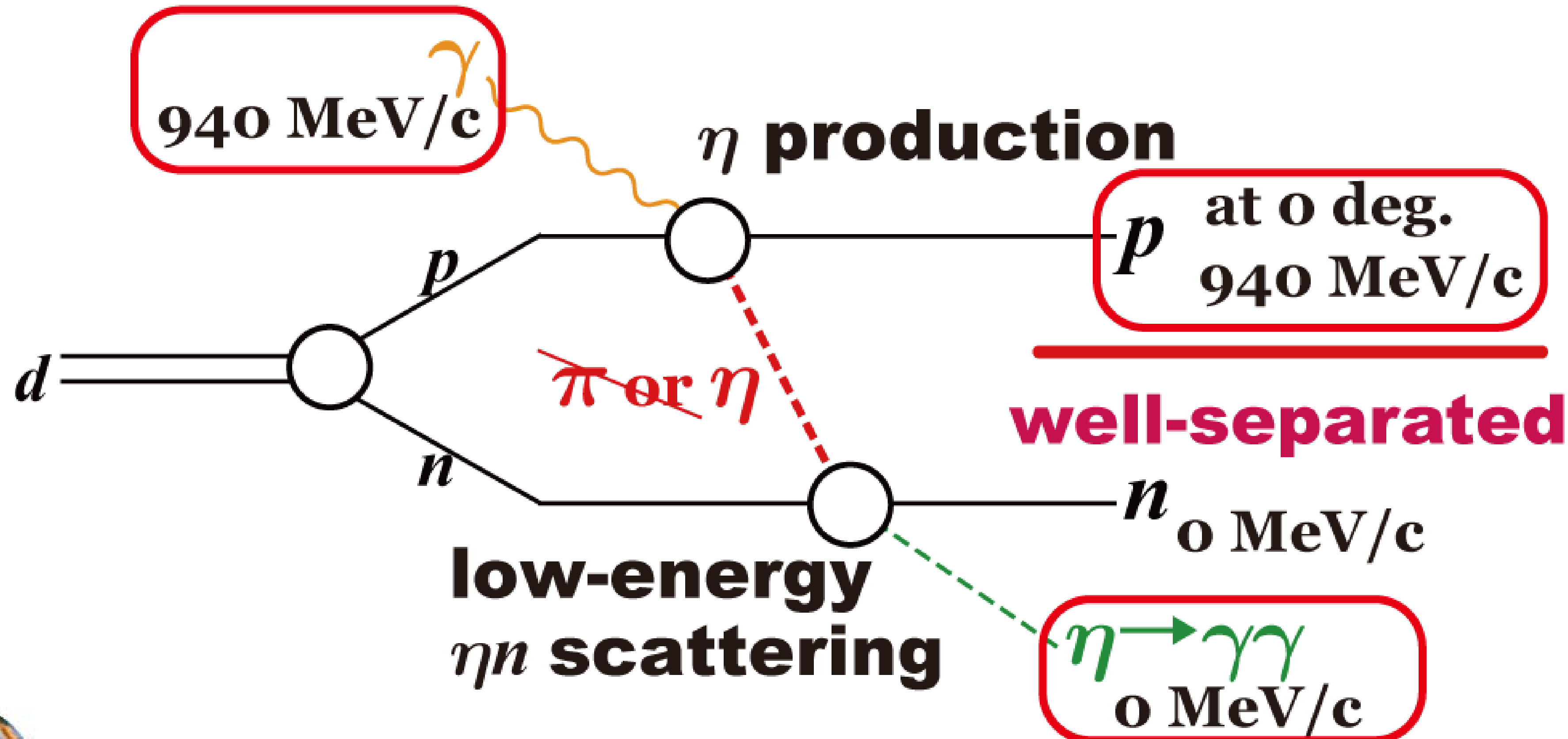

experiments

1) energy-tagged photon beam

2) eta-meson identification (EM calorimeter)

3) forward proton detection (spectrometer)

1.3 GeV Booster STorage Ring

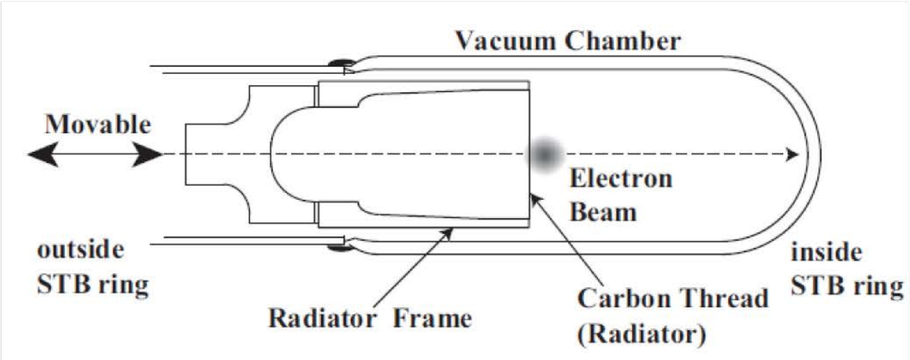

the energy of each produced photon:
determined by detecting the corresponding post-bremsstrahlung electron

$$E_\gamma = 0.80 \sim 1.25\ \mathrm{GeV}$$

T. Ishikawa *et al.*, NIMA 622, 1 (2010); T. Ishikawa *et al.*, NIMA 811, 124 (2016); Y. Matsumura *et al.*, NIMA 902, 103 (2018); Y. Obara *et al.*, NIMA 922, 108 (2019).

experiments

1) energy-tagged photon beam

2) eta-meson identification (EM calorimeter)

3) forward proton detection (spectrometer)

T. Ishikawa *et al.*, NIMA 832, 108 (2016).

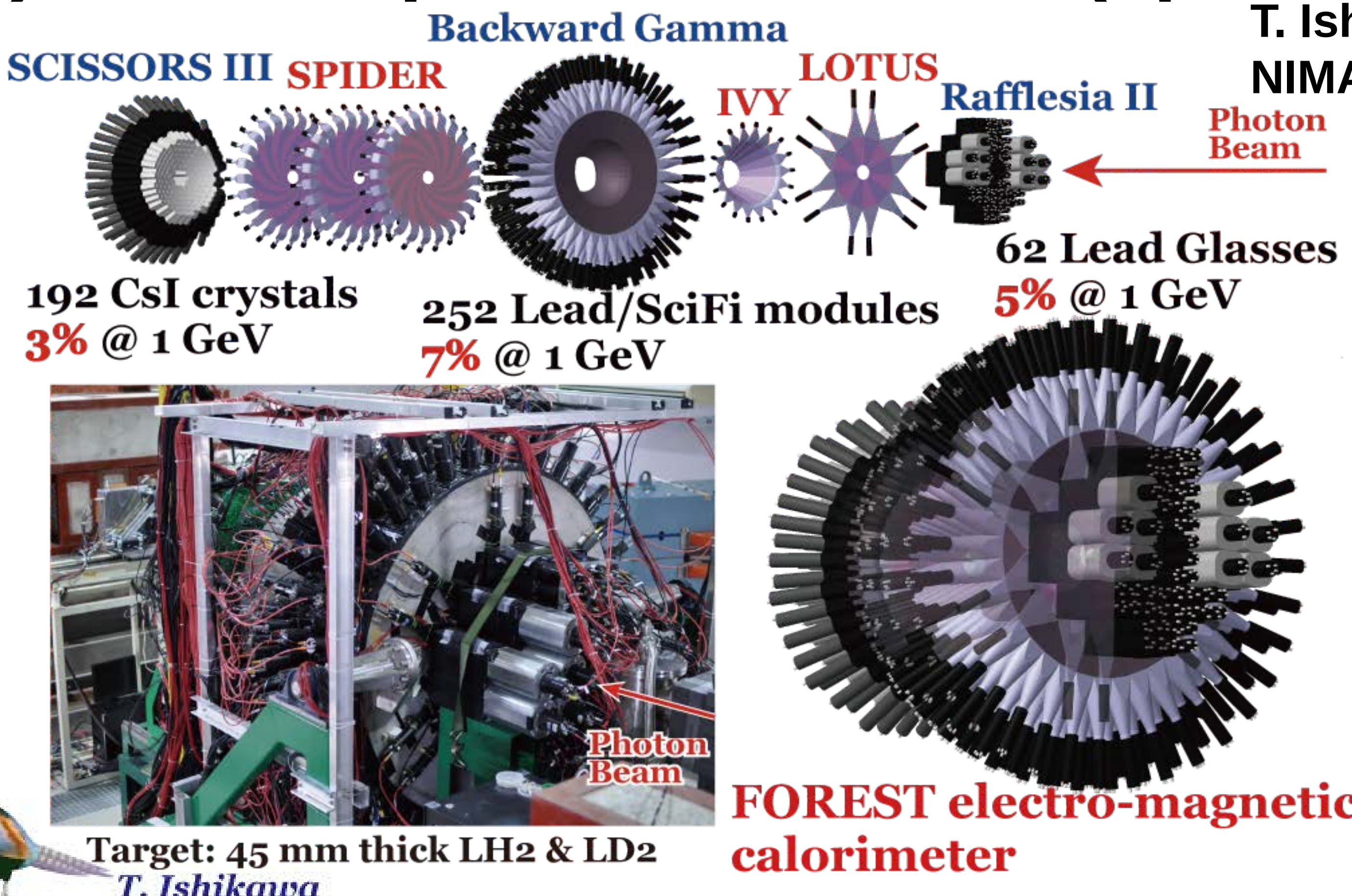

experiments

1) energy-tagged photon beam
2) eta-meson identification (EM calorimeter)
3) forward proton detection (spectrometer)

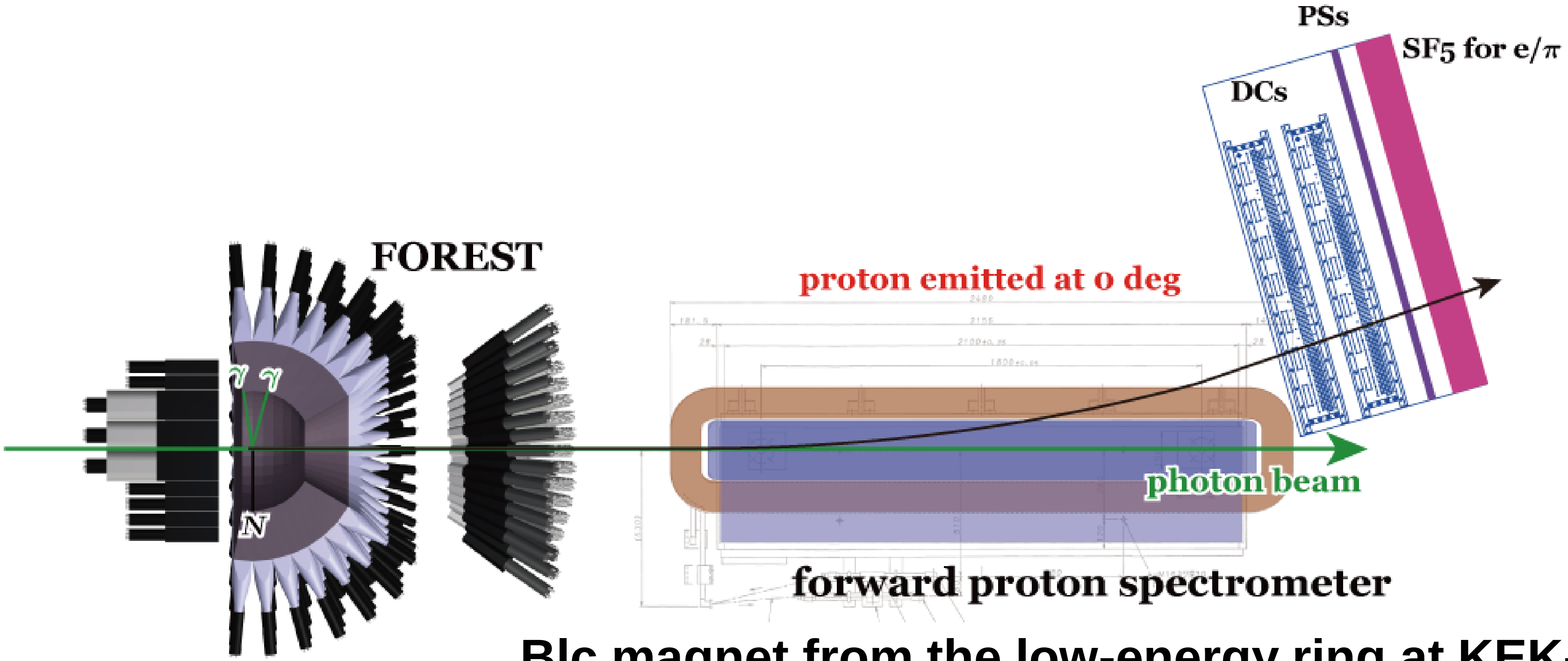

Blc magnet from the low-energy ring at KEK-B

current status

data acquired
two particles in FOREST

	hydrogen	deuterium	empty
2017.10.30~11.20	0.40 G	0.31 G	0.02 G
2017.11.23~11.30	0.20 G	—	0.05 G
2018.06.07~06.25	0.47 G	0.49 G	0.09 G
2018.10.12~11.04	0.75 G	0.88 G	0.07 G
2019.04.08~05.06	0.75 G	1.39 G	0.12 G
2020.04.09~	> 0.77 G	> 2.58 G	> 0.08 G

current statistics: ~½ of the original plan

ηn invariant mass distribution

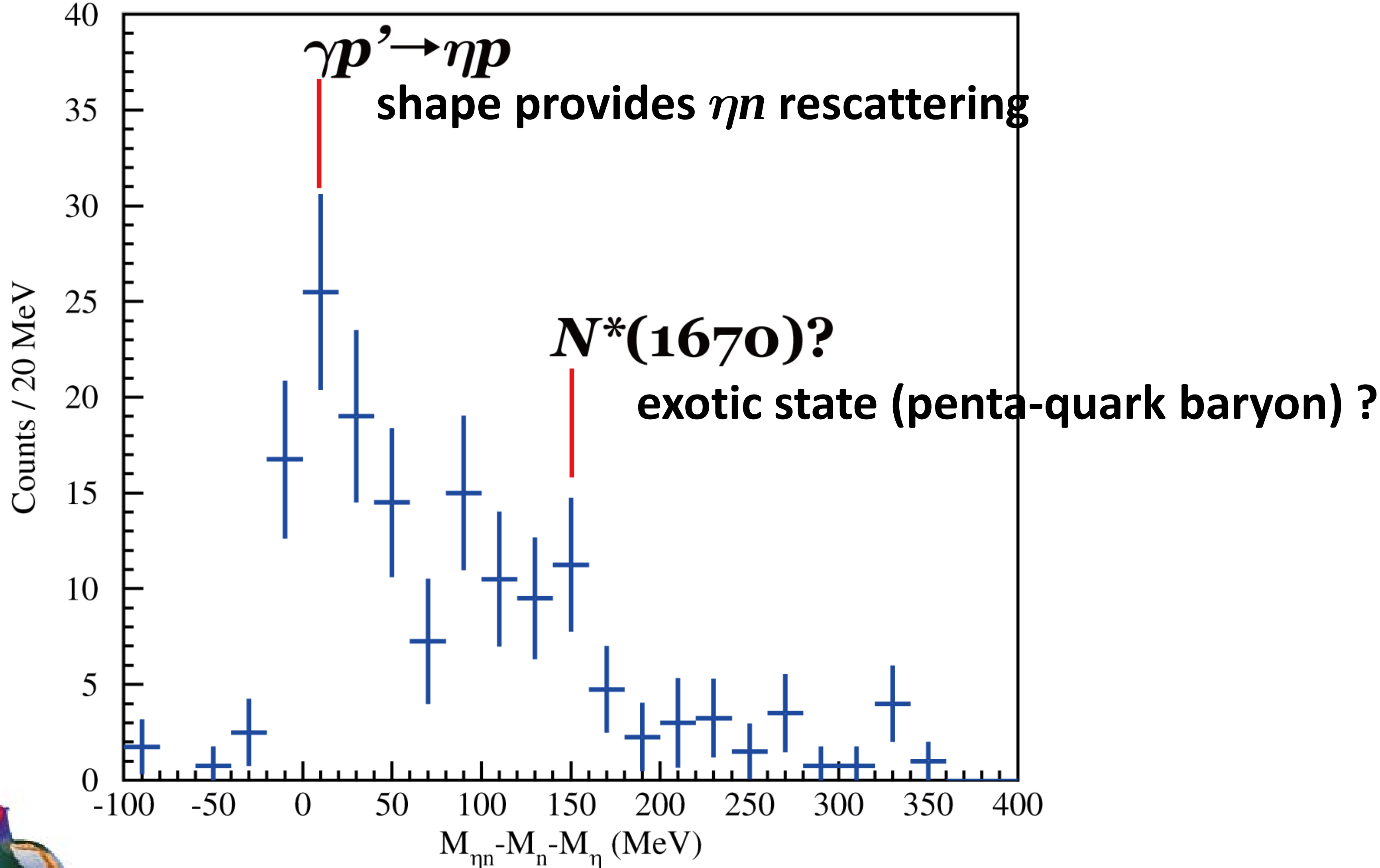

Backup slides ~ **ηN** (2)

Alternative method

coherent $\pi^0\eta$ photoproduction on the deuteron ($\gamma d \to \pi^0 \eta d$)

1. no Δ-Kroll-Ruderman or meson-pole Born term
2. final-state interaction is significantly enhanced

$$a_{\eta N} = 0.70 + i0.29\ \mathrm{fm}$$

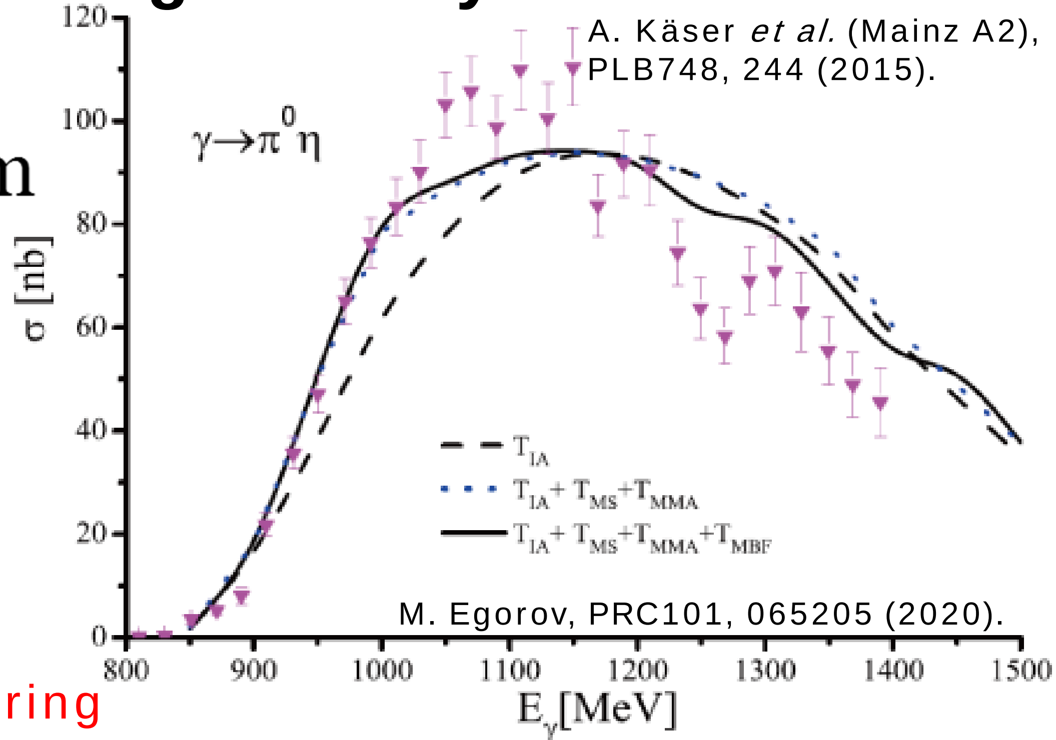

IA: impulse
MS: meson-nucleon scattering
MMA: absorption of an additionally produced meson
MBF: meson-deuteron scattering

Experiment ~ photo beam

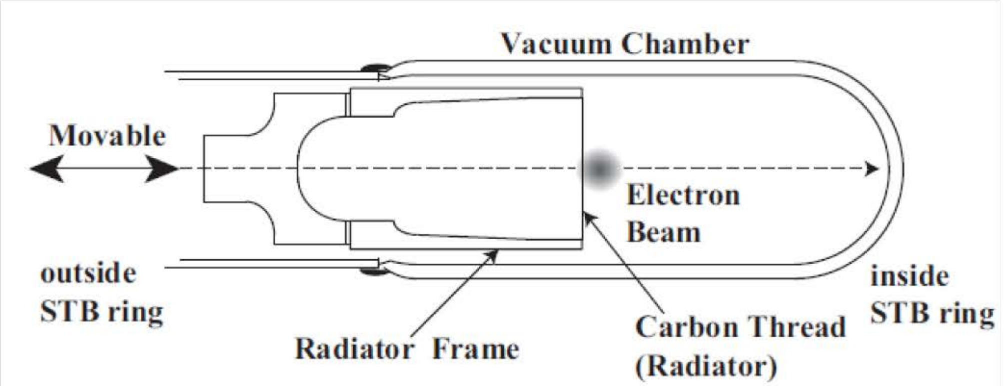

the energy of each produced photon: determined by detecting the corresponding post-bremsstrahlung electron

$$E_\gamma = 0.74 \sim 1.15\,\mathrm{GeV} \;\; (E_\gamma^{\mathrm{thr}} \simeq 0.81\,\mathrm{GeV})$$

tagging intensity ~ 20 MHz
(photon intensity ~ 10 MHz)

T. Ishikawa *et al.*, NIMA 622, 1 (2010); T. Ishikawa *et al.*, NIMA 811, 124 (2016); Y. Matsumura *et al.*, NIMA 902, 103 (2018); Y. Obara *et al.*, NIMA 922, 108 (2019).

Experiment ~ detector

Backward Gamma

SCISSORS III SPIDER IVY LOTUS Rafflesia II

Photon Beam

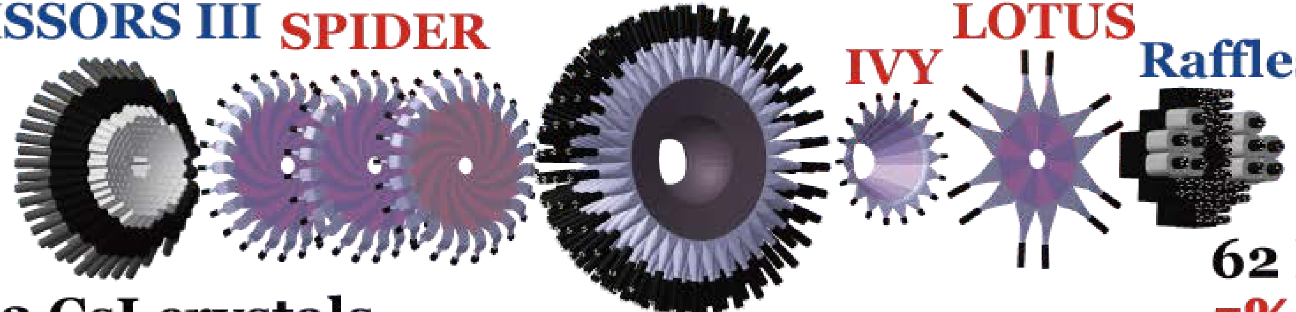

192 CsI crystals
3% @ 1 GeV

252 Lead/SciFi modules
7% @ 1 GeV

62 Lead Glasses
5% @ 1 GeV

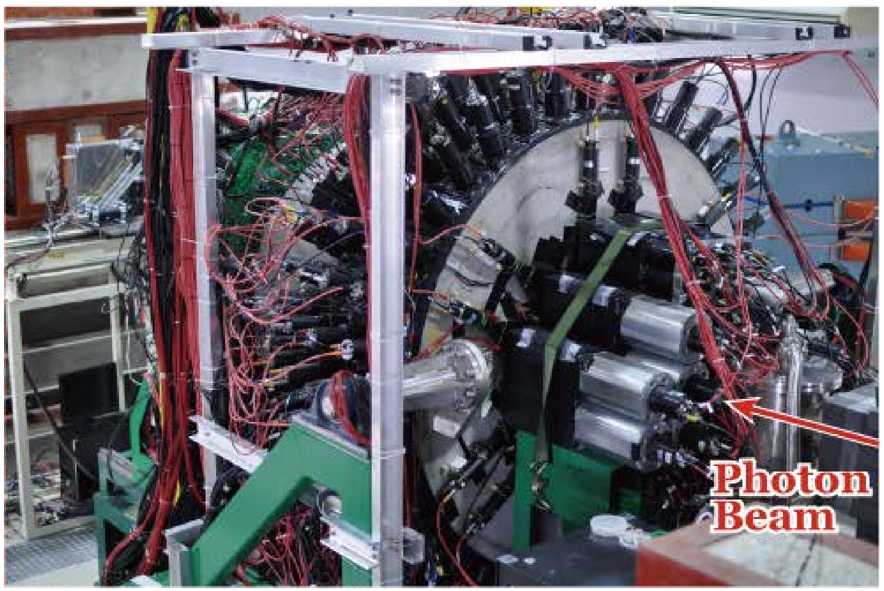

Target: 45 mm thick LH2 & LD2

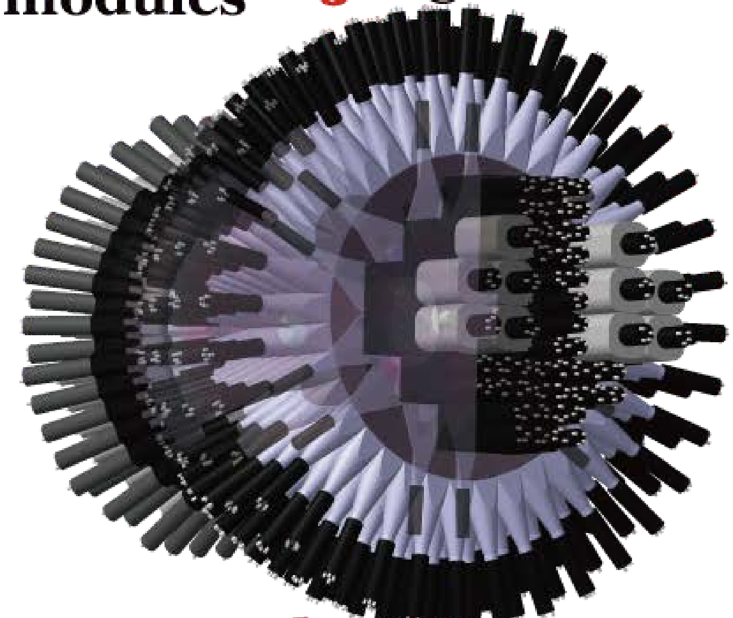

FOREST electro-magnetic calorimeter

T. Ishikawa *et al.*, NIMA 832, 108 (2016).

Analysis

event selection for $\gamma d \to \pi^0 \eta d$

1. 4 neutral particles and 1 charged particle
2. π^0: $\gamma\gamma$ decay
3. η: $\gamma\gamma$ decay
4. time difference is less than $3\sigma_t$ between every two neutral clusters out of 4
5. d is detected with SPIDER
   time delay is longer than 1 ns wrt $\gamma\gamma\gamma\gamma$
   energy deposit is higher than $2E_{\mathrm{mip}}$
6. sideband background subtraction
   to remove accidental coincidence
   between STB-Tagger II and FOREST

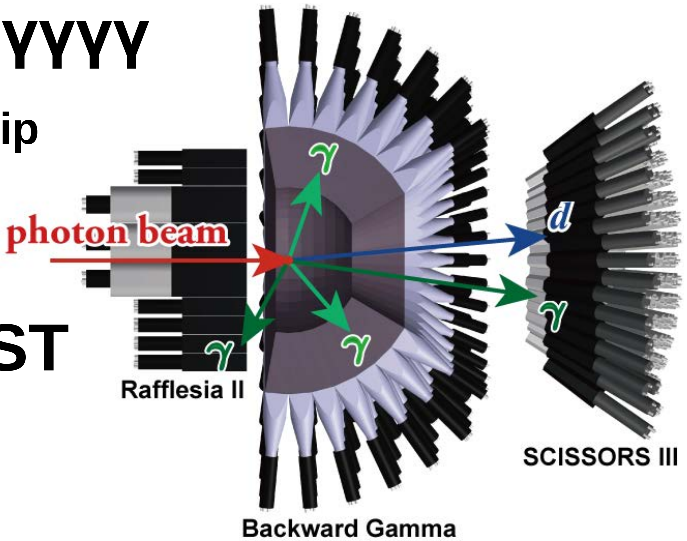

Analysis

6C kinematic fit (KF):

four momentum conservation, $M_{\gamma\gamma}^{(1)}=M_{\pi}$, $M_{\gamma\gamma}^{(2)}=M_{\eta}$

1. **π^2 probability > 0.2 in the kinematic fit for $\gamma d \to \pi^0 \eta d$**
2. **π^2 probability < 0.01 in the kinematic fit for $\gamma p' \to \pi^0 \eta p$**
   P_x, P_y, P_z measurement: 0±40 MeV/c for p'

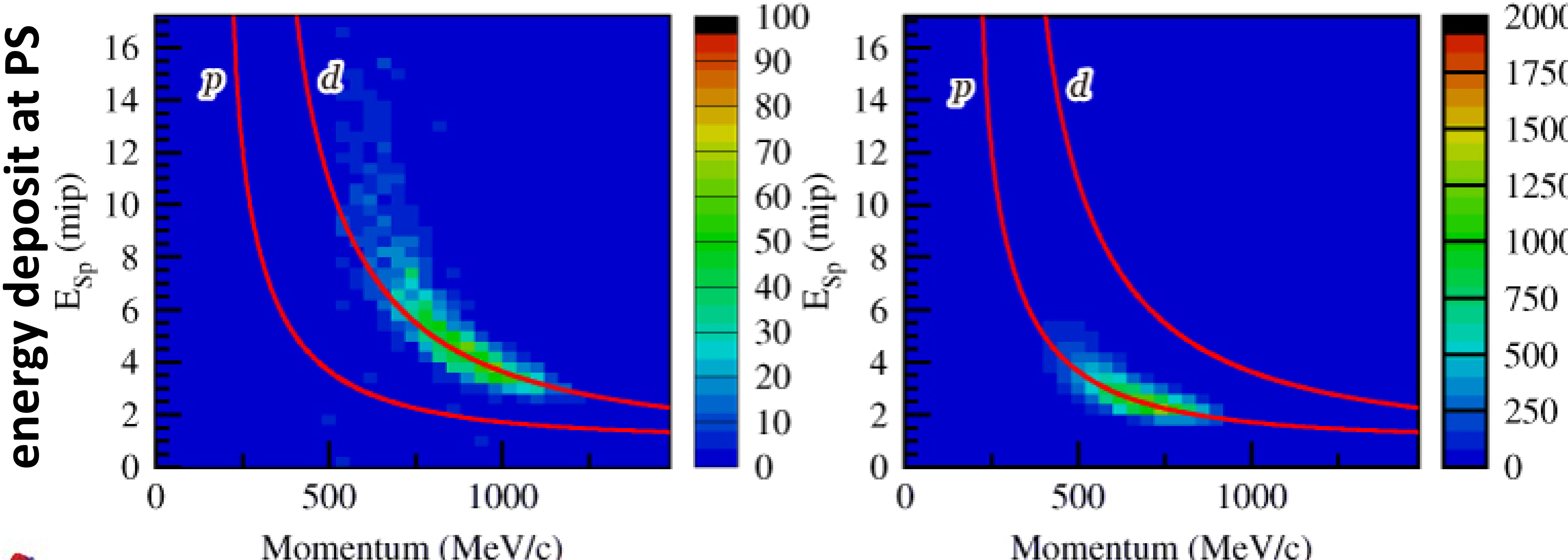

as a function of missing momentum d(γ, $\pi^0\eta$)

Total cross section

excitation function below 1 GeV is well-reproduced by the theoretical calculation with the final-state interaction

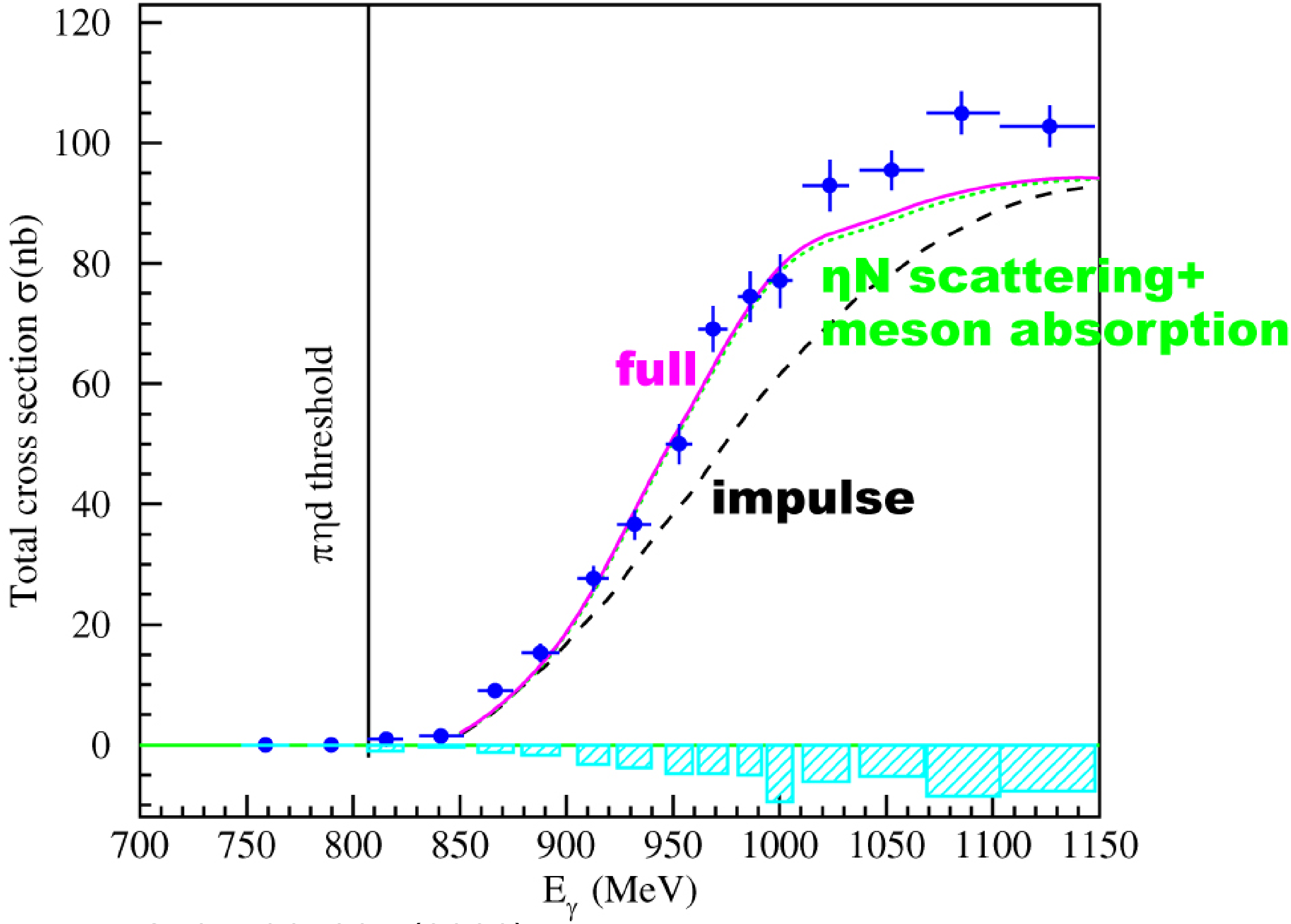

calculation: M. Egorov, PRC101, 065205 (2020).

Extraction of $a_{\eta N}$

the ηN scattering effect is assumed to be factorized in distortion from the impulse approximation

original calculation:

$$a_{\eta N} = 0.70 + i0.29 \text{ fm}$$

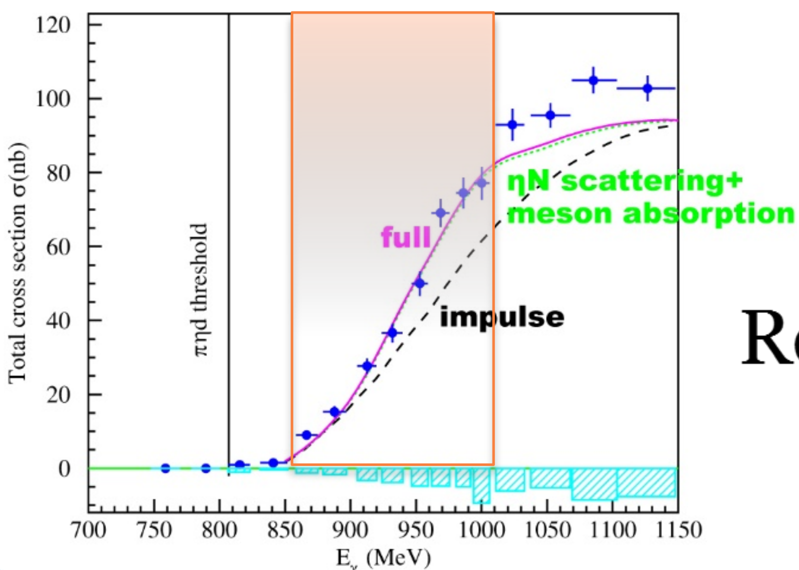

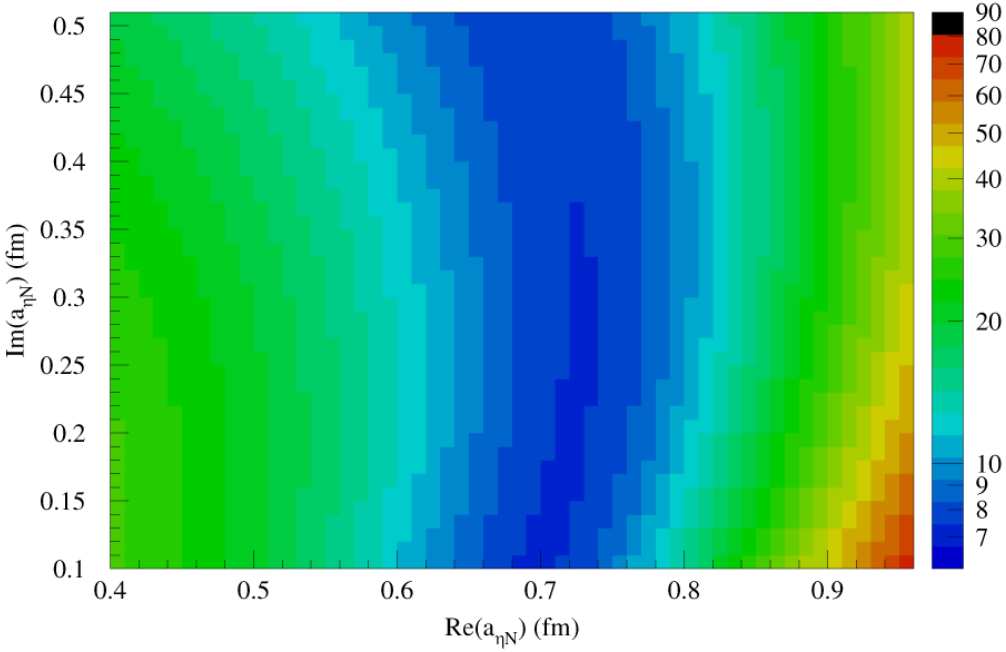

$$\mathrm{Re}[a_{\eta N}] = 0.72 \pm 0.05 \text{ fm}$$

$$\text{for } \mathrm{Im}[a_{\eta N}] = 0.2 \sim 0.4 \text{ fm}$$

angular distribution of deuteron emission is not reproduced, suggesting a sequential process:

$\gamma d \rightarrow \mathcal{D}_{IV} \rightarrow \pi^0 \mathcal{D}_{IS} \rightarrow \pi^0 \eta d$

ηd threshold enhancement

E$_\gamma$=1.01-1.15 GeV

E$_\gamma$=0.95-1.01 GeV

E$_\gamma$=0.86-0.94 GeV

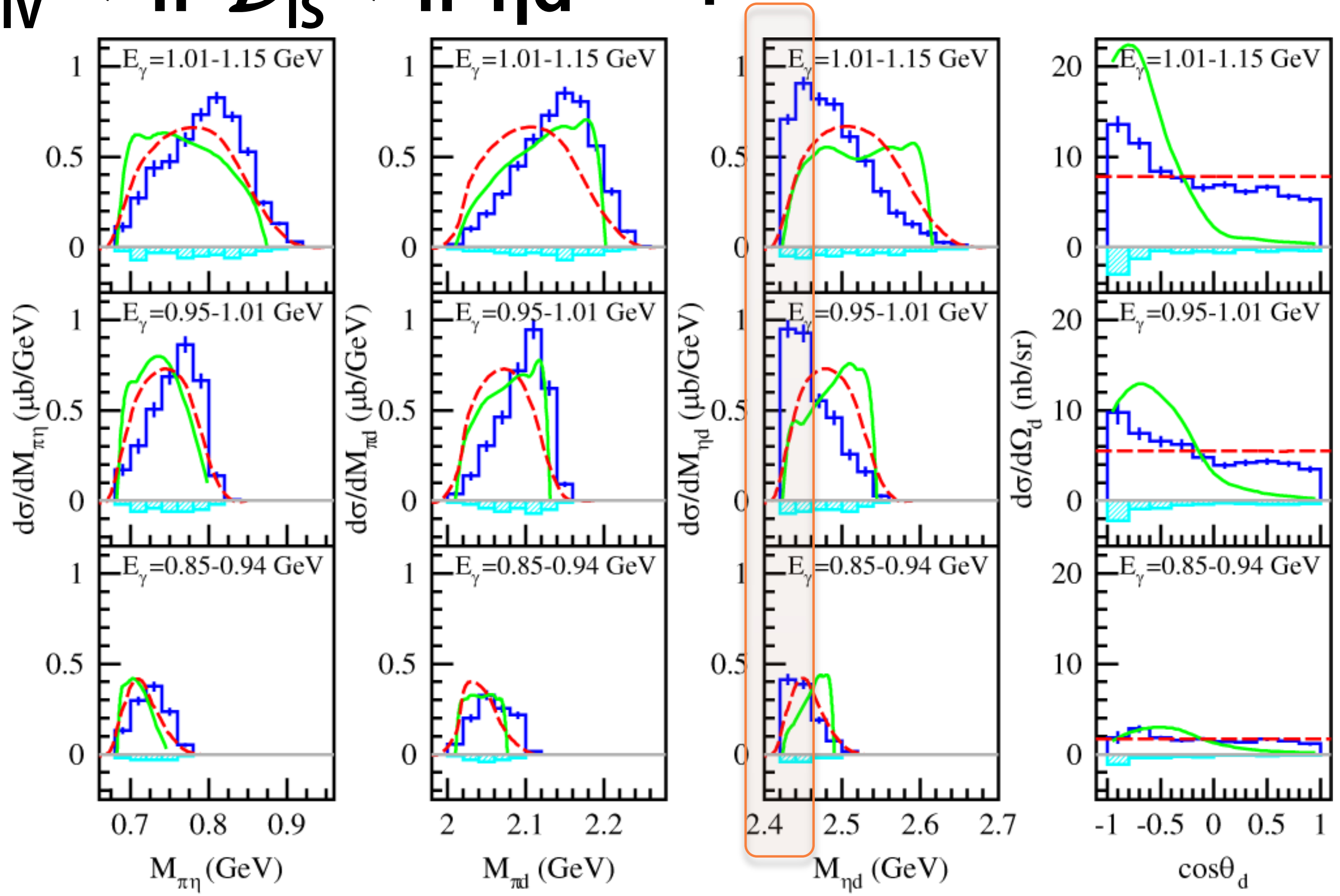

phase space calculation: M. Egorov, PRC101, 065205 (2020).

Intermediate state

prominent enhancement near the ηd threshold:

$\gamma d \to \mathcal{D}_{IV} \to \pi^0 \mathcal{D}_{IS} \to \pi^0 \eta d$ for $M_{\eta d}$<2.47 GeV $M_N + M_{N^*(1535)}$

only *L*=0 can produce
a threshold enhancement

$\mathcal{D}_{\rm IS} : 1^-$

angular correlation requires
(symmetry & convex)

***L*=2 component (~1/16)**

consistent with S-wave NN*,
and with L=2 component in d

η emission in ηd rest frame (z: -π⁰)

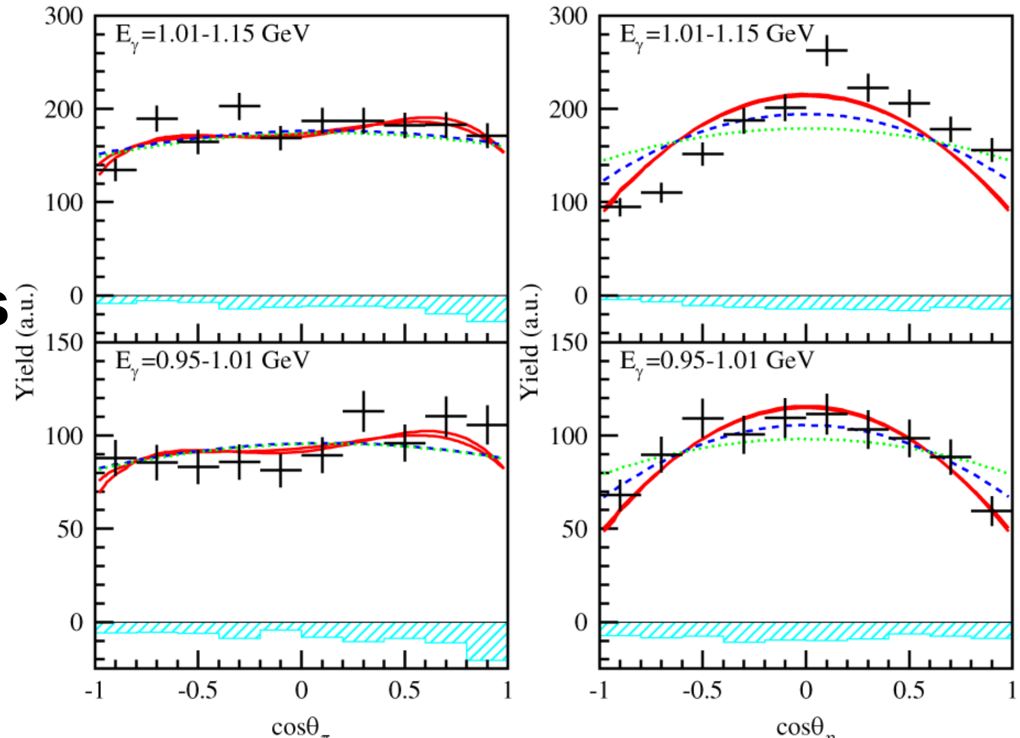

π⁰ emission in γd-CM (z: γ beam)

dominant process

$$d \xrightarrow{\gamma(L=1)} \mathcal{D}_{\rm IV}(0^-) \xrightarrow{\pi(L=1)} \mathcal{D}_{\rm IS}(1^-) \xrightarrow{\eta(L=0)} d$$

Extraction of $a_{\eta d}$

ηd scattering is investigated to fit the distorted phase space to the data

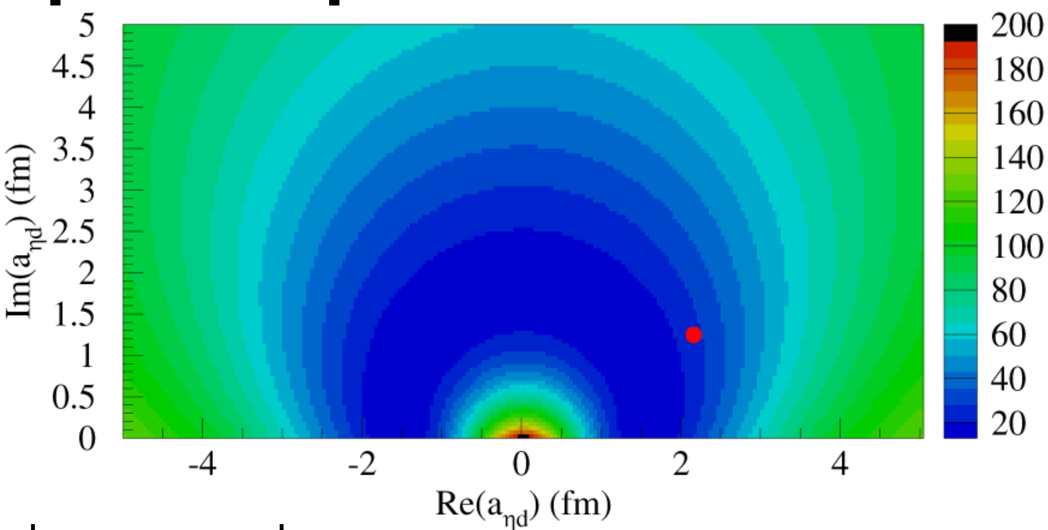

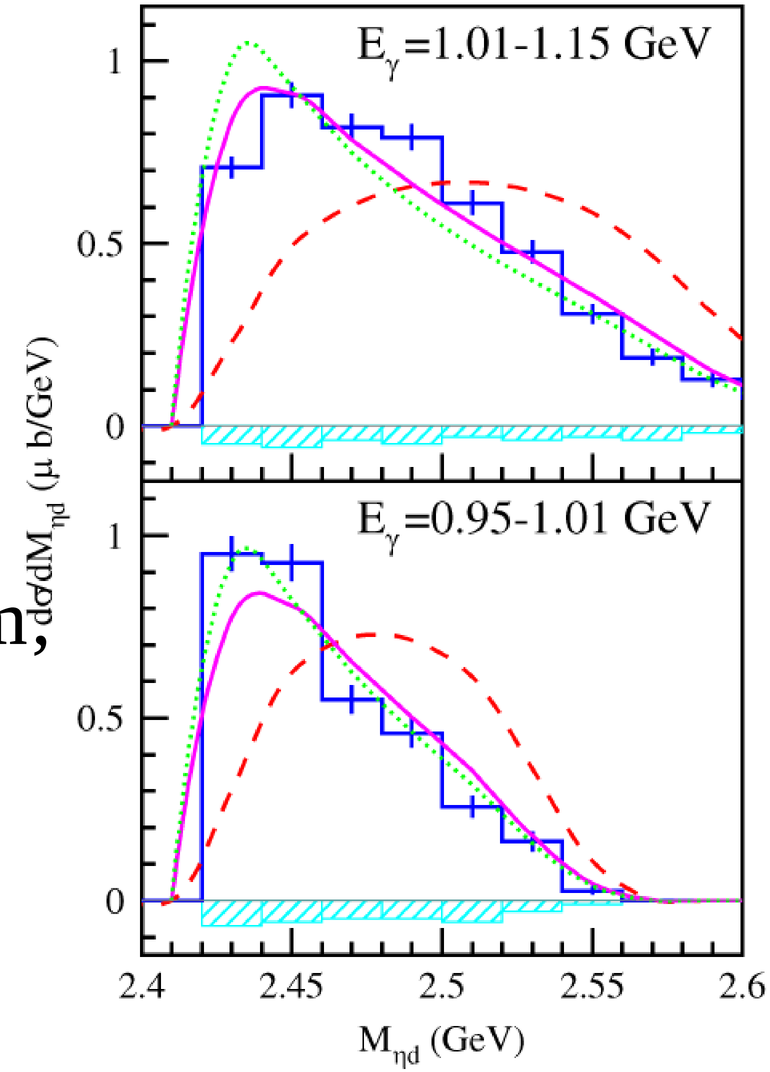

$$\left|\mathrm{Re}[a_{\eta d}]\right| < 2.7\ \mathrm{fm},\ \mathrm{Im}[a_{\eta d}] < 3.8\ \mathrm{fm},$$

$$0.9\ \mathrm{fm} < |a_{\eta d}| < 3.8\ \mathrm{fm}$$

$$a_{\eta d} = 2.16 + i1.25\ \mathrm{fm}$$

Fix and Kolesnikov, PRC97, 044001 (2018).

$$a_{\eta d} = (1.20 \pm 0.20) + i1.25\ \mathrm{fm}$$

present work